Boletín

Sociedad Española de Astronomía

ISSN 1575-3476
Depósito legal M-18326-1999
Número 10, julio 2003

Contenidos

Editorial

El contenido del boletín sigue superando, en cantidad y calidad, nuestras expectativas más optimistas. El número que tenéis entre manos es el más extenso de los publicados hasta el presente, siguiendo la tendencia de las ediciones anteriores. Agradecemos a todos los autores el trabajo que han dedicado a sus contribuciones en el boletín.

Los editores, por nuestra parte, también seguimos trabajando en la mejora del boletín. El cambio más visible es el nuevo diseño de la portada, que esperamos os guste y que hay que agradecer al trabajo de Benjamín Montesinos. Precisamente con esta edición Benjamín se despide como editor del boletín despues de diez años, por lo que el resto de editores quisieramos agradecerle la inmensa dedicación y esfuerzo que ha puesto en su labor, sin los cuales el boletín no habría llegado a su nivel actual. Podéis encontrar la despedida de Benjamín al lado de este editorial. De nuevo, Benjamín, muchas gracias por tu ejemplo y dedicación.

Con el mismo objetivo de mejorar la calidad del boletín, incluimos en esta edición una versión revisada y actualizada de las normas de publicación. El objetivo de estas normas es garantizar la coherencia y claridad de los contenidos del boletín, y constituirán la referencia para la publicación de contribuciones en el mismo. En particular, hemos clarificado en ellas un aspecto que conllevó una cierta polémica en la edición anterior: el idioma de publicación del boletín es el castellano. Esto no significa que no se acepten artículos en otros idiomas (en particular en inglés) para su publicación, pero creemos que esto debe ser la excepción y no la norma para el boletín.

En lo que respecta a los contenidos, esta edición cuenta en el apartado de contribuciones libres con la habitual revisión del estado actual del GTC, un artículo sobre el uso de estrellas de referencia por láser, una reseña de las actividades del programa "Adopta una estrella" del ESO y una reseña de las actividades de divulgación llevadas a cabo en torno al tránsito de Mercurio del 7 de mayo de este año. A continuación, en el apartado de artículos de revisión, podréis encontrar un par de magníficos (y extensos) textos sobre XMM y sobre la espectropolarimetría en astrofísica y, cerrando el boletín, los resúmenes de tesis doctorales.

Para concluir, sencillamente animaros a contactar con nosotros para publicar alguna contribución en el boletín.

Los editores

Despedida

Después de diez años como editor del Boletín de la SEA y de 18 números editados, es hora de despedirme. Xavier Luri, Ignasi Ribas y Jaime Zamorano continuarán con el trabajo. A ellos, a Javier Gorgas, y a Xavier Barcons, que comenzó conmigo la aventura, mi agradecimiento por toda su colaboración. A Agustín Sánchez-Lavega y al Comité Editorial, a los autores de contribuciones, artículos y resúmenes de tesis, también gracias, y por supuesto a las distintas Juntas Directivas, por su confianza. Y a todos, perdón por mi tozudez y por los mensajes "metiendo prisa" (*"twisting arms"* como dicen los anglos) con que inevitablemente os he inundado cada vez que se acercaba la fecha del cierre de la edición.

Benjamín Montesinos `bmm@laeff.esa.es`

Normas de publicación para el boletín

El Boletín de la Sociedad Española de Astronomía es una publicación semestral dirigida a los socios de la SEA. Diversas secciones del Boletín están abiertas a la publicación de contribuciones de los socios u otros miembros de la comunidad astronómica.

Normas generales

1. El objetivo del Boletín es la difusión de información u opiniones de interés general para la comunidad astronómica española. Las contribuciones al Boletín deberán ceñirse a este criterio y no se admitirán en ningún caso contenidos injuriosos o ataques personales.

2. Los contenidos del Boletín son determinados en última instancia por los editores, los cuales fijaran los criterios de publicación de las contribuciones, pudiendo posponer o anular su publicación en caso necesario.

3. El Boletín se publica en castellano y las contribuciones enviadas para su publicación deberán estar escritas en este idioma. En casos excepcionales podrán aceptarse contribuciones en otros idiomas previa autorización de los editores.

4. Las contribuciones al Boletín deberán entregarse en el formato requerido por los editores para su publicación. Actualmente este formato es LaTeX2e para el texto (usando el fichero de estilo proporcionado por los editores) y PostScript Encapsulado (EPS) para las figuras.

5. Las figuras incluidas en las contribuciones deben prepararse de forma que al ser impresas a una resolución de 300dpi o superior sean claramente legibles.

6. Las contribuciones presentadas deberán seguir las normas de redacción listadas en los apéndices de este documento.

7. Como orientación para la composición de toda clase de contribuciones o artículos, una página del Boletín sin figuras ni tablas tiene una extensión media de unas 800 palabras.

Cartas a los editores

El Boletín incluye una sección dedicada a la publicación de cartas de los miembros de la SEA. Siguiendo las normas del boletín, estas cartas deberán tratar temas de interés general para la comunidad astronómica española y no se admitirán contenidos injuriosos o interpelaciones personales. Las cartas a los editores deben de tener una extensión máxima de dos páginas del Boletín, incluyendo texto, figuras y tablas.

Artículos de revisión

El Boletín publica artículos de revisión y puesta al día de temas que son de amplio interés general para la comunidad de astrónomos españoles. Dichos artículos son solicitados mediante invitación del Comité Editorial del Boletín a los autores. Los manuscritos serán evaluados para su publicación por algún miembro del Comité Editorial o en su defecto y si se juzgase oportuno, por algún evaluador externo al Comité siguiéndose en todo caso, las pautas habituales de publicación de las revistas científicas. Se proporcionarán 25 separatas gratuitamente al autor principal de cada artículo.

Normas particulares

1. Los artículos deben tener un máximo de 12 páginas del Boletín, incluyendo texto, figuras y tablas.

2. Debe incluirse en los artículos un resumen (abstract) en castellano y en inglés.

3. Se enviará 1 copia impresa y otra por correo electrónico al Coordinador del Comité Editorial: Agustín Sanchez-Lavega, Dpto. Física Aplicada I, Escuela Superior de Ingenieros, Alda. Urquijo s/n, 48013 Bilbao (Vizcaya) (Tfno: 94-6014255, Fax: 94-6014871; e-mail: wupsalaa@bi.ehu.es).

4. El envío puede efectuarse en disquette o por los medios electrónicos habituales al presidente del Comité Editorial quien, una vez aceptado, lo remitirá finalmente al Editor del Boletín.

5. Dado que el artículo es de revisión, se tendrá especial cuidado con las citas bibliográficas que deberán llevar el nombre del primer autor seguido de et al. si se trata de mas de dos autores, el titulo del artículo, la revista (en nomenclatura indicada en el apéndice), el volumen, las páginas y el año. El listado de referencias se hará por orden alfabético

Contribuciones de tema libre

El Boletín incluye también una sección abierta dedicada a la publicación de pequeños artículos de tema libre (aunque con especial énfasis en la instrumentación, instalaciones y centros de divulgación científica) que pueden ser enviados a los editores bajo invitación o por iniciativa propia. Estas contribuciones deben tener una extensión máxima de cuatro páginas del Boletín, incluyendo texto, figuras y tablas.

Reseñas de tesis doctorales

Esta sección del Boletín está dedicada a la publicación de reseñas de tesis doctorales presentadas por astrónomos españoles. Las reseñas deberán ocupar un máximo de una página del Boletín, incluyendo texto, figuras y tablas.

Apéndice: unidades, símbolos, nomenclatura y abreviaturas

El texto debe distinguir claramente entre variables físicas, símbolos matemáticos, unidades de medida, abreviaciones, etc. según se indica a continuación:

1. En general, los nombres de variables deben escribirse en itálica y los vectores en itálica y negrita.
2. Las constantes físicas (como la velocidad de la luz o la constante de Hubble) deben escribirse en itálica
3. Las unidades de medida (por ejemplo km, erg cm^{-2}, s^{-1}) nunca deben escribirse en itálica, salvo si se incluyen en un pasaje que está totalmente escrito en itálica.
4. Deberán seguirse las recomendaciones de la UAI para la nomenclatura de objetos astronómicos.
5. Deberán usarse las siguientes abreviaciones para los títulos de revistas:

AJ	Astronomical Journal (the)
ARA&A	Annual Review of Astronomy and Astrophysics
AZh	Astronomiceskij Zhurnal
A&A	Astronomy and Astrophysics
A&AR	Astronomy and Astrophysics Review (the)
A&AS	Astronomy and Astrophysics Supplement Series
Acta Astron.	Acta Astronomica
Acta Astron. Sin.	Acta Astronomica Sinica
Afz	Astrofizica
ApJ	Astrophysical Journal (the)
ApJS	Astrophysical Journal Supplement Series (the)
Ap&SS	Astrophysics and Space Science
Ark. Astron.	Arkiv for Astronomi
Astron. Nachr.	Astronomische Nachrichten
Aust. J. Phys.	Australian Journal of Physics
Aust. J. Phys. Astrophys. Suppl.	Australian Journal of Physics Astrophysics Supplement
BAAS	Bulletin of the American Astronomical Society
C. R. Acad. Sci. Paris	Comptes Rendus de l'Académie des Science
Chin. Astron	Chinese Astronomy
IAU Circ.	International Astronomical Union, Circular
Icarus	Icarus
Ir. Astron. J.	Irish Astronomical Journal
J. R. Astron. Soc. Can.	Journal of the Royal Astronomical Society of Canada
JA&A	Journal of Astronomy and Astrophysics
MNRAS	Monthly Notices of the Royal Astronomical Society
Mem. R. Astron. Soc.	Memoirs of the Royal Astronomical Society
Mem. Soc. Astron. Ital.	Memorie della Societa Astronomica Italiana
Mitt. Astron. Ges.	Mitteilungen der Astronomischen Gesellschaft
Mon. Notes Astron. Soc. S. Afr.	Monthly Notes of the Astronomical Society of SouthernAfrica
Nat	Nature
Observatory	Observatory (the)
PASJ	Publications of the Astronomical Society of Japan
PASP	Publications of the Astronomical Society of the Pacific
PASPC	Ditto, Conference Proceedings
Phil. Trans. R. Soc. London, Ser. A	Philosophical Transactions of the Royal Society of London, Series A
Proc. Astron. Soc. Aust	Proceedings of the Astronomical Society of Australia
QJRAS	Quarterly Journal of the Royal Astronomical Society
Rev. Mex. Astron.	Astrofis. Revista Mexicana de Astronomia y Astrofisica
Ric. Astron. Specola Vaticana	Ricerche Astronomiche Specola Vaticana
Sci	Science
Sci. Am.	Scientific American
Sky Telesc.	Sky and Telescope
Space Sci. Rev.	Space Science Reviews
SvA	Soviet Astronomy

El GTC acaba de pasar la sexta revisión de progreso

Resumen

El GTC acaba de pasar su sexta revisión de progreso, en la que se ha examinado en detalle el estado del proyecto. Aunque según los revisores el proyecto va adelante, con los problemas normales de este tipo de proyectos, son evidentes una serie de retrasos que van a influir en la fecha de finalización.

Coincidiendo con esta reunión de revisión, se ha reunido también el Comité Científico, conocido por sus siglas inglesas (SAC), así como el Comité Internacional originado de los acuerdos de participación de México y de la Universidad de la Florida en el GTC.

En la montaña, el anillo de acimut está siendo ensamblado, paso previo a los demás elementos de la montura del telescopio.

El edificio está finalizado y con los necesarios documentos de fin de obra sellados por las autoridades competentes. Está siendo amueblado y preparado para acoger al equipo de operación. Los sistemas de refrigeración de la cúpula, pensados para mantener la cámara del telescopio a la temperatura prevista para la noche, han sido probados para permitir medidas del anillo de acimut a temperatura constante. El sistema de refrigeración parece funcionar correctamente.

La cúpula está acabada, si bien con algún problema por resolver. Esto es el resultado de la ruptura del contrato con la empresa que construyó la cúpula. Dicha empresa fue forzada a abandonar el recinto de obra ante su claro incumplimiento de fechas y de solucionar aspectos técnicos concretos. Por esta razón han quedado algunas partidas por acabar. Si bien la cúpula gira sin problema y las compuertas pueden operarse, hay dos problemas que necesitan atención para su adecuada resolución. Estos son los mecanismos de la compuerta de observación, que no funcionan correctamente y pueden desgastarse prematuramente, y los mecanismos de cierre estanco de las ventanas de ventilación, que no son precisamente estancos. Una vez rescindido el contrato con la compañía constructora de la cúpula, se están estudiando con otra empresa de ingeniería las acciones necesarias para solucionar estos problemas con el menor perjuicio posible para la actividad de montaje del telescopio.

Ya está en el ORM gran parte de la estructura metálica del telescopio, específicamente toda la estructura inferior, incluyendo el anillo de acimut, el sistema de canalización y recogida de aceite de los patinetes hidrostáticos, las patas de la montura, el suelo rotante y las plataformas Nasmyth. Para los menos familiares con la estructura del telescopio, esto significa algo más de la mitad de la misma. A día de hoy se está procediendo a alinear el anillo de acimut, ya instalado sobre el pilar del telescopio (Figura 1). El resto de la estructura, es decir el anillo de elevación y sus muñones, el tubo del telescopio, la araña del secundario y la celda del primario están siendo enviados al ORM o finalizando pruebas de fábrica. Este es el caso de los muñones de elevación, en los que se detectó cierta falta de concentricidad en sus superficies de referencia sobre la que apoyan los cojinetes hidrostaticos, los motores de elevación y el codificador de posición.

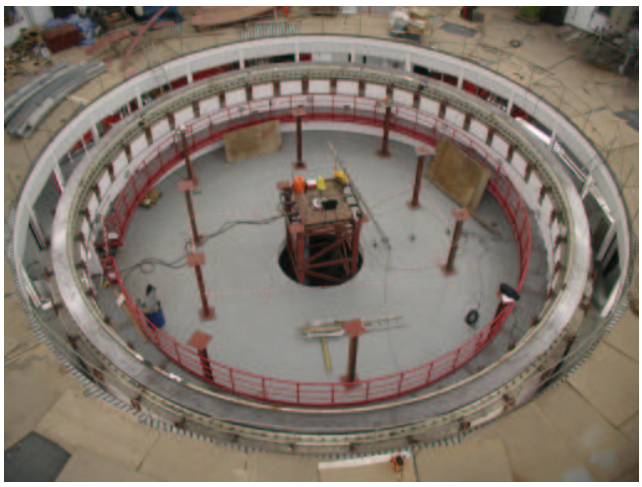

Fig. 1.: El anillo de acimut sobre el pilar del telescopio

En el montaje del anillo de acimut se ha detectado un problema de falta de homogeneidad en su superficie debido a un mal ajuste del anillo antes de fijarlo al pilar. Esto ha forzado a liberar de nuevo este anillo para su correcto alineado antes de fijarse definitivamente. Conforme escribimos este artículo, a finales de junio, se está procediendo a este realineado, que debiera estar completado en las próximas semanas. A partir de entonces se montará el sistema de alimentación y recogida del aceite de los patinetes hidrostáticos. Este sistema se encarga de mantener una película muy delgada de aceite a presión sobre la que deslizan los patinetes hidrostáticos y sobre ellos todo el telescopio. A continuación se montará el suelo rotante, que cierra la cámara del telescopio del resto del edificio, impidiendo que cualquier foco de calor o de luz de las zonas bajas del edificio pueda verse desde la cámara del telescopio.

Por último, los rotadores de instrumentos (Figura 2) y torre del terciario son los elementos mecánicos importantes de la estructura que quedan, y que a su vez están siendo terminados en sus respectivas factorías.

La óptica del primario avanza decididamente, si bien más despacio de lo que se quisiera. Este año es decisivo para la óptica del GTC por varias razones. Se terminará el primer lote de seis segmentos, las cajas de adquisición y guiado se recibirán en el ORM, así como la cámara de verificación, el secundario y el terciario. En la actualidad existen varios segmentos preparados para pasar a la fase última del pulido que es la fase

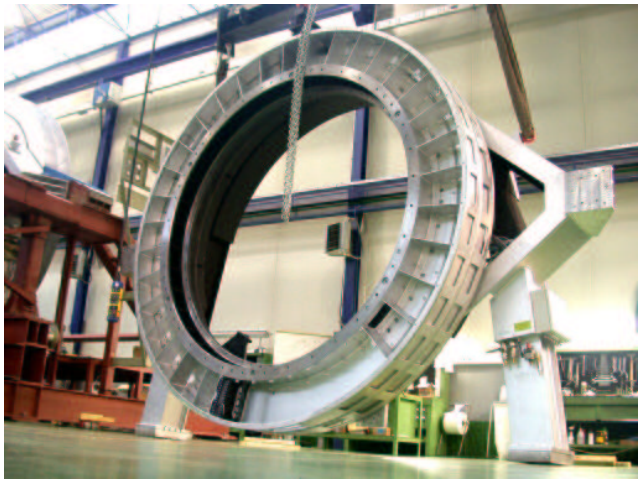

Fig. 2.: Rotadores de instrumentos en la factoria Tekniker

Fig. 3.: Substrato del secundario recubierto de níquel

de pulido iónico. El proceso de pulido, hasta ahora, se ha alargado debido a las dificultades de la empresa francesa SAGEM para conseguir la calidad requerida en los bordes de los segmentos. Escribimos esto volviendo de un viaje a SAGEM, una de las visitas periódicas (mensuales) que hacemos para examinar el avance del pulido de los segmentos. En ella hemos comprobado que el segmento maestro está listo para ser cualificado. Se acaban de ver franjas de interferencia en el sistema óptico que se ha montado para comprobar la figura de los segmentos del primario. El segmento maestro es un segmento que, una vez cualificado, se usará para contrastar los demás segmentos contra él, permitiendo la realización de pruebas ópticas de varios segmentos a la vez. En los próximos días el segmento maestro será sometido a un primer pase de pulido iónico. Esperamos que para final de julio este segmento maestro esté cualificado, con lo que el procesado de varios segmentos procederá, esperemos, más rápidamente. El plan es tener el primer lote de seis segmentos antes de final de año. Este primer lote se utilizará para la primera luz del telescopio.

El secundario ha salido de la situación de incertidumbre en que se encontraba el año pasado por estas fechas. El bloque de berilio fue, por fin, fabricado después de varios contratiempos de los que informamos en su día. En la actualidad, el bloque de berilio, ya provisto de una capa de níquel –que es la que se pule y luego aluminiza– está siendo pulido en la factoría de SAGEM, donde se está haciendo lo mismo con los segmentos del primario. Por su parte, el espejo terciario, una vez solventado un problema con algunas de las almohadillas por las que se sujeta a su montura, continua su pulido en Moscú.

Los instrumentos científicos parecen haber alcanzado la velocidad de crucero y se ven claros avances. OSIRIS, por ejemplo, tiene ya gran parte de la óptica fabricada o en proceso de fabricación. La estructura mecánica sin embargo va un poco atrasada ya que se ha avanzado su diseño hasta casi la fase de fabricación. Ahora se acaba de sacar el anuncio para la fase de fabricación que se hará en la industria. El esfuerzo de diseño de detalle ha supuesto un mayor costo en tiempo de lo que inicialmente se había estimado. Por ello la estructura mecánica de OSIRIS está ahora en lo que se denomina el camino crítico. Todo depende de dicha estructura y de su avance depende el calendario del proyecto OSIRIS. Esto significa que la integración de OSIRIS no empezaría hasta Marzo de 2004, previendo acabar la etapa de integración y pruebas de laboratorio hacia final de 2004.

OSIRIS ha celebrado varios talleres científicos sobre el uso o calibración de algunos de sus modos de observación, en particular sobre la calibración de los filtros sintonizables, y sobre espectroscopía multi-objeto. A dichos talleres han asistido numerosos colegas de todo el país, así como de México, y han sido de lo más instructivo y útil para entender los problemas asociados con el uso de alguno de los modos de observación de OSIRIS y ver como los han resuelto nuestros colegas en otros proyectos.

CANARICAM ha comenzado su integración una vez que el equipo de Florida ha terminado TRecs. En estos días, TRecs se está, de hecho, probando en el GEMINI sur. La imagen adjunta (Figura 5) es una de las primeras obtenidas por TRecs del planeta Marte. No se prevé ningún contratiempo en la integración de CANARICAM, toda vez que es un instrumento muy parecido a TRecs y que el grupo de Florida ya tiene una gran experiencia acumulada en la integración de este tipo de instrumentos infrarrojos.

ELMER comenzará su integración en los talleres del IAC el próximo mes de octubre y se espera esté terminado para la primavera de 2004. Toda la óptica de ELMER está ya lista y una gran parte de ésta se encuentra en los laboratorios de GTC. La que falta se recibirá en los próximos meses. Gran parte de la estructura

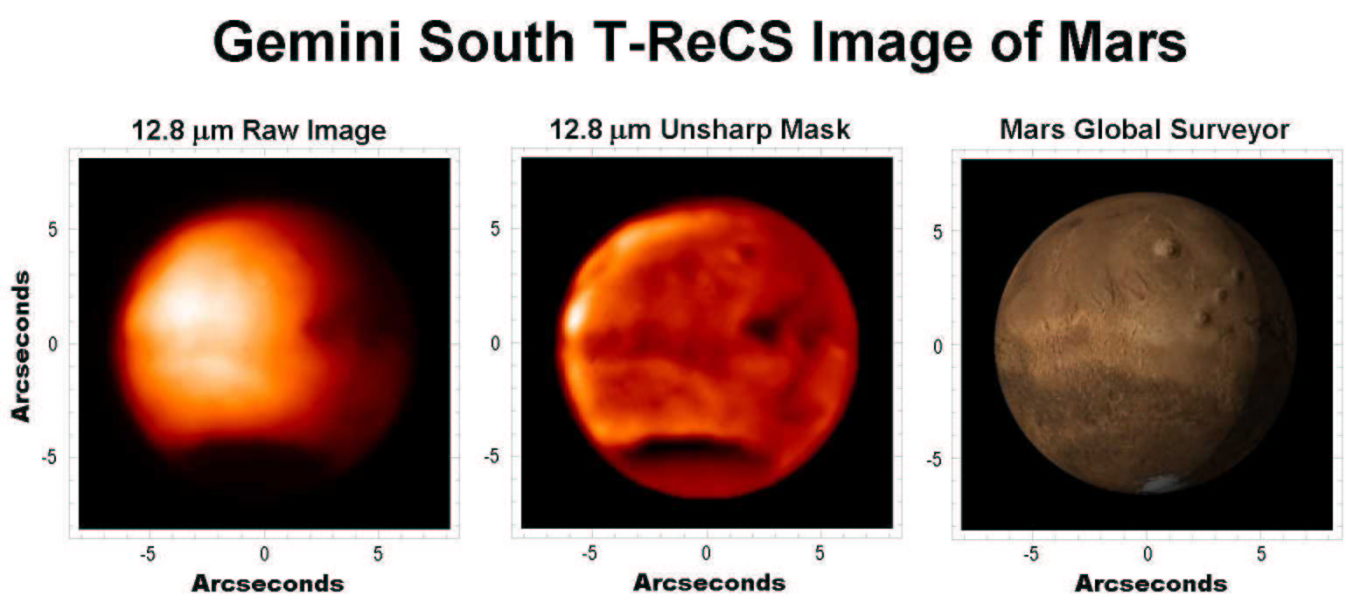

Fig. 5.: Imagen de Marte obtenida con Trecs en Gemini Sur (izquierda). La misma imagen procesada (centro). Marte con el Global Surveyor (derecha). Imagen cortesía del equipo de CanariCam.

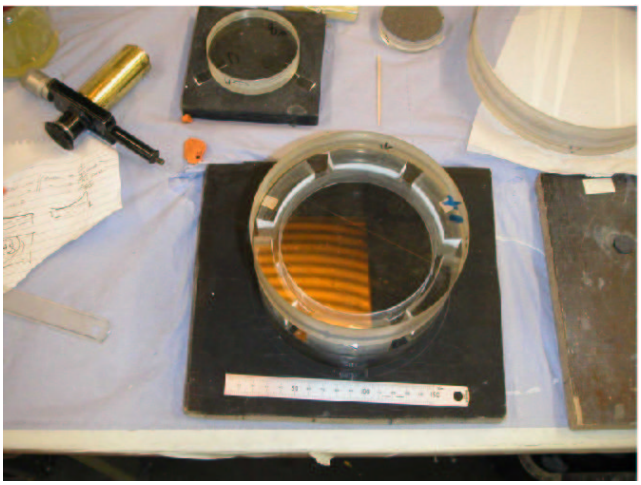

Fig. 4.: Uno de los filtros sintonizables de OSIRIS

Fig. 6.: La rueda que albergará los prismas (convencionales y escalonados) y los VPHs de ELMER

metálica está asimismo terminada o en proceso de terminación. Pronto será pues enviada a La Laguna para su integración y pruebas. Recientemente se ha diseñado y pedido un conjunto de redes holográficas (VPH) para dotar a ELMER de una dispersión cercana a 2.500, lo que añadirá aún más versatilidad a este instrumento.

EMIR ha pasado recientemente con éxito su revisión de diseño preliminar con lo que Paco Garzón y su equipo están avanzando rápidamente a la fase de diseño detallado con la idea de pasar a fabricación por subsistemas a lo largo de 2004. EMIR tenía dos elementos clave y no exentos de riesgo en su diseño conceptual. Estos eran el sistema cambiador de máscaras criogénicas, y el cómo conseguir la dispersión necesaria para resolver las líneas de emisión de los radicales hidroxilo de la atmósfera, ganando de esta manera hasta una magnitud en sensibilidad. En la revisión de diseño se discutieron profusamente estos aspectos. En lo que respecta al sistema para cambiar las máscaras criogénicas, se ha decidido utilizar un robot criogénico capaz de configurar un conjunto de hasta 52 rendijas (el número final que se adopte está en discusión) de anchura variable. Un prototipo de este robot ha sido cualificado para su utilización como tecnología de repuesto para el espectrógrafo infrarrojo del JCMT.

El otro aspecto clave de EMIR son los elementos dispersores que han de ser capaces de conseguir resolver las líneas de OH del cielo. En la reunión de revisión se pudo comprobar la solución adoptada por el equipo EMIR consistente en un seudo-prisma escalonado (*pseudo-grism*) en el que una lámina plano-paralela en

Fig. 7.: Uno de los prismas escalonados de alta dispersión prototipo de EMIR y los VPHs de ELMER

la que está grabado el patrón de dispersión se intercala entre dos prismas normales. Con este esquema se ha mostrado un prototipo con el que se puede conseguir la dispersión necesaria, a un precio y dificultad de fabricación razonables.

Al igual que OSIRIS, el equipo de EMIR está simultáneamente llevando a cabo una gran actividad científica de cara a preparar la ciencia que se hará una vez EMIR esté instalado en el GTC. Varios resultados de gran impacto han salido ya a la luz mucho antes de que EMIR haya podido llegar al telescopio.

Nuevos instrumentos

El Instituto de Astrofísica de Andalucía está iniciando las acciones pertinentes para llevar a cabo un diseño conceptual del instrumento de resolución espectral intermedia. Este instrumento, que el SAC ha priorizado como el próximo instrumento de segunda generación del GTC, debiera estar finalizado hacia finales de 2007. El IAA, que está poniendo gran interés en este proyecto, tendrá un diseño conceptual listo para la primavera de 2004. Se están dando asimismo los pasos necesarios para formalizar un consorcio que incluya a todas las personas e instituciones interesadas en dicho instrumento. En particular el INAOE en Puebla, México, ha expresado gran interés en participar desde el inicio en el diseño y fabricación de dicho instrumento. Las características fundamentales de este espectrómetro se obtendrán del cuestionario que se envió a la comunidad. De las respuestas obtenidas, que están aún por estudiar en detalle, se deduce que una gran mayoría de la comunidad se decanta por una resolución entre 5000 y 20000, y tanto de rendija larga como multiobjeto. Hay asimismo cierta preferencia por la espectroscopía de campo integral.

Instrumentos "visitantes"

La Universidad de Florida ha propuesto llevar a cabo el diseño y fabricación, totalmente a su costo, de una cámara infrarroja, denominada CIRCE, para trabajar en las bandas J, H y K. La financiación para la fabricación de dicha cámara proviene de la propia Universidad de Florida, como parte de los fondos de contratación del Profesor Steven Eikenberry, recientemente incorporado al claustro de Florida. El profesor Eikenberry ha formado un equipo científico en el que ha incluido a colegas españoles así como de México y Florida. La idea es dotar al GTC de una cámara para el infrarrojo cercano, viniendo a rellenar un hueco que, en el GTC, no estaría cubierto hasta la llegada de EMIR. A cambio de proporcionar CIRCE, la Universidad de Florida ha solicitado un cierto tiempo garantizado que dependería de la aceptación que CIRCE tuviera entre la comunidad de usuarios de México y España. La aceptación de CIRCE está siendo discutida por los comités relevantes.

Sexta reunión anual de revisión del proyecto

Los días 11, 12 y 13 de Junio ha tenido lugar una reunión del Comité Científico Asesor (SAC) y la sexta revisión anual del proyecto GTC. Como en anteriores revisiones, el panel de expertos es siempre el mismo, reforzado en cada caso con alguien experto en el tema que se quiere tratar más a fondo. En este caso se querían revisar con detalle los planes de la futura operación del GTC. En esta ocasión, por tanto, los miembros del panel de revisión fueron los habituales, Alvaro Giménez (actual director del Departamento de Ciencias Espaciales de la ESA, antiguo director del INTA y profesor del CSIC), Peter Gray (director técnico que supervisó la integración y puesta en marcha de los VLT, actual jefe de ingeniería de GEMINI encargado de optimizar la operación de GEMINI), Jerry Nelson (director científico y principal impulsor de los telescopios Keck, actual director del *Center for Adaptive Optics* de la NSF, y promotor del telescopio CELT de 30 metros de diámetro), y René M. Rutten (director del ING), complementados con Hilton Lewis (subdirector de operación del KECK) y Jason Spiromillio (Subdirector del Observatorio de Paranal). Disculparon su ausencia por problemas de calendario Torben Andersen (Profesor de la Universidad de Lund, antiguo director Técnico del NOT, actual director de ingeniería del EURO50, y encargado del paquete de óptica del proyecto de telescopio gigante europeo) y Thomas Sebring (director técnico del HET y del SOAR y actual director técnico del *Next Generation Lowell Telescope*).

En esta revisión se hizo especial hincapié en la escasez de personal con que cuenta el GTC en algunas áreas, especialmente las relacionadas con la integración,

y en la previsión optimista del esfuerzo necesario para la puesta a punto y operación científica del GTC. Si bien no era el tema de la revisión de este año, no se pudieron dejar de analizar los problemas por los que atraviesa el GTC, que en opinión del panel de expertos son similares a los problemas por lo que han pasado otros proyectos. Hicieron énfasis sin embargo en la necesidad de reforzar la plantilla, especialmente en algunas áreas. Se puso de manifiesto en la reunión el retraso en el calendario del GTC, debido a los problemas mencionados con los diversos contratistas. La fecha estimada a día de hoy para primera luz es otoño de 2004, con lo que la operación científica se retrasaría hasta casi finales de 2005. En el proyecto se está poniendo todo el esfuerzo para, en la medida de lo posible, acortar estos plazos.

El SAC también celebró su vigésima reunión y participó en la reunión anual de revisión del proyecto como se ha venido haciendo año tras año. Por último, el sábado 14 de junio se celebró una visita al ORM de los miembros del panel de revisión, del SAC y del Comité Internacional, para ver el estado de las obras. Pudo comprobarse la terminación del edificio y el inicio del montaje del telescopio. El Comité Internacional celebró su reunión esa misma tarde; dicho comité, del que varios de sus miembros habían asistido a la reunión de revisión, abundó en la necesidad de reforzar la plantilla y mantener al personal clave del GTC para la operación.

La reunión científica sobre Ciencia con el GTC que se había previsto inicialmente para noviembre de 2003 se ha pospuesto hasta febrero de 2004. Próximamente se lanzará el primer anuncio. La reunión se celebrará en la Ciudad de México, en el Castillo de Chapultepec, donde se instaló el primer observatorio astronómico de México.

En el próximo número trataremos de escribir sobre el sistema de control del GTC, que incluye las interfaces de usuario, es decir la cara visible del GTC ante la comunidad astronómica. Esto incluye los programas de preparación de propuestas, las cadenas de reducción de datos, el archivo, etc.

Pedro Alvarez Martín pam@ll.iac.es
J. Miguel Rodríguez Espinosa espinosa@ll.iac.es

Superando la limitación del ángulo isoplanático: estrellas de referencia por láser

Resumen

El reto de construir instrumentos de uso común para obtener imágenes y espectros desde la superficie de la Tierra con la misma resolución que desde el espacio es bastante atractivo. Distintos campos de la Astrofísica esperan disponer de un mayor poder resolutivo para seguir ahondando en el conocimiento del Universo. El ángulo isoplanático es la región angular alrededor de un objeto astronómico a observar con un instrumento de óptica adaptativa donde es preciso encontrar una fuente de referencia que nos permita muestrear la turbulencia atmosférica para corregir sus perturbaciones, siendo su valor típico de dos segundos de arco para los observatorios de alta montaña. Al ser una región tan pequeña, es necesario utilizar otras estrategias que permitan extender la técnica a cualquier objeto de interés, para ello un haz láser propagándose a través de la atmósfera puede ayudarnos a evaluar las perturbaciones introducidas por la turbulencia atmosférica en la radiación del objeto astronómico en su camino hacia la apertura del telescopio, y posteriormente, corregirlas en tiempo real. En particular, las estrellas de referencia en sodio se basan en la radiación retrodispersada resonantemente de los fotones de un láser al alcanzar la capa de este elemento situada a 90 km, en la región atmosférica conocida como mesopausa, permitiendo extraer las deformaciones introducidas por la atmósfera. Nuestro grupo está desarrollando una campaña de caracterización, en el Observatorio del Teide, de la distribución en altura del sodio dentro del experimento CALAS (Caracterización Atmosférica por LASer) que permita establecer los requerimientos necesarios para un sistema de estrellas láser sobre las Islas Canarias.

Alta resolución espacial

El poder resolutivo alcanzado con un telescopio de 15 cm es idéntico al poder resolutivo logrado con un telescopio de clase 10 metros. La turbulencia atmosférica es la responsable del emborronamiento de las imágenes al producir fluctuaciones aleatorias del índice de refracción en el camino de propagación de la luz, hecho que provoca que las imágenes obtenidas de un objeto puntual tengan una resolución menor que la resolución teórica para un telescopio perfecto sin atmósfera. Por ello, para una apertura superior a 15 cm en un observatorio de alta montaña, el poder resolutivo es el mismo para todas las aperturas.

El telescopio fue introducido en Europa por Galileo hace más de 400 años, iniciándose un desarrollo constante con la pretensión de detectar objetos cada vez más lejanos en el espacio-tiempo y resolver estructuras más pequeñas de los mismos. Pero desde los mismos inicios, la resolución de las observaciones realizadas a través de los telescopios terrestres no ha variado debido a que la radiación del objeto es modificada por la atmósfera de la Tierra. En 1953, Beckers planteó la posibilidad de utilizar elementos de óptica autoajustables para compensar en tiempo real las deformaciones introducidas por la atmósfera terrestre en las imágenes astronómicas. Pero no es hasta la década de los setenta cuando el gobierno de los Estados Unidos de América impulsa la investigación en este campo al tener una aplicación inmediata en la detección de los satélites soviéticos en órbita. Para lograr este propósito, comienzan programas donde se toman fotografías del cielo y cuyos resultados se ven condicionados por la resolución alcanzada al observar a través de la turbulencia atmosférica. Para solucionar el problema se inicia el desarrollo de la óptica adaptativa con el objetivo de construir telescopios capaces de corregir las imágenes en tiempo real, proporcionándonos el poder resolutivo máximo teórico para la apertura disponible.

En Europa, la investigación se desarrolla dentro del campo de la instrumentación astrofísica, donde los primeros experimentos con técnicas de óptica adaptativa fueron realizados en 1989 por Rouset (5), demostrando las potencialidades de su uso. Concretamente, en este primer experimento la técnica fue aplicada a una estrella binaria en el infrarrojo, donde se logró una ganancia en resolución y sensibilidad en 2.23 micras.

En la fig. 1 mostramos un diagrama conceptual de un sistema de óptica adaptativa que corrige las deformaciones en el frente de onda del objeto científico para aumentar la resolución de la observación: [1] Detector del frente de ondas, que mide las deformaciones, [2] elemento para aplicar la corrección, habitualmente se utilizan espejos deformables, [3] sistema de control que opera a una frecuencia de trabajo igual a la de las variaciones de la turbulencia atmosférica, y [4] un objeto de referencia en las proximidades del objeto astronómico a observar. En el óptico es más difícil conseguir imágenes corregidas ya que los sistemas tienen que operar a frecuencias más altas y las perturbaciones tienen una escala menor, por ello estas técnicas se están desarrollando en el infrarrojo.

El frente de ondas del objeto astronómico y de referencia, al estar separados una cierta distancia angular, atraviesan un volumen atmosférico ligeramente diferente en su camino de propagación. La primera limitación a la que se enfrentan los sistemas de óptica adaptativa es encontrar un objeto de referencia en las proximidades del objeto a estudiar. La separación angular máxima tal que la turbulencia atmosférica introduce deformaciones similares en el frente de ondas del objeto científico y de referencia es el **ángulo isoplanático**.

En el Observatorio del Roque de los Muchachos,

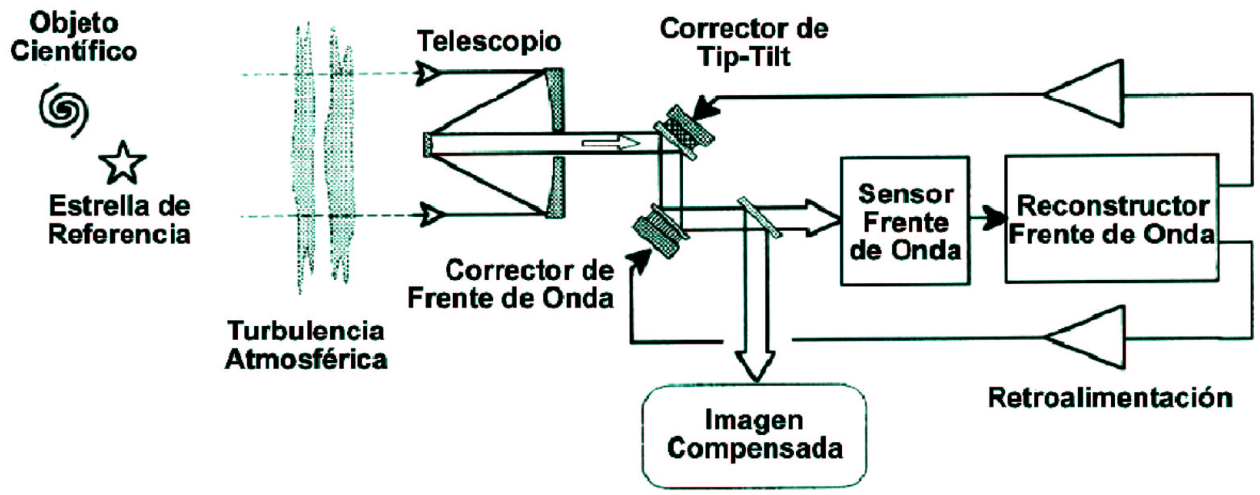

Fig. 1.: Diagrama conceptual de un sistema de óptica adaptativa

utilizando perfiles de turbulencia medidos en noviembre de 1995 por Jean Vernin y Casiana Muñoz-Tuñón, se llegan a obtener valores para el ángulo isoplanático de 2.8" (6). Es decir, la estrella de referencia puede estar alejada hasta casi tres segundos del objeto de estudio para que la corrección en el frente de ondas por el sistema de óptica adaptativa sea satisfactoria. Esta información es complementaria a la del *seeing*, porque aunque el ángulo isoplanático medido en dos ubicaciones diferentes sea el mismo, el *seeing* puede ser distinto dependiendo de la estructura específica de la turbulencia sobre el observatorio. De esta forma, cuanto más próxima a la superficie del suelo estén las capas turbulentas las resoluciones alcanzadas con el sistema de óptica adaptativa van a ser mayores.

Estrellas de referencia y óptica adaptativa multiconjugada

Gran parte de los objetos de interés científico quedaron lejos de su estudio en alta resolución espacial al no disponer de estrellas naturales de referencia en sus cercanías. La primera idea planteada para solucionar esta limitación procede de Foy & Laberie, que en 1984 sugieren la posibilidad de generar una fuente de referencia utilizando la dispersión de la radiación de un láser propagándose en la atmósfera, generando artificialmente una estrella situada a una distancia angular del objeto de estudio menor que el ángulo isoplanático. A partir de su trabajo se abre un nuevo campo de investigación: las **Estrellas de Referencia por Láser (LGS)**. Durante el quinquenio 1996-2001 se implanta en Europa una red (*Training Mobility Research*, TMR) con el objetivo de resolver los problemas existentes para construir un sistema de óptica adaptativa utilizando estrellas de referencia en los telescopios de clase 8 metros. Actualmente, se están explorando dos métodos para generar los objetos de referencia: [1] utilizando la dispersión Rayleigh de las capas entre 10 - 15 km, [2] utilizando la dispersión resonante de una capa de sodio situada a 90 km. En concreto, las estrellas de referencia en sodio presentan, a priori, unas mejores prestaciones al generarse a una altura mayor sobre el telescopio, permitiendo un mejor muestreo de la turbulencia en las capas altas. En la figura 2 mostramos una imagen de una estrella de referencia en sodio generada en el Observatorio del Teide, para ello focalizamos un láser en la capa de sodio excitando resonantemente la transición D_2 del sodio atómico a 5891.58 Å.

Los primeros experimentos con estrellas de referencia por láser se realizaron en Mauna Kea durante 1987, obteniéndose las primeras imágenes de la estrella de referencia en sodio (8). Pero ha sido en la década de los noventa, en el Observatorio de Calar Alto, donde se desarrolló el sistema ALFA que permitía obtener imágenes corregidas con una estrella artificial de sodio (9). Este proyecto concluyó en el 2000, pero ha servido de base para el nuevo proyecto de un instrumento con estrella de referencia en sodio de la ESO para el Very Large Telescope (VLT). Actualmente, todos los grandes telescopios (GTC, GEMINI, VLT, Keck, Subaru) están desarrollando instrumentos que hacen uso de estrellas de referencia por láser de sodio.

Los sistemas de óptica adaptativa convencionales corrigen el frente de ondas en una región de tamaño angular definido por el ángulo isoplanático, pero Becker (3) planteó la posibilidad de incrementar esta región situando varios espejos deformables en planos conjugados a la altura de las capas turbulentas más intensas. Esta estrategia de trabajo se conoce como **óptica adaptativa multiconjugada (MCAO)**, aunque actualmente no es independiente de las estrellas de referencia por láser debido al mismo problema, no es posible siempre encontrar estrellas naturales de referencia en las posi-

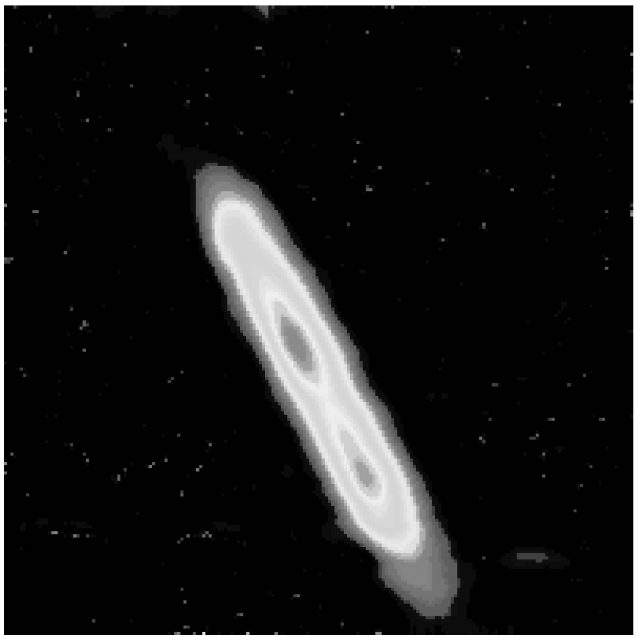

Fig. 2.: Imagen de una estrella de referencia en sodio generada en el Observatorio del Teide con el Experimento CALAS durante Diciembre de 2001. El haz láser excita resonantemente la transición D_2 del átomo de sodio reemitiendo los fotones dispersados isotrópicamente y generando un objeto de referencia en las proximidades del objeto científico de interés.

ciones adecuadas para aplicar la técnica (4).

Un método para evaluar el ángulo isoplanático generalizado alcanzado con los sistemas de óptica adaptativa multiconjugada ha sido desarrollado por Tokovinin (7), atendiendo únicamente a consideraciones de la estructura en altura de la turbulencia sobre el observatorio. A partir de los perfiles experimentales de turbulencia medidos durante la campaña de Jean Vernin y Casiana Muñoz-Tuñón de 1995, hemos encontrado los valores para el ángulo isoplanático generalizado, resultado que mostramos en la tabla 1. El valor para cada uno de los 12 perfiles utilizados es similar durante la noche al valor promedio, es decir, la alturas de conjugación para la noche de estudio fueron bastante estables en el tiempo. De todas formas es necesario el desarrollo de un estudio estadístico de este parámetro ya que no se pueden extraer conclusiones definitivas con el número de perfiles de que disponemos actualmente.

Las hipótesis que se asumen para definir el ángulo isoplanático generalizado son tales que proporcionan un valor independiente del instrumento y permiten comparar la calidad de dos observatorios diferentes para instalar un sistema de óptica adaptativa con óptica multiconjugada. Si comparamos con el ángulo isoplanático para el Observatorio del Roque de los Muchachos, pasamos de casi tres segundos a disponer de una región de medio minuto de arco para encontrar el objeto de referencia donde se puede medir la perturbación en el

Número de espejos	Θ_G	H_1	H_2	H_3
1	2.8			
2	20.76	3.1	13.5	
3	35.88	2.6	7.5	15.0

Tabla 1: Alturas óptimas de multiconjugación para un sistema de óptica adaptativa con varios espejos deformables conjugados a la altura de las capas más intensas y el ángulo isoplanático generalizado asociado. Estos datos se han extraido a partir de 12 perfiles de turbulencia medidos el 11 de noviembre de 1995 en el Observatorio del Roque de los Muchachos.

frente de ondas del objeto.

Características de la estrella de referencia en sodio

Los parámetros más relevantes para caracterizar la estrella son: (1) su tamaño angular observable desde el telescopio y (2) su magnitud. El tamaño angular depende a su vez de dos factores: el perfil de turbulencia y la distribución en altura de la capa de sodio; la magnitud depende de la densidad columnal de átomos de sodio. Con estos datos podemos modelar como será la estrella de referencia generada y establecer las especificaciones técnicas del láser para el instrumento de óptica adaptativa. Con el láser se excitan los átomos de sodio en el volumen más pequeño posible, consiguiendo una fuente puntual que permita evaluar las perturbación introducidas en el frente de ondas por la turbulencia. Para ello, mediante un sistema óptico se concentra la máxima cantidad de energía del láser en la capa de mayor densidad de átomos de sodio. Un desenfoque del sistema se produce cuando hay un diferencia entre la altura de focalización del haz y la región de densidad máxima de la capa de sodio, aumentando el tamaño de la estrella de referencia y disminuyendo la eficiencia global de la corrección del frente de ondas. Las dos fuentes de error de focalización son: [1] la variación de la turbulencia , y [2] la variación en la estructura de la capa de sodio. Por ello es interesante disponer de un estudio estadístico de las variaciones diarias y estacionales de la capa que permita evaluar sus prestaciones bajo diversos escenarios de operación.

El experimento CALAS

En el año 1997 nos propusimos construir un instrumento que permitiera evaluar las características de una estrella de referencia sobre los Observatorios de Canarias. El sistema que operamos actualmente en el Observatorio del Teide utiliza dos de sus telescopios: el IAC80 y la OGS. En el banco óptico del *Optical Ground Telescope* (OGS) está situada la infraestructura de generación y

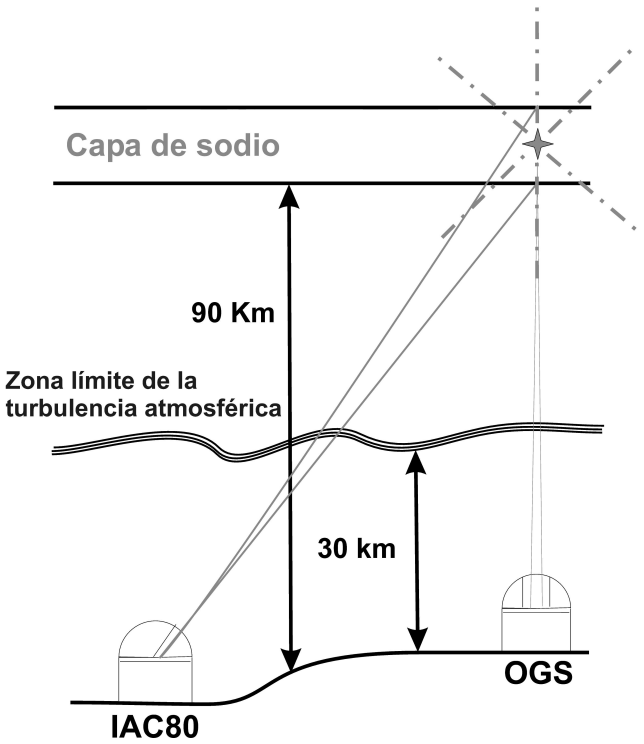

Fig. 3.: Diagrama de la configuración observacional del experimento CALAS. Lanzamos un láser en la longitud de onda de la transición D_2 del sodio desde la OGS, observando el dispersión resonante desde el telescopio IAC80, situado a 165 metros, con lo que obtenemos información en altura de la distribución de sodio sobre el observatorio.

lanzamiento del láser a través de una apertura de 1 metro de diámetro. La estrella creada se observa desde el telescopio IAC80, emplazado a 165 metros de distancia y proporcionando una imagen de la estrella de 1 minuto, con lo que permite resolver la estructura de la capa con una resolución de 300 metros para un *seeing* de 3".

El láser de colorante utiliza una disolución de Rodamina que nos proporciona una potencia de salida de 1 W cuando es bombeado por un láser de Argón con una potencia de 25 W. La sintonización del láser a la longitud de onda de la transición D_2 del sodio se realiza utilizando un filtro birrefringente dispuesto en la cavidad resonante. La estabilización en la longitud de onda se hace con un juego de etalones y un sistema de control obteniendo un ancho de banda de 10 mÅ para el haz de salida. La longitud de onda se mide con un interferómetro Fabry-Perot que opera con la longitud de onda en el vacío, ya que esta es independiente de la temperatura y presión.

La altura donde se focaliza el láser depende del ángulo de divergencia del haz a la salida del telescopio, modificándose mediante un expansor de haz diseñado por el área de instrumentación del IAC. Al comienzo de cada periodo de observación calibramos el foco Coudé de la OGS para evaluar el cero en la tabla de focalización del telescopio. En particular, para el estudio de la mesosfera focalizamos el haz a 90 km, observando la estrella generada con tiempos de exposición de 15 minutos durante toda la noche, estableciendo las variaciones en altura de la capa y la densidad columnal de átomos de sodio a partir de la señal de dispersión resonante. La potencia emitida del láser es calibrada utilizando la señal de dispersión Rayleigh a 20 km. Por ello, cada dos horas se realiza una exposición a esta altura del haz.

Esta capa se estudia en geofísica debido a que el sodio es un trazador de las ondas de gravedad interna de la atmósfera de la Tierra. Entre las características globales podemos destacar que se sitúa en el rango de alturas entre 90 y 95 km, con variaciones diurnas y estacionales, con una densidad de columna típica de 3×10^9 atomos/cm^2 (10). Debido a la dependencia de la abundancia y la altura de la capa con la ubicación geográfica es necesario un estudio detallado sobre el observatorio. La altura del centroide ($z_{\rm Na}$) y el error en la medida ($\rho_{\rm Na}$) lo expresamos en función del momento estadístico definido por:

$$m_i = \int dz\ z^i\ N_{\rm Na}(z) \qquad (1)$$

donde la $z_{\rm Na} = m_1/m_2$ y $\rho_{\rm Na} = [m_2/m_0 - (m_1/m_0)^2]$ y $N_{na}(z)$ es el perfil de dispersión Rayleigh medido por el experimento CALAS. En la figura 4 mostramos la evolución de la capa durante el 18 y el 19 de septiembre de 2002. La variaciones relativas entre los centroides de la capa de sodio más alta y más baja es de 2 km durante el 18 de septiembre y de 8 km durante el 19 de septiembre.

La densidad de sodio columnal se puede evaluar a través de

$$\rho_{\rm Na} = \frac{\sigma_{\rm Na}\ z^2_{Ray} \Delta z_{\rm Na}}{\rho_{air}\sigma_{Ray}\ z^2_{\rm Na} \Delta z_{Ray}} \frac{N_{\rm Na}}{N_{Ray}} \qquad (2)$$

donde $N_{\rm Na}$ es el número de fotones detectado de la capa de sodio, $\Delta z_{\rm Na}$ es la anchura de la capa de sodio, N_{Ray} es el número de fotones de dispersión Rayleigh. De esta forma determinados que la densidad columnal media es del orden de 10^9 atomos/cm^2, valor que no podemos precisar más actualmente por problemas con la estabilidad de la longitud de onda emitida.

Otro efecto interesante es la aparición de capas esporádicas, estás se desarrollan entre el centro de la capa estable de sodio y los 110 km de altura, con una anchura típica de varios kilómetros (11). La densidad de la capa esporádica se expresa a través del factor de proporcionalidad entre el pico de densidad de la capa estable y el pico de la esporádica, factor que oscila entre 1 y 10. La vida media de una capa esporádica es de varias horas, formándose en tan sólo unos minutos y desvaneciéndose lentamente. Con el experimento CALAS estamos elaborando una estadística de la frecuencia de las capas

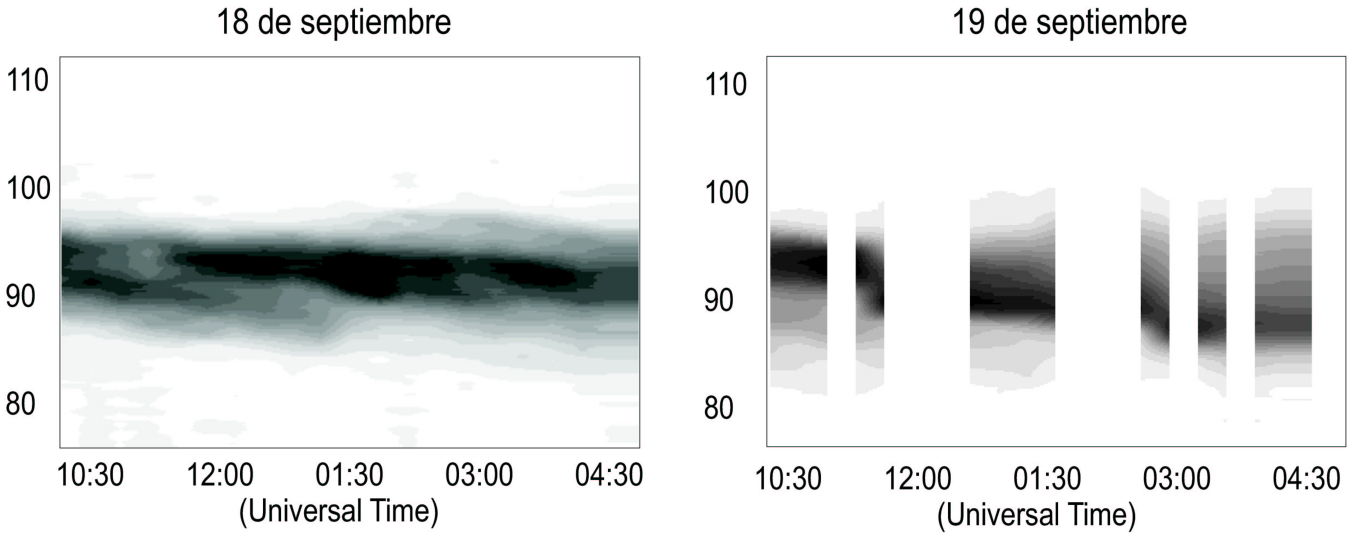

Fig. 4.: Evolución de la densidad de la capa de sodio (mayor concentración en negro, ausencia en blanco). El diagrama de la izquierda corresponde a la variación durante el 18 de septiembre y el de la derecha durante el 19 de septiembre.

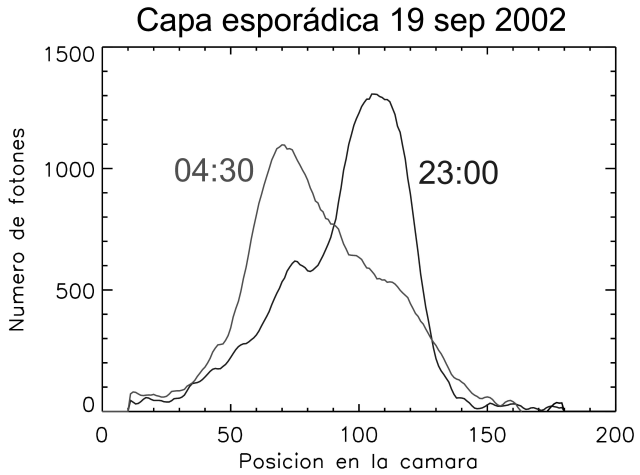

Fig. 5.: Evento de capa esporádica detectado el 19 de septiembre sobre el Observatorio del Teide. El pico de concentración máxima está desplazado 8 kilómetros cuando comparamos un perfil al comienzo de la noche con otro medido al final de la misma. Esto afecta seriamente a la focalización de la estrella de referencia cambiando su magnitud y el tamaño angular.

esporádicas de sodio para evaluar las noches que un sistema de óptica adaptativa sufrirá perturbaciones en la eficiencia al incrementarse la magnitud y el tamaño angular de la estrella. En los datos adquiridos haste el momento hay un claro ejemplo de capa esporádica durante la noche del 19 de septiembre. En la figura 5, mostramos el perfil de emisividad de la estrella con la altura durante esa noche, constantando una diferencia de 8 km entre el pico de concentración máxima al principio y al final de la noche.

Todos los grandes observatorios están comenzando campañas de caracterización de la capa de sodio; entre los grupos que trabajan actualmente en esta línea están el Imperial College de Londres, la Universidad de Illinois, el proyecto Gemini y la ESO. En los próximos años veremos como se desarrollan instrumentos de óptica adaptativa multiconjugada en aquellos lugares con las mejores condiciones observacionales. El reto es obtener imágenes de alta resolución de forma rutinaria. Con este estudio pretendemos aportar datos estadísticos de las características de la capa de sodio que permitan definir con mayor precisión los parámetros de diseño de los instrumentos con estrellas de referencia de sodio sobre los observatorios de Canarias.

Referencias

[1] Foy, R., Labeyrie, A. 1985, A&A, 152, L29

[2] Sergio Chueca, "Estrellas de referencia por láser: estructura y dinámica de la mesosfera terrestre", Tesis Doctoral, Instituto de Astrofísica de Canarias, 2002

[3] Beckers, J.M., Proceedings of a ESO Conference on Very Large Telescopes and their Instrumentation, 1988, p. 693

[4] Berkefeld, T. 1999, BAAS, 31, 837

[5] Rousset, G., Fontanella, J.C., Kern, P., Gigan, P., Rigaut, F. 1990 A&A, 230, L29

[6] Varela, T., comunicación personal

[7] Le Louarn, M., Hubin, N., Sarazin, M., Tokovinin, A. 2000, MNRAS, 317, 535

[8] Thompson, L.A., Gardner, C.S. 1987, Nature. 328, 229

[9] Hippler, S., Kasper, M.E., Feldt, M., Weiss, R. et al. 2000, SPIE, 4007, 41

[10] Butler, D.J., Davies, R.I., Fews, H., Redfern, R.M. et al. 2000, SPIE, 4007, 358

[11] Ageorges, N., Hubin, N. 2000, A&AS, 144, 533

Sergio Chueca chueca@ll.iac.es
Jesús J. Fuensalida jjf@ll.iac.es
Marcos Reyes mreyes@ll.iac.es
Angel Alonso aas@ll.iac.es
Casiana Muñoz-Tuñon cmt@ll.iac.es
Toñi Varela avp@ll.iac.es

La componente española de proyectos europeos sobre enseñanza de la Astronomía

El Departamento de Educación del Observatorio Europeo Austral (ESO) interesado en divulgar contenidos de astronomía en los currícula de los diversos países europeos inició un nuevo proyecto que dio en llamar *Catch a Star*. La idea central era sencilla: un grupo de estudiantes de secundaria, coordinados por un profesor, eligen un determinado cuerpo celeste y se dedican a estudiarlo desde diferentes perspectivas.

La primera edición del concurso *Catch a Star* que en versión española se ha traducido por "Adopta una Estrella" ha propiciado ya la generación de un conjunto de materiales de interés que pueden consultarse en la web de ESO. Por supuesto, tales materiales han servido fundamentalmente para el aprendizaje de los estudiantes inmediatamente implicados, pero la vinculación del profesor ha sido fundamental en todos los casos.

Adopta una Estrella

Este concurso fue en nuestro país la versión nacional de *Catch a Star* y se integró dentro del programa "Física en Acción" organizado por la Real Sociedad Española de Física en cooperación con el Instituto de Astrofísica de Canarias. El primer premio consistió en un viaje del profesor coordinador del equipo a Canarias para visitar las instalaciones del IAC, así como un lote de materiales editados por el IAC para los estudiantes. El ganador del concurso en España fue el equipo del IES de Sestao con el trabajo titulado "Mercurio".

En estos momentos se está preparando la segunda edición del concurso para el presente año. Así que, ¡todos a punto!. Si queréis viajar a Canarias o a diversos países europeos conviene participar en "Adopta una Estrella - Catch a Star 2". Las bases del concurso son similares a las del año anterior. Fases que hay que desarrollar:

1. Seleccionar una estrella u otro cuerpo celeste. Estudiar sus principales características.
2. Conseguir fotografías (por medios propios o a través de la red).
3. Comparar con otra estrella u objeto, con la que marcar analogías y/o diferencias.
4. Realizar actividades prácticas (desplegar algún tipo de observación, redactar posibles ejercicios, diseñar algún experimento, etc.)

Os invitamos a participar en el concurso nacional "Adopta una estrella 2" organizado de nuevo este año dentro del programa "Física en Acción" de la Real Sociedad Española de Física junto con la Real Sociedad Matemática Española en colaboración con el Instituto de Astrofísica de Canarias. Todos los interesados podéis enviar vuestros trabajos a la RSEF y optar así al premio nacional. Más detalles del concurso nacional se hallan en `http://www.ific.uv/fisicaenaccion`

Catch a Star

Si además se desea participar en el concurso internacional, basta traducir el trabajo presentado a "Adopta una Estrella" al inglés y optar a los premios de varios viajes fuera del territorio nacional.

El objetivo del programa *Catch a Star* es impulsar a los estudiantes hacia el mundo de la Astronomía. El grupo de alumnos de secundaria, bajo la tutela de su profesor, elige un objeto celeste y tal como actúa un detective logra saber el máximo sobre él. Este estudio se puede plantear como un trabajo interdisciplinar Al final del proceso se pretende que el objeto sea un "amigo" más o una mascota para el grupo.

Para presentarse al concurso internacional *Catch a Star*, hay que inscribirse en la web de ESO

`http://www.eso.org/outreach/eduoff/catchastar/`

En la primera edición el premio principal consistía en un viaje a Chile de todos los miembros del equipo

para visitar los grandes telescopios de ESO en Paranal. El segundo premio era un viaje a Alemania para visitar las instalaciones de ESO en Garching donde se procesan las imágenes obtenidas por sus instrumentos situados en Chile. El tercer premio era un viaje a Austria del equipo para visitar el Observatorio y Planetario de Königsleiten en los Alpes y finalmente el cuarto viaje era a Francia para visitar en Toulouse la "Cité de l'Espace". Además había otros 16 premios consistentes en diversos materiales editados por ESO (CD–Roms, Videos, DVDs, libros y posters).

Debido a las propias características del concurso, abierto a cualquier grupo de alumnos de primaria, secundaria o bachillerato, se estableció que a todos los trabajos que pasasen la selección del jurado se les asignaría un número para una lotería final. De esta forma cualquier trabajo que verificara las reglas del concurso tenía opción a obtener el gran premio del viaje a Chile. Todos tenían las mismas posibilidades.

En la primera edición de *Catch a Star* en total se presentaron 174 trabajos procedentes de 20 países (Alemania, Austria, Bélgica, Bulgaria, Dinamarca, España, Finlandia, Francia, Holanda, Hungría, Italia, Letonia, Lituania, Luxemburgo, Polonia, Portugal, Reino Unido, Rusia, Suecia y Suiza) para competir por diversos premios.

El jurado del premio formado por miembros de ESO y de la EAAE (European Association for Astronomy Education) seleccionó 134 de los 174 trabajos presentados. Todos los trabajos españoles pasaron esta prueba previa y a todos ellos se les asignó un número de lotería que se podía consultar en la página web de *Catch a Star*, pero ninguno de ellos consiguió uno de los importantes premios que se ofrecían. La suerte es la suerte. Todos los equipos que consiguieron un número de lotería recibieron un conjunto de cuatro camisetas especiales del evento que ESO les remitió a sus respectivos centros de enseñanza. Realmente todos los seleccionados son los reales ganadores del concurso por haber superado el juicio del jurado. Los 134 trabajos seleccionados están en la web de ESO. Sin duda estos materiales serán muy útiles a profesores y alumnos de Astronomía de todos los países. Están clasificados por objetos y presentan, de acuerdo con el esquema del concurso, una introducción del objeto, una colección de imágenes del mismo, una comparación con otro objeto similar o diferente, y una actividad práctica de laboratorio o algún ejercicio que pueda ser interesante para llevar a cabo.

Los trabajos españoles presentados que pasaron a la fase final y consiguieron un número de lotería para el sorteo, fueron seis: Plutón del IES de Sestao, Marte del IES Juan de Garay, Mercurio del IES de Sestao, Tuban de la Fundación Masaveu de Madrid, La Luna de la Tierra del IES La Roca de La Roca del Valles, Barcelona y Saturno del IES Pérez Galdós de Madrid.

La final, que se retransmitió en directo en webcast, –se puede ver la lista de galardonados en la web de ESO– . Cabe mencionar que el primer premio fue para el equipo de la escuela SOU "P.K.R. Javorov" de Bulgaria que concursaba con la Constelación de Cassiopeia. El segundo lugar fue para el equipo de Bulgaria correspondiente al Observatorio Galileo Galilei que presentó un trabajo relativo a la Constelación Ursa Major. El tercer premio fue para el grupo del Liceo Scientifico *A.Genoino* de Italia que concursaba con un trabajo titulado Cometa Hale-Bopp y el cuarto premio fue para el equipo alemán del Kopernikus-Gymnasium que concursó con un trabajo sobre el Cúmulo abierto NGC 1960.

Además se introdujo un premio sorpresa al final para la escuela que presentó más trabajos. Este correspondió al HTBLuVA Wr. Neustadt de Austria, que presentó seis trabajos, todos ellos bajo la tutoría del mismo profesor. Esta escuela va a recibir la visita personal del Dr. Richard West, bien conocido por sus trabajos y por ser el descubridor del cometa que lleva su nombre. El Dr. West actualmente es el Director de la Oficina de Educación de ESO, responsable máximo del proyecto *Catch a Star*.

Ejercicios de Astronomía de ESA/ESO

La Agencia Espacial Europea ESA y el Observatorio Europeo Austral ESO han producido un conjunto de ejercicios para su uso en secundaria de gran interés para todos los miembros de ApEA (Asociación para la Enseñanza de la Astronomía). El objetivo principal de estos consiste en transmitir a los estudiantes la satisfacción y excitación que comportan diversos descubrimientos actuales. Cual científicos, los estudiantes podrán deducir diversos parámetros acerca del universo usando las magnificas fotografías obtenidas por ESA y ESO gracias a sus proyectos.

Hasta ahora han sido publicados cuatro ejercicios acompañados de una "Introducción General" que contiene la información del telescopio espacial Hubble y del telescopio VLT de ESO así como de un librito de "Herramientas" que incluye información básica que los estudiantes van a necesitar sobre contenidos de Astronomía y Matemáticas. Así pues, en total se han publicada seis pequeños libros que se pueden usar de forma independiente e individual.

Los cuatro ejercicios publicados hasta ahora se centran en el tema de la medida de distancias en el Universo utilizando diversos recursos. Los títulos son:

Ejercicio 1 Medida de la distancia a la Supernova 1987 A,

Ejercicio 2 La distancia a M100 determinada por las estrellas Variables Cefeidas,

Ejercicio 3 Medida de la distancia a la Nebulosa Ojo de Gato y

Ejercicio 4 Medida de la distancia y la edad de un cúmulo globular de estrellas.

En la actualidad ambas instituciones están trabajando en la elaboración de dos nuevos ejercicios que seguro serán también de sumo interés.

Además de disponer todas las publicaciones de gran numero de maravillosas fotografías y disfrutar de una cuidada edición hay que destacar de forma especial el particular interés mostrado por ESA y ESO en ofrecer unos materiales con cuestiones planteadas para los alumnos y las respuestas suficientemente desarrolladas para que sirvan de material de ayuda al profesor.

Tanto la "Introducción General", las "Herramientas" y los cuatro ejercicios mencionados han sido traducidos al español y pueden conseguirse en la dirección `http://www.astroex.org/spanish/`

Rosa M. Ros `ros@mat.upc.es`

El tránsito de Mercurio y la divulgación de la Astronomía

Introducción

Quizá la principal diferencia entre la Astronomía y otras ramas de la Física sea la facilidad con que ciertos fenómenos astronómicos despiertan el interés del público en general. Eclipses de Sol y de Luna, pasos de cometas, lluvias de estrellas fugaces o conjunciones múltiples de planetas suelen obtener cierto eco en los medios de comunicación y entre los ciudadanos de a pie. Son fenómenos que cumplen las condiciones de ser fáciles de observar, no demasiado frecuentes (a lo sumo una vez al año en el caso de las lluvias de estrellas fugaces) y relativamente espectaculares.

De las tres condiciones citadas, el tránsito de Mercurio por delante del Sol del pasado 7 de mayo, tan solo cumplía la de excepcionalidad (el último visible desde España lo fue en noviembre de 1973). Pero ni se trataba de un acontecimiento fácil de observar, pues era imposible de ver sin la ayuda de algún instrumento óptico, ni era en absoluto espectacular, ya que en realidad se trataba de despertar el interés de la gente por un minúsculo punto negro desplazándose sobre el disco solar.

Sin embargo, el tránsito de Mercurio tenía un interés especial: era el preámbulo perfecto al esperado tránsito de Venus de junio de 2004. Cualquier iniciativa a llevar a cabo para el tránsito de Venus (un fenómeno que no se ha repetido desde el año 1882 y que como veremos más abajo está aglutinando gran número de proyectos educativos a nivel internacional) debía ser probada ahora. Bajo esta premisa, los departamentos de Astrofísica y CC. de la Atmósfera de la Universidad Complutense de Madrid (UCM) y el Departament d'Astronomia i Meteorologia de la Universitat de Barcelona (UB) prepararon sendos proyectos de divulgación con motivo de dicho tránsito[1].

El papel de internet

Cuesta trabajo imaginar hoy en día alguna iniciativa de divulgación en que internet no tenga un papel preponderante. Es por ello que tanto el proyecto de la UCM como el de la UB se construyeron en torno a la posibilidad de ofrecer a través de internet imágenes del tránsito en tiempo casi real. Nuestro objetivo era tomar imágenes con telescopios situados en las respectivas facultades y ofrecerlas a través de sendas páginas web[2] donde se incluia información complementaria sobre el tránsito.

[1] Estas no fueron las únicas iniciativas tomadas en nuestro país: diversos observatorios permitieron el acceso para seguir el tránsito en directo y varias asociaciones de aficionados a la Astronomía facilitaron la observación al público. También se habilitaron diferentes páginas web con información e imágenes del tránsito.

Fig. 1.: Estudiantes de la Facultad de CC. Físicas de la UCM esperando un claro.

Fig. 2.: Aspecto de la azotea de la Facultad de Física de la UB durante el tránsito.

En el caso de la UCM se utilizó una cámara digital Nikon Coolpix 995 con el Celestron 11"Schmidt-Cassegrain de la cúpula W del observatorio UCM situado en la terraza de la facultad de CC. Físicas para obtener imágenes de la fotosfera. En la misma montura se instaló un telescopio refractor con filtro Hα para tomar imágenes de la cromosfera. El detector era un ocular electrónico de Meade que proporciona señal video que se iba grabando y digitalizando simultáneamente. Estaba previsto colocar ambas imágenes en la red según se fueran tomando y ofrecer instantáneas del ambiente en las terrazas. En ellas se prepararon varios telescopios para el público en general. Para llevar el espectáculo a más personas, los estudiantes aficionados colocaron telescopios en la entrada de la facultad y explicaron sobre la marcha las imágenes que ofrecían las páginas web con ayuda de un cañón de video acoplado a un ordenador en el vestíbulo de la facultad.

Por su parte la UB dispuso una cámara CCD Ce-

[2] `http://mercuri.am.ub.es/mercurio.html`
`http://www.ucm.es/info/Astrof/obs_ucm/tran_mer_03/transito_mercurio_mayo03.html`

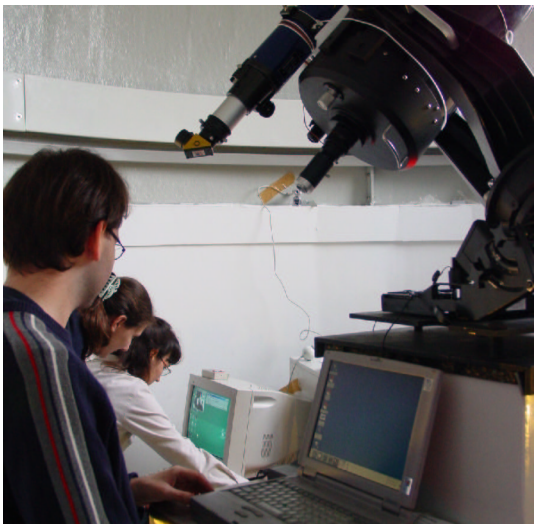

Fig. 3.: Interior de la cúpula W de la Facultad de CC. Físicas de la UCM durante el tránsito.

lestron Pixcel 237 acoplada a un pequeño telescopio reflector de 10 cm con la que tomar una imagen cada 5 minutos (en total unas 70 imagenes en las 5 horas y 20 minutos que duraba el tránsito). El día del tránsito se instaló un cañon de proyección en el aulario de la facultad desde donde los alumnos podían seguir el tránsito a través de la página web. También se dispusieron diversos telescopios portátiles en la azotea de la facultad para aquellos que quisieran realizar una observación directa. Una webcam retransmitía imágenes del ambiente de la azotea.

7 de mayo de 2003

El tránsito del 7 de mayo se iniciaba a las 7:11 hora oficial, con el Sol a tan solo 4 grados de altura en Barcelona y antes de que saliese en Madrid. Con una importante borrasca situada sobre la mitad Este de la península, el día amaneció con la mayor parte del cielo cubierto en ambas ciudades.

En Madrid el aspecto del cielo a primera hora del día era desalentador: seguía lloviendo como toda la noche anterior. Sólo se pudo ver el Sol durante un corto espacio de tiempo a media mañana. Para desesperación de los aficionados, las prácticas de observación solar se pudieron realizar por la tarde cuando ya Mercurio había terminado su tránsito. Mientras, en Barcelona la nubosidad fue variando a lo largo de la mañana y, finalmente, los pocos intervalos de cielo despejado permitieron obtener 10 imágenes del tránsito.

Los problemas con el tiempo pudieron ser en parte subsanados gracias a que muchas instituciones y particulares en diversas partes del mundo (La Palma, Bélgica, India, Australia,...) ofrecian imágenes en directo. Sus páginas fueron enlazadas desde las nuestras

Fig. 4.: Imagen del tránsito tomada desde la Facultad de Física de la UB.

para poder ofrecer imágenes durante los largos intervalos en que las nubes nos impedían cualquier tipo de observación. De esta forma se consiguió que la gente conectada a nuestras páginas no se quedase sin ver imágenes del tránsito.

Pese al relativo fracaso ocasionado por el mal tiempo, la experiencia fue altamente positiva: las páginas web recibieron más de 20000 visitas a lo largo del día (entre ellas las de numerosos institutos de enseñanza secundaria que habían sido previamente avisados del fenómeno) y muchos alumnos, profesores y personal administrativo siguieron el tránsito a través de las imágenes proyectadas en un momento u otro. Muchas personas interesadas se acercaron para mirar directamente a través de los telescopios habilitados al efecto. Cabe destacar también el seguimiento por parte de diversos medios de comunicación.

El tránsito de Venus de 2004

El tránsito de Venus del 8 de junio de 2004 es un acontecimiento único. No tan solo por su rareza (el último fue en 1882 y el próximo visible desde España lo será en el siglo XXII –el tránsito del 2012 no es visible desde nuestro país–, sino porque en un tránsito de Venus confluyen la Astronomía y la Historia. Al interés del tránsito en sí, se une el interés por las épicas expediciones de los siglos XVIII y XIX que, con el propósito de medir la paralaje solar, constituyeron los primeros proyectos científicos internacionales de la historia. A modo de ejemplo y por sernos más próxima, podemos citar la expedición hispano-francesa que se desplazó hasta la península de California (por entonces la región más occidental de Nueva España) para observar el tránsito de Venus de 1769.

Es por tanto una gran oportunidad de hacer llegar la Astronomía y parte de su historia al público en general,

y muy especialmente a los estudiantes de ESO y bachillerato. Son ya varios los proyectos educativos internacionales que se han puesto en marcha[3]. Básicamente se trata de proyectos dirigidos a los estudiantes, que obtendrán un valor para la Unidad Astronómica a partir de los instantes de contacto de Venus con el disco solar, al igual que los astrónomos profesionales de la época hicieron en los tránsitos pasados.

Estos proyectos tienen además el aliciente de precisar de la colaboración entre centros de paises repartidos por todo el mundo. De nada sirven las medidas que pueda obtener un solo centro, o incluso diferentes centros de un solo país, si no son comparadas con las observaciones realizadas en otros lugares (cuanto más distantes, mejor) de la Tierra.

A modo de conclusión

Con el tránsito del 7 de mayo se puso de manifiesto, como ya sabíamos, el gran interés que existe en la calle y en los centros de enseñanza por la Astronomía, así como la facilidad con que los medios de comunicación son convocados ante acontecimientos como éste.

Las experiencias de divulgación organizadas por la UCM y la UB con el tránsito de Mercurio demostraron que con unos medios no demasiado sofisticados es posible desarrollar proyectos de este tipo. Un equipamiento tan sencillo como una cámara web apuntando a una pantalla donde se proyecte la imágen del Sol capturada a través de un pequeño telescopio podría ser suficiente (y de hecho lo fue en el caso de una página francesa) para transmitir el tránsito a través de Internet.

El próximo año tenemos una nueva oportunidad. La experiencia llevada a cabo con el tránsito de Mercurio será repetida, a ser posible a mayor escala y con una colaboración más estrecha entre los centros implicados, para el tránsito de Venus del 8 de junio de 2004. Desde aquí os animamos a participar.

Por otro lado, posiblemente serán muchos los centros de enseñanza de nuestro país que puedan estar interesados en participar en los proyectos educativos que se están poniendo en marcha con motivo del tránsito de Venus del próximo año. Creemos que la Sociedad Española de Astronomía no debería dejar escapar esta gran ocasión de llegar a los que son potencialmente los futuros astrónomos de nuestro país, divulgando y coordinando en la medida de lo posible la participación de los centros en dichos proyectos.

[3] Véase por ejemplo
`http://didaktik.physik.uni-essen.de/~backhaus/VenusProject.htm`
`http://www.eso.org/outreach/eduoff/vt-2004/index.html`

Agradecimientos

Las diferentes actividades que la UB llevó a cabo el día 7 de mayo fueron posibles gracias a la colaboración y el esfuerzo de más de 20 personas, miembros del Departament d'Astronomia i Meteorologia, en especial de David Fernández-Barba, Ignasi Ribas y Salvador Ribas. La organización, preparación y desarrollo de esta experiencia en la UCM implicó a profesores y doctorandos del Departamento de Astrofísica y CC. de la Atmósfera y en particular a David Montes y Jesús Gallego. Deseamos destacar la magnífica colaboración de los miembros de la Asociación de Astrónomos Aficionados de la UCM (ASAAF).

Eduard Masana `emasana@am.ub.es`
Jaime Zamorano `jaz@astrax.fis.ucm.es`

Highlights from XMM-Newton

Xavier Barcons[1] barcons@ifca.unican.es

Ignacio Negueruela[2] ignacio@dfists.ua.es

[1]Instituto de Física de Cantabria (CSIC-UC), Facultad de Ciencias, Avda. Los Castros s/n, 39005 Santander
[2]Departamento de Física, Ingeniería de Sistemas y Teoría de la Señal, Universidad de Alicante, Carretera San Vicente del Raspeig s/n, Escuela Politécnica Superior Apartado 99, 03080 Alicante

Abstract

The launch of the Chandra (NASA) and XMM-Newton (ESA) X-ray observatories in 1999 has revolutionized our view of the Universe, by providing astrophysical information about many classes of sources with unprecedent detail. The high throughput of XMM-Newton makes it the ideal instrument to provide low to moderate resolution spectroscopy of faint and extended sources. After 3 years of operations, XMM-Newton has observed all types of astronomical sources and delivered very interesting results in many areas. In this review, we highlight a few points where the contribution of XMM-Newton has significantly furthered our knowledge of the energetic Universe.

Resumen

El lanzamiento de los observatorios de rayos X *Chandra* (NASA) y *XMM-Newton* (ESA) en 1999 ha revolucionado nuestra visión del Universo, al proporcionar información astrofísica detallada sobre muchos tipos de fuentes. La alta eficiencia de *XMM-Newton* lo convierte en el instrumento ideal para obtener espectroscopía de resolución baja y moderada de fuentes débiles y extensas. Después de 3 años de operaciones, *XMM-Newton* ha observado todo tipo de fuentes astronómicas y ha proporcionado resultados de la mayor importancia en muchas áreas. En esta revisión, destacamos unos pocos aspectos donde la contribución de *XMM-Newton* ha incrementado de forma significativa nuestro conocimiento del Universo energético.

Introduction

X-ray Astronomy is at the very heart of the enormous progress that our astrophysical knowledge of the Universe has undergone over the last decades. X-rays are emitted in a wide range of physical situations in the Universe, invariably linked to the presence of hot gas and strong gravitational fields. These phenomena, largely unsuspected in the early days of X-ray astronomy, are nowadays seen to be ubiquitous in a variety of astronomical objects. X-ray observations of previously known objects have often revealed phenomena (e.g., the presence of an accreting black hole) just not seen at other wavelengths. In addition, new sources serendipitously discovered in X-ray surveys have uncovered new classes of objects, totally inconspicuous at optical wavelengths. One datum that illustrates the impact of X-ray observations in Astronomy is that 20% of the papers published by the 3 main Astrophysics journals in 2002 (Astrophysical Journal, Monthly Notices of the Royal Astronomical Society and Astronomy & Astrophysics) contain the "X-ray" keyword in the abstract. The 2002 Nobel Prize in Physics given to Riccardo Giacconi (father and leader of X-ray Astronomy), is also a sign of the good health reached by this discipline, as it is one of the very few granted to astronomers.

Some history

X-ray Astronomy began in 1962, when a rocket flown to detect the Moon in scattered X-rays from the Sun, discovered instead the first extra-solar X-ray source (Sco X-1) and the cosmic X-ray background (Giacconi et al. 1962). This already showed that the Universe out there could be radically more energetic than what was known before, as Sco X-1 had a much larger X-ray to optical flux ratio than the Sun. More rockets followed this pioneering discovery, but there was a basic limitation in the amount of observing time available for observations in a single flight.

UHURU (which means *freedom* in swahili) was the first orbiting X-ray observatory. It was launched from Italy's San Marco station in Kenya on the 12th of December of 1970, coinciding with the independence day of this country (thence the name). The *UHURU* payload weighed less than 60 kg. It scanned the sky for over 2 years and produced the first all-sky catalogue of X-ray sources, containing a few hundred of them. Subsequent work demonstrated that outside the galactic plane, most of the sources were Active Galactic Nuclei (AGN) and clusters of galaxies. In the Galactic plane, *UHURU* found X-ray binaries, supernova remnants and other diffuse structures. This rough picture (but with varying fractions of objects) still describes to zero-th order the present knowledge of the X-ray Universe.

This early generation of X-ray orbiting observatories (which also included *HEAO-1* and more recently *Ginga*, Japanese word for Milky Way) were equipped with a mechanical collimator as the only means to limit the field of view covered by the (usually gas-filled proportional counter) detectors, without any further optics. This provided a very rough angular resolution, of the order of several degrees, which ultimately limited the sensitivity of the observatory because of confusion of fainter sources.

Proper imaging X-ray optics was first featured for

soft X-rays (below 4.5 keV) with the *Einstein Observatory*. With an angular resolution of a couple of arc minutes, *Einstein* discovered many new X-ray sources (including many at cosmological distances), showing that the word *experiment* was in the way of being replaced by *observatory* in X-ray missions. *Einstein* made it possible to discover new classes of sources by their X-ray emission, resolved the spatial structure of the intracluster gas in galaxy clusters and produced large catalogues of X-ray sources that were subsequently used to conduct detailed astrophysical studies. It also showed, for the first time, that a significant fraction of stars are X-ray emitters. *ROSAT*, in some sense a successor to *Einstein*, deepened our knowledge of the X-ray Universe, by conducting first an all-sky survey (this yielded the, so far, largest catalogue of X-ray sources, exceeding 50000), and for almost a decade, targeted observations of a full range of astronomical objects, from comets to distant QSOs.

Focusing X-ray photons is not an easy task. In a standard reflecting optical telescope, photons are directed almost normally to the reflector's surface and collected in the focal plane. If the same setup is used for X-rays, they end up either transmitted or absorbed, but never reflected. Grazing incidence is needed to achieve total reflection for X-rays, the maximum angle with respect to the surface being of a few degrees for a photon of ~ 1 keV. Reflection becomes more difficult at higher photon energies, as the angle for total reflection becomes smaller and the mirrors need to be placed almost parallel to the optical axis. It is easy to see that the effective area that a photon sees is very small with a mirror placed in grazing incidence, and therefore several (or many) mirrors are nested one inside each other to increase the collecting area. It is also clear that an X-ray focusing telescope of higher energy photons will have less effective area and longer focal length than a similar one focusing soft X-ray photons.

The start of the nineties brought X-ray observatories able to produce images with photons of up to 10 keV, such as the Japanese *ASCA*. *ASCA* also opened the door to a more modern type of X-ray detector (the *Charge Coupled Device* or CCD) that ended up burying the proportional counters. CCD-based detectors deliver an order of magnitude better spectral resolution for single photons than proportional counters. At the energy of the Fe Kα line (6.4-6.7 keV), the resolution of ~ 50 achieved by these detectors enables a detailed study of the physical environment where it is produced.

Other X-ray observatories have been launched during the 1990's, including *BeppoSAX* (which also featured higher energy detectors sensitive to many tens of keV) and *Rossi X-ray Timing Explorer* (RXTE) which is tailored to timing analysis of bright sources. However, at the turn of the new millenium, both *NASA* and *ESA* decided to launch their respective large X-ray observatories: *Chandra* (launched July 1999) and *XMM-Newton* (launched December 1999). The coincidence of operations between both missions (being just by chance, as *Chandra* was over-delayed for several years) has brought what can be called the *golden age* of X-ray Astronomy. By virtue of their respective designs *Chandra* is mostly an imaging observatory, while *XMM-Newton* has its major capabilities at spectroscopy. Having both of them operating at the same time has opened a huge window to X-ray astrophysics, whose dimensions are just beginning to be realized after the first few years of operations.

XMM-Newton

XMM-Newton is an X-ray observatory launched and operated by the European Space Agency (ESA), with instruments contributed and funded by ESA member states and NASA (USA). *XMM-Newton* was successfully launched by an Ariane 5 on the 10th of December of 1999. Its orbit is highly eccentric with a period of $\sim$ 2 days. Although the original *XMM-Newton* project was approved for 2 years of scientific operations, all systems and payloads are designed to last for ~ 10 years. Specifically, fuel (hydrazine) is currently thought to last for more than that. In fact, an extension of the *XMM-Newton* operations has already been approved to 2006 with a further 2 year period being revised by mid 2003. For comparison with early missions, the full *XMM-Newton* satellite weighs more than 3000 kg. Currently, the *XMM-Newton* spacecraft is operated by ESOC at Darmstadt (Germany), but the instruments and science operations in general are managed from VILSPA (Villafranca del Castillo, Spain).

XMM-Newton consists of 3 co-aligned grazing incidence X-ray telescopes (Jansen et al. 2001), with angular resolution of 4-6 arcsec (FWHM) and 13-15 arcsec (Half Energy Width). Each X-ray telescope nests 58 grazing incidence mirror pairs, with a total collecting area of $\sim 4000\,\mathrm{cm}^{-2}$ (see Fig. 1 for a schematic of the X-ray optics in the *XMM-Newton* X-ray telescopes). One of these telescopes focuses all X-rays into a single spectroscopic imaging detector (EPIC-pn, Strüder et al. 2001), which has a pixel size of 4 arcsec and covers a field of view of about 30 arcmin in diameter. About half of the X-rays focused by the other two telescopes go undispersed to similar imaging spectrographs called EPIC-MOS (Turner et al. 2001) . The EPIC instruments can measure the energy of individual photons with a resolution of $\sim 20-50$. EPIC is sensitive to photons from 0.2 to 12 keV and can detect X-ray sources as faint as $\sim 10^{-15}\,\mathrm{erg\,cm^{-2}\,s^{-1}}$ in the 0.5-2 keV band in a few tens of kiloseconds (ks). Its main limiting sensitivity in soft X-rays is caused by confusion, due to the modest angular resolution of the X-ray telescopes. At higher photon energies the main limiting factor is photon counting, with an expected confusion limit in the 2-10 keV band reached in a several Ms exposure only.

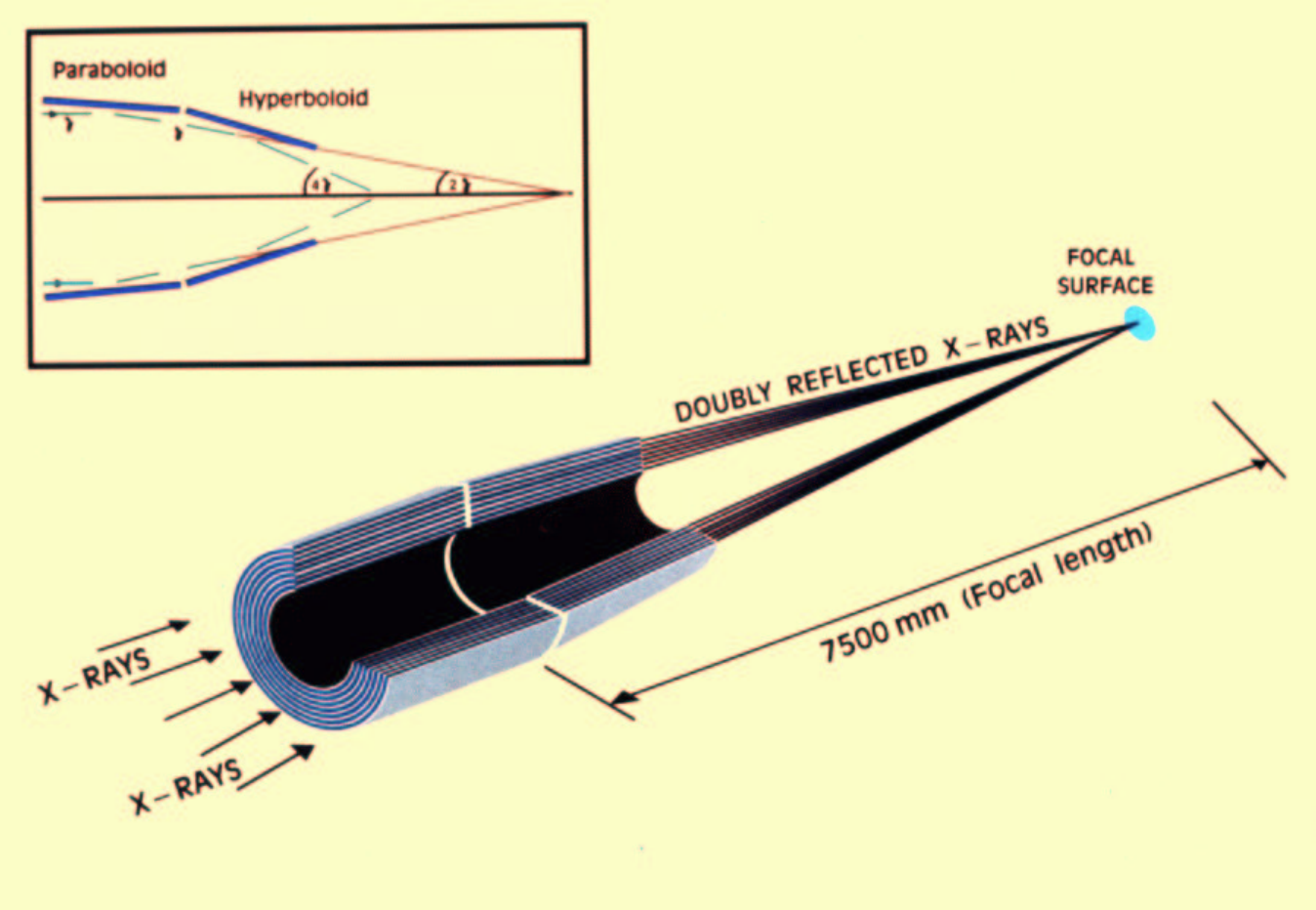

Fig. 1.: Scheme of the grazing incidence optics on the *XMM-Newton* X-ray telescopes (from ESA)

The two X-ray telescopes that focus the X-rays into the EPIC-MOS detectors are equipped with difraction gratings working by reflection. These disperse the remaining X-rays according to their wavelength and these are recorded in a further chain of CCD detectors. This wavelength-dispersive instrument is called the Reflection Grating Spectrometer (RGS) and delivers a spectral resolution ~ 200 in first order dispersion (i.e., ~ 0.06 Å) in the soft X-ray domain (5-35 Å, or 0.3-2.4 keV). The sensitivity of the RGS can be viewed in terms of a source with 0.5-2 keV flux of $\sim 10^{-11}$ erg cm^{-2} s^{-1} producing peak S/N$\sim$ 10 per spectral resolution element in 100 ks. It is therefore an instrument designed to observe bright sources with relatively high spectral resolution. The moderate angular resolution of the *XMM-Newton* mirrors makes it possible to obtain integrated moderate resolution of *extended* sources, a capability that is producing extremely interesting results (see later).

Besides that, *XMM-Newton* has a co-aligned optical/UV telescope (the Optical Monitor - OM) which operates in the range from 1600 to 6600 Å. At its focal plane the OM has a photon counting device (Mason et al. 2001), which delivers time-resolved information for the detected photons. The field of view of the OM is 17 arcmin, with a point-spread-function of FWHM between 1.3 and 2.5 arcsec, with a limiting sensitivity of 23.5 magnitudes for 1000 sec integration. The OM is equipped with a number of UV and optical filters, plus low resolution UV and optical grisms, whose calibration is being conducted at the time of writing this report. All three *XMM-Newton* instruments (EPIC, RGS and OM) are simultaneously operated.

The ground segment operations of *XMM-Newton* are conducted by the SOC at Villafranca del Castillo (Spain) with the assistance of an ESA member-state funded consortium called *Survey Science Centre* (SSC). The SSC tasks include the development of Science Analysis Software tasks in collaboration with the SOC; the pipeline processing of all *XMM-Newton* data and the identification of the *serendipitous* sources discovered by *XMM-Newton*. This last task is specially demanding, as it is likely that *XMM-Newton* will find about 50000 new X-ray sources per year. Identifying and cataloguing these data will constitute a major legacy of *XMM-Newton* (see Watson et al. 2001).

ESA has already released the first version of the *XMM-Newton* catalogue provided by the SSC, which contains over 30000 good-quality X-ray sources. Some of these sources are identified thanks to the extensive

archival search conducted by the SSC. At the time of writing this report the SSC has imaged in various optical filters a large fraction of fields that contain the catalogued sources. Besides that, well over 500 of these X-ray sources have been spectroscopically identified. All this optical imaging and spectroscopic information will be included in future versions of the *XMM-Newton* catalogue, delivering an extremely powerful tool to investigate the X-ray sky.

Normal stars

One of the areas where the impact of *XMM-Newton* has been strongest is the study of X-ray emission from "normal" stars. The possibility that stars without compact companions could be X-ray emitters had not been initially foreseen. Though some normal stars had been detected by previous experiments (e.g., Topka et al. 1978), only after the observations by *Einstein* was it fully realised that many solar-type stars emitted soft X-rays (Vaiana et al. 1981). Equally surprising was the discovery that hot OB stars also appeared to be substantial soft X-ray sources.

The X-ray emission from low-mass stars was quickly interpreted in terms of coronal activity, similar to that observed in the Sun, but on a much larger scale. Many M-type stars were found to display relatively strong X-ray emission, which correlated with other indicators of activity, such as emission in Hα or the Ca II doublet (Noyes et al. 1984; Vilhu 1984, Fleming et al. 1989).

It was also found that there was a strong correlation between age and X-ray activity. In this sense, the all-sky survey by *ROSAT* greatly changed the previous view on the evolution of low-mass stars towards the main sequence. It was seen that many stars not displaying the typical characteristics of T Tauri stars could be identified as very young objects because of their X-ray emission (e.g., Neuhäuser 1997). This led to the discovery of whole new associations of young stars. As previous missions lacked spectral resolution in the soft X-ray range, *XMM-Newton* and *Chandra* offer the possibility of obtaining, for the first time, information about the physical causes of this emission.

Coronal activity

Coronal activity in chromospherically active low-mass stars is thought to result in X-ray emission through mechanisms similar to those observed in the Sun. Observations with *XMM-Newton* provide spectra showing lines from a large variety of elements (O, Ne, Mg, Fe, N, etc), many of them in at least two different ionisation states. ¿From them, coronal abundances, which are in many cases very different from the stellar atmospheric abundances, are derived. In the Sun, elements with low first ionisation potential are overabundant with respect to their photospheric abundances, while elements with high first ionisation potential are not. In a survey of RS CVn binaries (tidally locked binaries containing a highly active slightly evolved G-K star), Audard et al. (2003) find that the most active stars display a behaviour opposite to that seen in the Sun, suggesting that fractionation mechanisms should be revised. They indicate that this opposite effect is seen in all stars with high coronal activity, while stars with lower activity seem to present an effect similar to the Sun.

Simultaneous observations of σ Gem, an RS CVn binary with a K1III primary, with *XMM-Newton* and the VLA have allowed the discovery of a correlation between the radio luminosity of a large flare and the time derivative of the X-ray luminosity (Güdel et al. 2002). This relationship is observed in solar flares, where it is known as the Neupert effect, and supports flare mechanisms causing chromospheric evaporation.

The presence of X-ray emission from young (pre-main-sequence) stars is now recognised as a widespread phenomenon (Feigelson & Montmerle 1999). It is assumed to be a consequence of the same magneto-centrifugal processes that drive the outflows and winds associated with classical T Tauri stars (e.g., Shu et al. 1994). Large-scale surveys with *XMM-Newton* will allow an understanding of these phenomena. As a first example, Favata et al. (2003) have observed the L1551 star forming complex. They find that the characteristics (both temporal evolution and spectrum) of classical T Tauri stars and weak-lined T Tauri stars are very different, suggesting that while weak-lined T Tauri stars show an enhanced version of the coronal activity seen at older ages, classical T Tauri stars have a different X-ray emission mechanism, related to their accretion disks.

Massive stars

Although emission from low mass stars can be understood in terms of coronal activity, the existence of relatively soft X-ray emission from massive stars came as a bit of a surprise (Harnden et al. 1979). Models trying to explain it invoke hydrodynamic shocks resulting from intrinsic instabilities in their radiatively driven winds (see Feldmeier et al. 1997). *XMM-Newton* RGS spectra have allowed the exploration of physical conditions in the regions where the emission is produced. Observations of the O4Ief star ζ Puppis have provided confirmation that the X-ray emission consists mostly of broad emission lines from H-like and He-like charge states of N, O, Mg and Si, as well as Ne-like ions of Fe (Kahn et al. 2001). In this object with a very strong radiative wind, X-ray emission reaching us seems to be produced at large distances from the star.

Conversely, the X-ray spectrum of the B0.2V MK standard τ Scorpii is not very consistent with standard models. Emission lines in its *XMM-Newton* RGS spec-

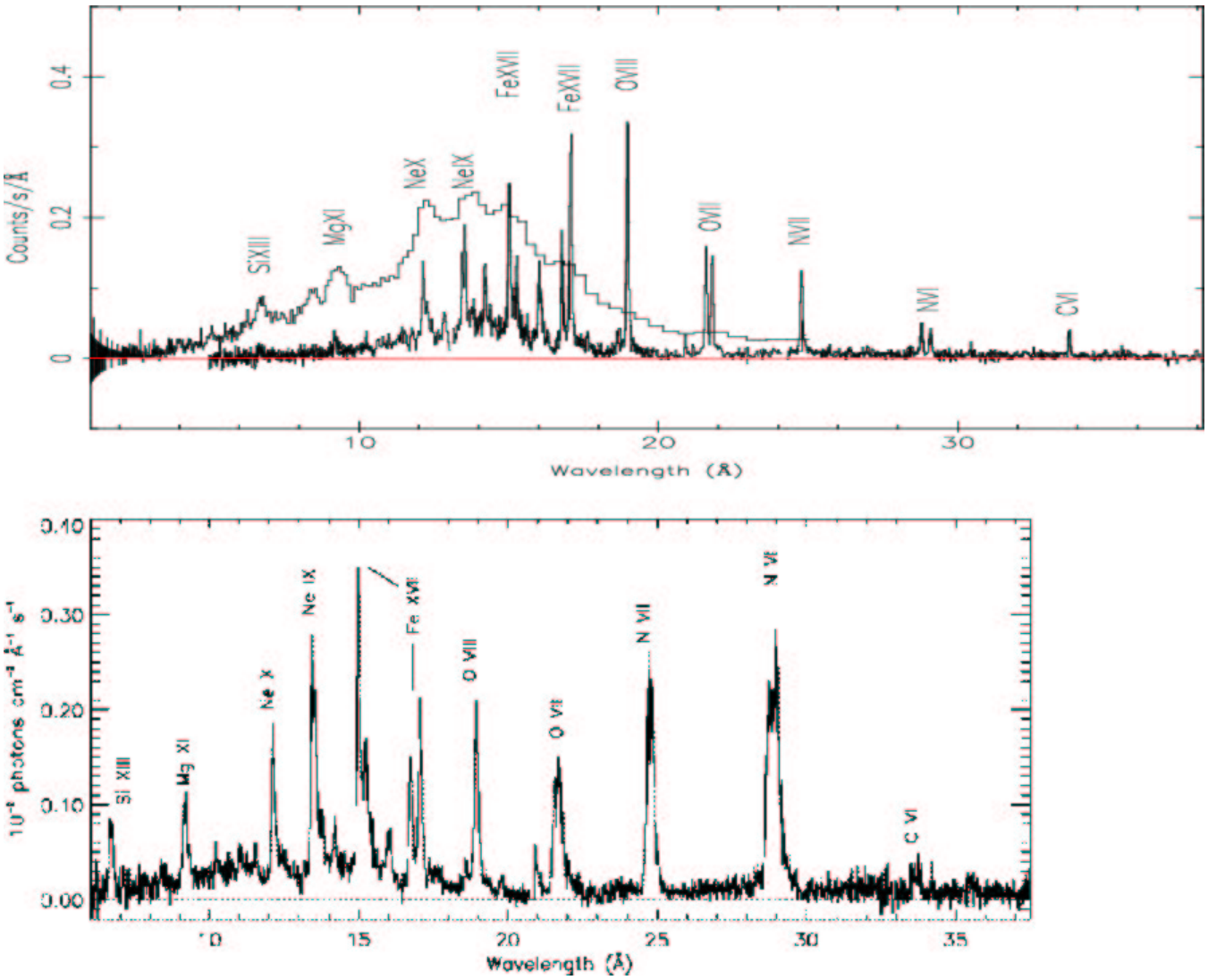

Fig. 2.: Top panel: The RGS spectrum of τ Sco, rebinned by a factor 3, compared to the EPIC MOS spectrum of the same star. The impressive spectral resolution of the RGS stands out. Prominent lines are labelled with the emitting ions (from Mewe et al. 2003). Bottom panel: The RGS spectrum of ζ Pup from Kahn et al. (2001). The lines are clearly much broader than in τ Sco.

trum are as narrow as the instrumental profile, suggesting that they are produced much closer to the star (Mewe et al. 2003). X-ray emission shows a hot component corresponding to a temperature in excess of 20×10^6 K. This is supported by a *Chandra* observation of the same star by Cohen et al. (2003), who suggest that the spectrum of τ Scorpii is intermediate between those of O-type stars and coronal emitters. As there is rather strong evidence against the possibility of a cool companion for τ Scorpii, a model in which dense clumps in the wind stall and decelerate, perhaps falling back onto the stellar surface, such as that presented by Howk et al. (2000), is preferred. The hard X-rays would then originate in bow shocks around those clumps.

In some cases, emission from relatively hot stars seems to be due to late-type companions. Simultaneous observations of Castor with *XMM-Newton* and *Chandra* allow the resolution of its three components, all of which are close binaries. Castor C is a pair of M1V stars, both of which appear to be moderately active (Stelzer et al. 2002). Both Castor A and Castor B contain an A-type star and a low-mass companion, but their emission appears typical of coronal activity in the low mass stars (Stelzer & Burwitz 2003).

Another interesting result obtained with *XMM-Newton* is the lack of X-ray emission from C-rich Wolf-Rayet stars. Oskinova et al. (2003) failed to detect WR 114 with *XMM-Newton*, implying a lower limit on its X-ray luminosity $L_{\rm x}/L_{\rm bol} \leq 4 \times 10^{-9}$. Until now, no single WC star has been detected in X-rays, while several WN star have. An example is WR 110, detected with *XMM-Newton* by Skinner et al. (2002). Surprisingly, the X-ray spectrum of this very hot star also shows a hard component which cannot be explained

with current models.

In some cases, a relatively hard X-ray spectrum is produced when the winds of two massive stars forming a close binary collide. This is the case of HD 93403 (O5.5I + O7V), where clear orbital modulation has been detected with *XMM-Newton* (Rauw et al. 2002).

Accreting binaries

X-ray binaries (XRBs) are systems in which high energy radiation is emitted as a consequence of the accretion of material from a donor star (in most cases, a hydrogen-burning "normal" star) onto the surface of a compact object (see Lewin et al. 1995, for extended reviews). Binary systems in which the accreting compact object is a white dwarf are generally considered as a separate subclass, known as Cataclysmic Variables, though there are no strong physical reasons for this separation.

XRBs emit most of the X-ray flux detected from normal galaxies, including the Milky Way. They have been discovered in large numbers by previous satellites and now a sufficiently large sample exists for population studies to be statistically significant (e.g., Helfand & Moran 2001). *XMM-Newton* offers several potentialities for their study. On the one hand, it opens up the opportunity of obtaining spectra of Galactic sources with moderate resolution and high signal-to-noise ratio. On the other hand, because of its large collecting area and moderately high spatial resolution, it provides an excellent opportunity for studying the populations of nearby galaxies. Last but not least, *XMM-Newton* offers the possibility of obtaining X-ray spectra of faint Galactic sources, opening the door to studies of low-luminosity accreting binaries.

XRBs are generally divided into two main subclasses, high mass (HMXBs) and low mass (LMXBs), depending on the nature of the donor star (either an OB star or G−M spectral type). Additionally, depending on the temporal behaviour, they can be divided in persistent and transient sources. LMXBs containing an accreting neutron star can be either persistent or transient, but systems with black holes are generally transient.

Low mass X-ray binaries

Classical low mass X-ray binaries (LMXBs) consist of a neutron star with a moderately strong magnetic field ($\sim 10^8$ G) accreting from a low-mass star. The light-curves of these objects are rather complex (displaying temporal features such as eclipses and dips). There is a large variety of behaviours among LMXBs, likely due to the complexity of their accretion geometries, which has prevented the creation of a unified model. As a matter of fact, while all LMXBs observed with *ASCA* could be well fit with a two component model, a blackbody representing the accretion disk and an extended Comptonising region (Church & Balucinska-Church 2001), this model failed to fit observations of several LMXBs with *BeppoSAX* (e.g., Oosterbroek et al. 2001).

Many LMXBs also display bursts, very rapid increases in the X-ray flux followed by exponential declines (typically lasting seconds to minutes). The bursts are interpreted as thermonuclear explosions on the stellar surface, after material has accumulated due to accretion (Lewin et al. 1993). During this bursts, X-ray emission from the vicinity of the neutron star dominates that coming from the disk.

XMM-Newton has allowed the study of the accretion environments of low mass X-ray binaries , with the discovery of complex narrow absorption features in their X-ray spectra, corresponding to H-like and He-like ions of O and Fe, and likely other elements (Cottam et al. 2001; Sidoli et al. 2001; Parmar et al. 2002). For example, comparing the number of absorbed photons at the O VII and O VIII edges with the number of photons emitted in the O VIII Lyα and O VII He-like complexes, Cottam et al. (2001) argue that absorbing material must be aligned with the accretion disk and extend along our line-of-sight.

Jimenez-Garate et al. (2002) are able to derive elemental abundance ratios from recombination emission lines seen in the spectrum of the LMXB Her X-1. They derive very high N/O ratios, which they interpret as proof of strong interactions during the formation history of this binary.

Soft X-ray transients

LMXBs containing a black hole (and a few transient sources containing neutron stars) are generally termed Soft X-ray transients (SXTs) or X-ray novae. This is because they display very strong X-ray and optical outbursts (generally also accompanied by radio emission) separated by long periods of quiescence (see Tanaka & Shibazaki 1996). They are "soft" in the sense that their outburst spectra are dominated by a soft blackbody component at $\sim$ 1 keV. The X-ray spectra of SXTs are very variable and characteristic low/hard and high/soft states have been identified. The geometry of the accretion flow and the source of soft photons during the outbursts is currently debated. In order to explain their long quiescent states optically thin advection-dominated accretion flows (ADAFs) have been invoked (Narayan et al. 1996; Esin et al. 1998). Some authors have argued that the very low X-ray fluxes during quiescence could be due simply to coronal activity from the donor.

The large collecting area of *XMM-Newton* allows the observation of very faint sources in quiescence. The SXT GU Mus was observed in quiescence as a very faint source. The X-ray flux was characterised by a

power law, ruling out coronal activity and apparently supporting ADAF models (Sutaria et al. 2002). Similar conclusions were drawn from an observation of the SXT GRO J1655−40 (Hameury et al. 2003). However, observations of the black hole candidate and micro quasar GRS 1758−258 found a very soft spectrum in the off state, against the predictions of simple ADAF models (Miller et al. 2002).

Another source, XTE J1650−500, was observed in the very high state by Miller et al. (2003a). Its spectrum displayed broad Fe Kα lines, whose shape suggests that rotational energy is being extracted from a spinning black hole.

Cataclysmic variables

Cataclysmic variables (CVs) are systems containing a white dwarf accreting from a low-mass hydrogen-burning star (e.g., Sion 1999). As such, CVs may manifest themselves under the guise of classical novae, dwarf novae, recurrent novae, nova-likes and similar objects (Patterson 1984). X-ray emission is generally detected from those CVs in which the white dwarf exhibits a strong magnetic field, the polars or AM Her stars, or a moderate magnetic field, the intermediate polars or DQ Her stars (Patterson 1994). The interest of CVs stems from the fact that they allow a detailed study of accretion processes, with wide applications in several astrophysical contexts.

As the X-ray spectra of CVs are not as hard as those of accreting neutron stars and their luminosities are also not very high, sensitive instruments are needed to detect their emission. *ROSAT* surveys resulted in the discovery of large numbers of new faint CVs and it is expected that *XMM-Newton* will provide spectral information for a large number of sources, making statistical studies possible. Such work is already in progress, with large numbers of CVs having been observed (e.g., Ramsay & Cropper 2002; Ramsay & Cropper 2003), allowing determination of their basic parameters, such as white dwarf mass and mass transfer rate.

Of particular interest is the observation of the recent nova V2487 Oph 1998. This classical nova was detected with signatures of an accreting white dwarf less than three years after its nova outbursts (Hernanz & Sala 2002). This detection suggests that the system was back to its standard configuration after the phenomenal thermonuclear explosion which originated the nova outburst.

Supersoft sources

Discovered originally in the LMC, supersoft X-ray sources (SSSs) display X-ray spectra peaking at energies much lower than traditional X-ray binaries (~ 40 eV). Because of this, they are heavily affected by interstellar absorption and unlikely to be detected in the Milky Way, unless they are very close. They are generally interpreted as white dwarfs accreting from a more massive hydrogen-burning donor. The mass transfer is therefore unstable and proceeds on the thermal timescale (van den Heuvel et al. 1992). Because of their soft spectra, they have only been studied in any detail with *ROSAT*. *XMM-Newton* provides now the opportunity to observe their spectra.

The first RGS spectrum of an SSS, CAL 83 in the LMC, proved that the X-ray emission originated from the photosphere of a very hot white dwarf by showing a rich spectrum of absorption complexes due to several elements (Paerels et al. 2001b). Even though this spectrum is qualitatively similar to expectations from white dwarf atmosphere models, RGS observations of the Galactic SSS MR Vel reveal a wealth of emission lines displaying P-Cygni profiles, indicative of a strong wind from the white dwarf's surface, which cannot be reproduced with current models (Motch et al. 2002). Also interesting is the likely detection of Doppler shifts due to orbital motion in the X-ray emission lines of MR Vel, probably the first detection of orbital motion at high energies (Motch et al. 2002).

In *XMM-Newton* pointings, Osborne et al. (2001) have found a transient SSS close to the nucleus of M31 displaying an 865-s periodicity. King et al. (2002) interpret this as the spin period of a white dwarf and hence argue (see also Schenker et al. 2002) that CVs are descendants from SSSs.

Supernova Remnants

Supernova explosions have a very profound impact on the Interstellar Medium (ISM), both as sources of mechanical energy and heavy elements. Supernova Remnants (SNRs) provide information about these issues and can be observed as high-energy sources. The interaction of high velocity ejecta with the ISM generates very high temperatures, giving rise to line emission from heavy elements. By studying the spatial distribution of elements, we can gain insight into nucleosynthesis in the progenitor and the geometry of the explosions. SNRs are also possible sites of cosmic ray acceleration.

The characteristics of the RGS make it possible to obtain spectral information from relatively extended sources. RGS spectra of SNRs allow the study of physical conditions all over the remnant (e.g., Rasmussen et al. 2001). By measuring the mass, temperature and bulk velocity of material, it is possible to obtain information about the supernova explosion. Using *XMM-Newton* observations of the young SNR Cas A, Willingale et al. (2002) have derived kinematic information and abundance ratios for the supernova ejecta. From analysis of those data, they find evidence for beaming in the supernova explosion, suggesting that most of the material was ejected in two jets (Willingale et al. 2003).

They also suggest that the progenitor was a very massive Wolf-Rayet star.

The compact object born in the Cas A supernova explosion has been identified with a point-like *Chandra* source, CXO J232327.8+584842. A long pointing with *XMM-Newton*, however, has failed to detect the X-ray pulsations that would be expected from a neutron star (Mereghetti et al. 2002a). The spectral properties of this source are also difficult to interpret in terms of a rapidly spinning neutron star.

No pulsations have been detected either from the SNR G21.5−0.9, which in many aspects resembles the Crab SNR, where a central pulsar is injecting high energy electrons (La Palombara & Mereghetti 2002). In this SNR, the X-ray spectrum of the nebula softens as one moves out from the centre, reflecting the energy losses of the electrons due to synchrotron radiation, as they diffuse out (Warwick et al. 2001). Similar conclusions are reached for the SNRs G0.9+0.1 (Porquet et al. 2003) and 3C 58 (Bocchino et al. 2001). While the central compact object of G0.9+0.1 has been detected with Chandra (CXOU J174722.8−280915), no obvious emission from a central object is seen in 3C 58.

The SNR IC 443 is specially interesting, because it is interacting with a dense molecular cloud rather than with the low density ISM. *XMM-Newton* has resolved several discrete hard X-ray sources, which could be fragments of the SNR interacting with the dense cloud (Bocchino & Bykov 2003).

Neutron stars

Young neutron stars in supernova remnants

The previous generation of imaging X-ray satellites (mainly *ROSAT* and *ASCA*) have detected a large population of young neutron stars which appear as rotation powered X-ray pulsars. X-ray emission in these systems may arise from a variety of physical processes. In many of them, non-thermal emission from relativistic particles accelerated in the pulsar magnetic field shows a power law spectrum over a broad energy range.

The large collecting area of *XMM-Newton* has provided for the first time spectral information for many of these weak X-ray sources. Its spatial resolution has also been necessary to separate them from their surrounding supernova remnants (SNRs). Preliminary results have been advanced by Becker & Aschenbach (2002), and the publication of many interesting results is expected in the near future.

Millisecond pulsars

Millisecond pulsars were first detected as radio sources (see Lorimer 2001) and only detected as X-ray pulsars with *ROSAT* (Becker & Trümper 1993). It is generally believed that millisecond pulsars are "recycled" pulsars, which have been spun up to their present high rotational velocities by accretion in a low mass X-ray binary and therefore objects of the highest interest for our understanding of binary evolution (Bhattacharya & van den Heuvel 1991).

Because of this, the recent detections of millisecond pulsars in accreting binaries (Wijnands & Van der Klis 1998) has sparked enormous interest. *XMM-Newton* observations of two of the currently four known accreting millisecond pulsars have been reported. The first accreting millisecond pulsar SAX J1808.4−365 has been detected in quiescence (Campana et al. 2002) and at a slightly higher luminosity (Wijnands 2003). In both cases, its spectrum was dominated by a power law, incompatible with thermal emission from the cooling surface of the neutron star (heated by accretion). A much better spectrum was obtained for the 2.3-ms accreting millisecond pulsar XTE J1751-305 (Miller et al. 2003b). However, no spectral features were detected.

The apparently isolated 4.86-ms pulsar PSR J0030+0451 was detected by *XMM-Newton*, which was able to measure its pulsed fraction. Its spectrum could be fitted by a two component model (either blackbody plus power law or two blackbodies) or a broken power law (Becker & Aschenbach 2002). Current models accounting for the spectra of millisecond pulsars predict that PSR J0030+0451 should be detectable at optical wavelengths. However, a very deep search in its *XMM-Newton* error circle conducted with the VLT has failed to detect any source down to B=27.3, casting into doubt such models (Koptsevich et al. 2003).

Thermal emission from neutron star atmospheres

Observations of isolated neutron stars (or neutron stars in quiescent X-ray binaries) are extremely important in fundamental physics, as thermal emission from the surface of a neutron star carries signatures of its gravitational field, which may be used to infer its mass and radius. Detection of absorption lines corresponding to elements on the neutron star atmosphere and measurement of their gravitational redshift would provide rather accurate data (e.g., Özel & Psaltis 2003). From the gravitational redshift at the surface of the neutron star, the ratio between its mass and radius may be measured, providing a very strong constraint on neutron star models. Such models give Physics an experimentally testable handle on properties of matter at (supra-)nuclear densities.

Unfortunately, observations so far have not been very successful at detecting these atmospheric features. The first *XMM-Newton* observation of an isolated neutron star (RX J0720.4-3125) yielded no spectral features on top of the blackbody continuum in a 62.5 ks exposure (Paerels et al. 2001a). Also, the isolated neu-

tron star RX J1856.5−3754 was observed for 57 ks with *XMM-Newton* without revealing any spectral feature. An extremely long (505 ks) exposure was then performed with *Chandra*, also failing to detect any feature (Burwitz et al. 2003). This result is against predictions by most current model atmospheres for neutron stars.

The spectrum of RBS 1223 does show a very broad absorption line, but this is interpreted as a cyclotron feature caused by electrons moving in its very high magnetic field of $2 - 6 \times 10^{13}$ Gauss (Haberl et al. 2003). No lines have been seen in the spectra of several other isolated neutron stars observed with *Chandra* or the anomalous X-ray pulsar 1E1048.1−5937 observed with *XMM-Newton* (Tiengo et al. 2002). The only secure detection is that of two absorption features, discovered with *Chandra*, in the isolated neutron star 1E 1207−5209. *XMM-Newton* observations have shown a phase dependence in at least one of these features (Mereghetti et al. 2002b), but their identification is still not clear.

Absorption features from the surface of a neutron star have likely been identified during a burst from the LMXB EXO 0748−676 (Cottam et al. 2002). If the identification of the observed features with Fe XXVI and XXV and O VIII lines is correct, they imply a $z = 0.35$ gravitational redshift.

Normal galaxies

As indicated above, X-ray emission from normal galaxies arises from their populations of X-ray binaries. By comparing the populations of different galaxies, we are able to obtain information about their star forming histories (e.g., Grim et al. 2003). In order to resolve the populations, imaging capabilities are necessary. Because of this, thorough exploration of the most nearby galaxies, the Magellanic Clouds, started only with *Einstein* and flourished with *ROSAT* (e.g., Sasaki et al. 2000; Haberl et al. 2000). *ROSAT* also allowed the study of other nearby galaxies such as M31 (Supper et al. 2001) or M33 (Haberl & Pietsch 2001).

The potentialities of *XMM-Newton* for this sort of study are enormous. Deep pointings of the Magellanic Clouds result in the detection of a wealth of X-ray sources, many of which are accreting binaries. The sensitivity of *XMM-Newton* permits the detection of effectively any active XRB. A pointing at the North of the LMC resulted in the detection of 150 discrete sources, among which a newly discovered HMXB, a new likely SSS and several new SNRs (Haberl et al. 2003). A pointing to the SMC resulted in the detection of the pulse periods of two previous candidates to HMXBs and the discovery of two new candidates (Sasaki et al. 2003). The wide field allows a large number of sources to be observed at the same time, considerably improving our knowledge of HMXB populations.

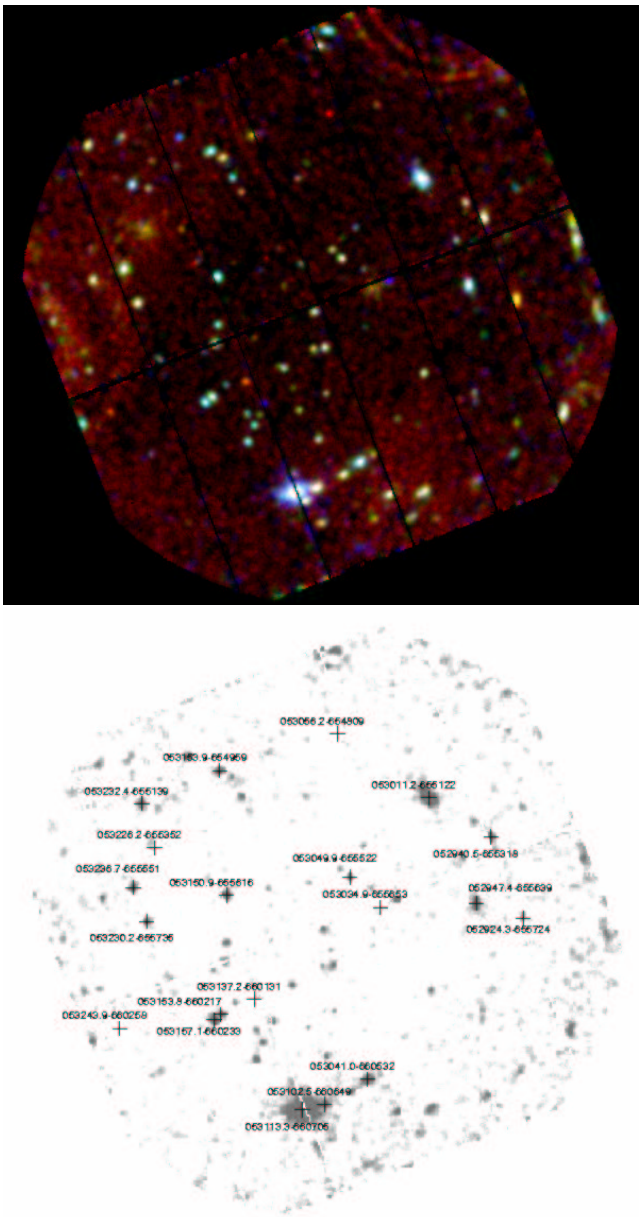

Fig. 3.: Top: False colour image of a field in the LMC generated from EPIC-pn data (red, green and blue represent images in the 0.3-1.0 keV, 1.0-2.0 keV and 2.0-7.5 keV bands respectively). Bottom: Grey-scale image of the same field showing the whole 0.3-7.5 keV band and the identification of several sources (from Haberl et al. 2003).

XMM-Newton can also extend this sort of work to more distant galaxies. Pointings to M 31 have allowed the detection of sources down to a luminosity of $L_x = 6 \times 10^{35}$ erg s^{-1} (Osborne et al. 2001), resulting in the characterisation of the whole XRB population. As expected, the bulge population is dominated by bright LMXBs, while the disk population appears to be composed mostly of young HMXBs (Trudolyubov et al. 2002a). The temporal evolution of some bright transients has been studied with both *XMM-Newton*

and *Chandra* (Trudolyubov et al. 2001). Among them, a bright LMXB has been detected in a globular cluster of the M 31 system (Trudolyubov et al. 2002b). All this work suggests an overall galactic XRB population similar to that of the Milky Way.

Even further, *XMM-Newton* has identified the first eclipsing X-ray binary outside the Local Group (Pietsch et al. 2003). This is RX J004717.4−251811 in the nearby starburst galaxy NGC 253.

Ultraluminous X-ray sources

One of the most interesting problems in extragalactic X-ray Astrophysics is the existence of Ultraluminous X-ray sources (ULXs). These sources are variable on short timescales, but their luminosities are typically much higher than those observed in Galactic and Magellanic Cloud XRBs, approaching in many cases $L_{\rm x} \approx 10^{40}$ erg s^{-1}. As this luminosity is much higher than the Eddington limit for a neutron star or a low-mass black hole, it seems to require massive black holes with masses of the order of $\sim 100 M_{\odot}$ (generally called intermediate-mass black holes, as their masses are between those of stellar-mass black holes and the supermassive objects at the heart of galaxies). Severe problems are found when trying to understand the formation mechanism of such black holes, leading to the thought that perhaps ULXs can be explained as normal XRBs in which the X-ray emission is beamed towards the observer, requiring thus much lower fluxes (King et al. 2001).

A very important result obtained with *XMM-Newton* has been the discovery of quasi-periodic modulation in the flux from an ULX in M82 (Strohmayer & Mushotzky 2003). Such modulation must arise in the immediate vicinity of the compact object and represents evidence against beaming. Unfortunately, because of the relatively low spatial resolution, the identification of the ULX is not completely certain and a simultaneous observation with *Chandra* seems desirable.

Further evidence supporting intermediate-mass black holes has been collected from analysis of the spectra of two ULXs in the nearby spiral galaxy NGC 1313. The blackbody temperatures inferred from the fits are a factor of ten lower than those of typical SXTs, suggesting rather more massive black holes (Miller et al. 2003c)

Clusters of galaxies

One of the very first discoveries of X-ray astronomy was that clusters of galaxies are strong X-ray emitters (see Sarazin 1986 for an early review and Mushotzky 2001 for a much more up-to-date compilation). Their X-ray spectrum is well fitted by plasma emission at a temperature of $10^7 - 10^8$ K, which includes thermal bremsstrahlung and line emission, most notably the Fe K emission line at ~ 6.7 keV. The inferred Fe abundance is about $\sim 0.3 - 0.5$ solar, with possible gradients across the cluster, but remarkable homogeneity across the cluster population. Clusters (and groups) of galaxies are therefore filled with enriched gas (likely deposited by the mass loss of the member galaxies), which appears to be trapped in the cluster potential well.

The intracluster medium appears to be close to hydrostatic equilibrium Except for the core (with a few $\times 100$ kpc), cluster gas is isothermal (or perhaps with a slowly decaying temperature) out to the distances where X-ray emission can be detected (less than the virial radius). Relaxed clusters often exhibit a *cooling flow* phenomenon, whereby the gas in the central part of the cluster is significantly cooler and the density higher probably due to a highly subsonic inflow amounting typically to $\sim 100\,{\rm M}_{\odot}\,{\rm yr}^{-1}$ (see Fabian 1994 for an extensive review).

The physical structure of the intracluster medium

One of the best studied clusters with *XMM-Newton* is A1795 ($z = 0.063$). This cluster shows a smooth gas density profile along the lines of the β profile adopted for many clusters (Arnaud et al. 2001). The temperature of the gas is seen to be constant from 0.1 to 0.4 virial radii, but dropping significantly at smaller distances from the cluster centre. This is now seen as a common feature in many clusters, like A496 (Tamura et al. 2001), A1413 (Pratt & Arnaud 2002).

The possibility of mapping the intracluster gas structure with unprecedent detail is now also opening big questions on its physical state. In their detailed analysis of the $z = 0.143$ A1413 cluster, Pratt & Arnaud (2002) argue that the gas departs from hydrostatic equilibrium when approaching the virial radius, as expected from the very long timescales involved. They also find evidence for a cuspy central density profile (at variance of the usually assumed β-profile). The mass profile of the cluster, as derived under the assumption of hydrostatic equilibrium, is not far from the predictions of standard Cold Dark Matter computations.

Another important contribution of *XMM-Newton* to cluster science has been illustrated with the observations of the $z = 0.54$ cluster CL0016+16, a working horse for the use of the Sunyaev-Zel'dovich effect to determine accurate values of the Hubble constant. Worrall & Birkinshaw (2003) have been able to derive accurate values for the gas temperature (to within 2.5%) and of the emission measure (electron density integrated along the line of sight) to within a similar accuracy. The subsequent revised value of $H_0 = 68 \pm 8\,{\rm km\,s^{-1}}$ is now in agreement with the latest determinations using the *Hubble Space Telescope* and the Cosmic Microwave Background power spectrum obtained by WMAP.

Building up clusters

For many years it has been thought that clusters build up from smaller structures, as predicted by popular cosmological scenarios. For instance, evidence for hierarchical merging in the Coma cluster was provided by *ROSAT* observations of X-ray emission of a merging sub-structure (White, Briel & Henry 1993).

With its much improved sensitivity, *XMM-Newton* is able to map intracluster gas down to very low surface brightness limits and therefore to strengthen or disprove the merging hypothesis. Indeed, the very first EPIC images of the Coma cluster (Briel et al. 2001) confirm the presence of the probably infalling lump from the SW (around NGC 4839) already detected by *ROSAT*, but they also find a further lump probably ahead of this one on its infall into the Coma cluster. N-body simulations do predict indeed that the infall into large clusters of galaxies proceeds along filamentary structures! The structure of the gas around NGC 4839 does show clear traces of being into its first infall into Coma (Neumann et al. 2001). The tail of the X-ray emission is very hot (~ 4.5 keV) and indeed hotter than the temperature of the galaxy itself. Together with a displacement of the X-ray emission with respect to the galaxy NGC 4839 (well placed at the centre of the optical group) this provides confirmation of the subgroup gas being ram pressure stripped in its infall into the Coma cluster.

Evidence for filamentary structures infalling onto clusters is also seen in *XMM-Newton* observations of the cluster A 85 (Durret et al 2003). Early *ROSAT* reports on a large ~ 4 Mpc filamentary structure towards the south of the central cD galaxy of A 85 are confirmed, together with a determination of the gas temperature of around ~ 2 keV. This suggests that the filamentary structure is made of a chain of several galaxy groups.

Further evidence in favour of clusters being built by merging blocks comes from observations of distant clusters. De Filippis et al. (2003) observed the cluster CL 0939+4713 at $z = 0.47$ and showed that it exhibits significant gas structure, with the gas in between the two dominant galaxies being the hottest. This implies a largely non-relaxed state with a likely collision between the two merging blocks within a few million years. Hashimoto et al. (2002) observed the very distant cluster RX J1053.7+5735 at $z = 1.26$ and also detected a double structure suggestive of a merger.

Therefore, *XMM-Newton* has brought evidence for merging activity in clusters of galaxies, particularly at significant redshifts. Assessing the incidence of mergers in the building up of galaxy clusters (there are examples of dynamically relaxed clusters at high redshift, see Arnaud et al. 2002, for observations of RX J1120.1+4318 at $z = 0.6$) has just started but will ultimately provide the most direct evidence on how large-scale structure forms in the Universe.

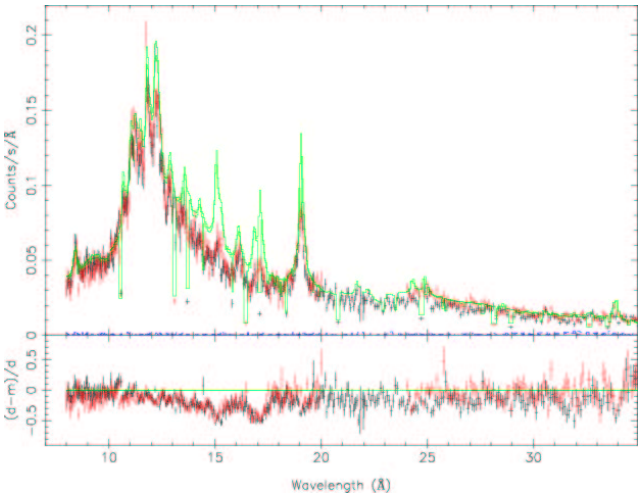

Fig. 4.: *XMM-Newton* RGS spectrum of the core of the Virgo cluster around the M87 galaxy (from Sakelliou et al. 2002). The discrepancy between the standard cooling flow model prediction (top green line) and the data (bottom lines) is most evident by the lack of Fe L lines around 12-17 Å.

Challenging cooling flows

Perhaps one of the most unexpected discoveries by *XMM-Newton* has been the challenge to the standard picture of the cooling flow phenomenon. The cooling time in the centres of galaxy clusters is significantly smaller than the age of the Universe, and therefore that gas will cool if no other phenomena prevent it (see, e.g., Fabian 1994 for a comprehensive review). Maintaining hydrostatic equilibrium with the hotter outer gas implies that gas should be steadily flowing inwards, increasing the density towards the cluster centre. Mass deposition rates are of the order of $\sim 100 - 1000\,\mathrm{M}_\odot\,\mathrm{yr}^{-1}$, which integrated over a Hubble time result in a substantial contribution to the mass of a large galaxy. Cooling flows manifest themselves as a peaked surface emissivity at the centre of the cluster, where the X-ray spectrum shows cooler gas. They occur almost invariably in cD clusters (i.e., those dominated by a large central-dominant early type galaxy), but very rarely happen in more non-relaxed structures, possibly due to the disruption of cooling flows by mergers.

Previous to the operation of *Chandra* and *XMM-Newton* there were doubts about the physics governing cooling flows. Conduction need to be suppressed to prevent the gas from thermalising in the hotter cluster environment, but lower temperature gas was unambiguously seen. The most intriguing question was (and still is) where does all this gas go. cD galaxies present at the centres of cooling flow clusters are red and, although they do form some stars (see the extensive work by Cardiel 1999 on star formation in cooling flow clusters), they certainly do not form $\sim 100 - 1000\,\mathrm{M}_\odot$ *normal* stars every year. A high pressure ambient as that

present in cooling flows could favour the formation of low-mass stars.

A major *XMM-Newton* result has been to show that the gas in cooling flow clusters does not cool below a temperature which is 1/2 to 1/3 of the outer intracluster medium temperature (see, e.g., Kaastra et al. 2001, Peterson et al. 2001, Tamura et al. 2001, Peterson et al. 2003, Sakelliou et al. 2002). Cluster gas at temperatures ~ 1 keV should cool mostly through Fe L lines, which should be very strong. Instead they are almost absent of the *XMM-Newton* RGS spectra. The amount of gas that cools is probably 1/10 of the gas expected from simple cooling flow models (Fabian & Allen 2003), suggesting a much modest role of cooling flows in galaxy formation (see also Molendi & Pizzolatto 2001).

The reasons for that are still unclear. Both conduction and heating by the central source (usually a powerful AGN) have been revived. Conduction should probably be decreased by the presence of magnetic fields, as a temperature gradient is indeed seen. Heating is also non-trivial, as it should deposit heat uniformly over a large volume, but on the contrary *Chandra* images show lots of structure in cluster cores.

A further complicating point is that, despite the fact that the amount of gas seen at temperatures of millions of degrees is much smaller than predicted by the simplest cooling flow models, *FUSE* observations reveal in some cooling flow clusters large OVI emission lines (Oegerle et al. 2001, Bregman 2003, priv comm). The amount of gas cooling at a few 10^5 K is paradoxically in agreement with the *cooling flow* models, but the few million degree gas is missing. There is clearly much to learn in the coming years from this phenomenon.

Active Galactic Nuclei

Active Galactic Nuclei (AGN) are the most populous class of X-ray sources in the Universe, particularly at high galactic latitude. The large variety of AGN manifestations results in distinctive X-ray emission properties. Radio-loud AGNs were early claimed to have flatter X-ray spectra than radio-quiet ones (Wilkes & Elvis 1987), with flat spectrum radiosources having an even flatter X-ray spectrum (Canizares & White 1989). This is now understood in terms of radio-loud AGNs being absorbed by cold gas (Sambruna et al. 1999), plus relativistic beaming affecting the X-ray emission in core-dominated radio sources.

Radio-quiet type 1 AGN (Seyfert 1 galaxies and QSOs) where optical broad emission lines are seen and type 2 AGN (Seyfert 2s) where these broad components are not seen in unpolarized light, should have different X-ray properties. Indeed, the simplest version of the AGN unified scheme (Antonucci 1993), where the type 1/type 2 dichotomy results from different viewing directions of the same (or very similar) central engine, predicts that X-rays emerging from the nucleus would be directly seen in type 1 AGNs but absorbed/scattered in type 2 AGNs.

The standard AGN model, i.e., that of a supermassive black hole fed by a geometrically thin accretion disk and collimated jets along the rotation axis, has found some of its best support in the X-ray observations. Hard X-ray photons at a rate of $10^{44}\,\mathrm{erg\,s^{-1}}$ are very difficult to produce by other means in a galactic centre. Additionally, some spectral features, as a broad relativistic Fe Kα emission discussed below, are distinctive tracers of accretion onto massive compact objects.

X-ray emission from AGN is characterised by an underlying power law with photon index $\Gamma \sim 1.5 - 2$ (on the steep side for radio-quiet AGN), which probably rolls over at energies ~ 100 keV (see the review by Mushotzky et al. 1993 summarizing the situation pre-*XMM-Newton*). For radio-quiet objects and those which are radio-loud but the beaming towards the observer is not important, this power law is interpreted as the Compton up-scattering of the UV photons produced in the accretion disk by the disk's relativistic electron atmosphere.

An Fe Kα emission line at 6.4-6.7 keV is the most prominent emission feature, along with a high-energy 'bump' at > 20 keV (Pounds et al. 1990), both of them probably arising from reflection of the X-rays in some thick material. For Seyfert 1 galaxies the equivalent width of the Fe line lies in the range 100-300 eV, while for Seyfert 2 galaxies the emission line is much stronger (up to 1 keV of equivalent width), in particular in Compton-thick Seyfert 2s. The most striking feature of the Fe line is that it is very broad (inferred Doppler velocities up to $\sim c/3$). In the best studied case of the Seyfert 1 galaxy MCG-6-30-15 it exhibits a relativistically broadened shape interpreted in terms of Doppler shifts produced by the disk rotation, aberration and gravitational redshift in the red horn due to the proximity to the black hole's event horizon (Tanaka et al. 1995). Similar shapes were observed in other Seyfert 1 galaxies, suggesting that this is a relatively general feature of type 1 AGNs. In the best studied Seyfert 2 galaxies (e.g. NGC 1068), *ASCA* showed a more complex emission line structure (Iwasawa et al. 1997).

AGN often exhibit photoelectric absorption features in excess of those produced by cold gas in our Galaxy. Radio-loud AGNs at high redshifts, often exhibit large cold (neutral) absorbing gas columns (Cappi et al. 1997) but in radio-quiet AGN the situation is more complex. In this case, type 1 AGN appear to have little neutral absorbing gas (Nandra & Pounds 1994), but they often exhibit signs of ionised gas along the line of sight in the form of absorption edges, most notably OVII K at 0.74 keV and OVIII K at 0.87 keV (Reynolds 1997, George et al. 1998). On the contrary Seyfert 2 AGN usually display large absorbing columns of neu-

tral gas (Smith & Done 1996), which is attributed to the "dusty torus" that the unified AGN scheme predicts to hide the broad line region. The average good correlation between optical spectral properties of radio quiet AGN and the amount of neutral absorbing gas along the line of sight has been clearly shown in Risaliti et al. (1999) on the basis of an [OIII]-selected sample of AGN (the [OIII] emissivity is believed to originate further away than any obscuring material in AGN, and therefore is regarded as an isotropic measure of the true intrinsic AGN luminosity).

The complex Fe line

Chandra and to a larger extent *XMM-Newton* have provided a qualitative leap forward in the study of Fe K lines, due to the large increase (in particular for *XMM-Newton*) of effective area at ~ 6 keV with respect to previous missions while preserving or improving the spectral resolution.

The best-studied Seyfert 1 galaxy MCG–6-30-15 has indeed been the subject of several long *XMM-Newton* observations. Fabian et al. (2002) discuss a 300 ks observation, where they confirm the existence of a very broad Fe line feature. A careful physical modeling of this feature shows that the line emissivity comes in two parts: the blue part of the line arises from the outer accretion disk (radius $> 6r_g$, where $r_g = GM/c^2$ is the gravitational radius of the black hole with mass M), but to account for the very extended red tail displayed by the line (extending down to 4 keV) a very concentrated emission at much lower radii is required. This unambiguously confirms early claims based on *ASCA* that reflection features arise from radii as close as $\sim 2\,r_g$ from the black hole, requiring a rapidly rotating (Kerr) hole. In fact Wilms (2001) caught the same source in the "low" state where the red wing of the Fe line dominates, suggesting extraction of energy from the spinning black hole through magnetic fields. In any case it is clear that the Fe line diagnostic of MCG–6-30-15 can only be understood in the context of reflection in an accretion disk around a Kerr black hole.

Observations of many other Seyfert galaxies have shown that the profile of the Fe line varies very much from source to source. In general, the reflection Fe line arises either in the inner part of the accretion disk, where it is likely to be highly ionised and broad, and/or at much more distant regions (perhaps the "dusty torus") where it betrays mostly neutral Fe with a narrow line. Prototypical cases showing both a narrow component at 6.4 keV and a broad component centered at 6.7 keV are Mkn 205 (Reeves et al. 2001) and NGC 5506 (Matt et al. 2001).

Interestingly, one of the cases claimed to have a broad Fe line with *ASCA* data, NGC 5548, does only show a neutral narrow line in *XMM-Newton* observations (Pounds et al. 2003). Although the Fe line

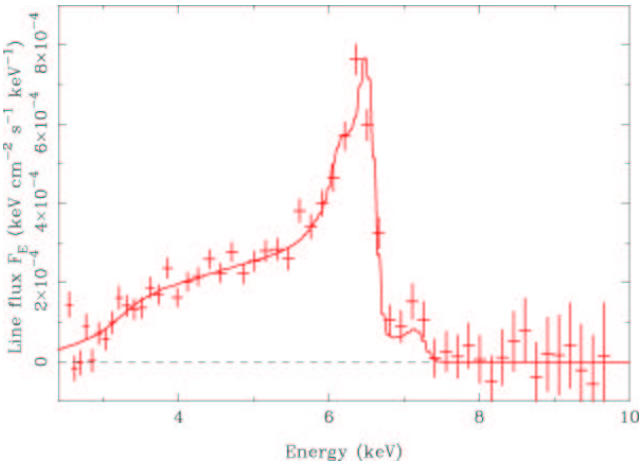

Fig. 5.: *XMM-Newton* EPIC-MOS spectrum of the Seyfert 1 galaxy MCG-6-30-15, around the Fe emission line, fitted to a relativistic disk model (from Fabian et al. 2002).

appears to vary less than the continuum in some of the best-studied Seyferts (such as MCG–6-30-15), there are reports of varying Fe lines. Guainazzi (2003) studies non-simultaneous *ASCA*, *XMM-Newton* and *BeppoSAX* observations of ESO198-G24, and he reports a broad component appearing and then fading away along with a narrow component.

It must also be stressed that the "holy grail" of using reverberation mapping (i.e., the response of reflected components, such as the Fe line, to continuum variations) to measure the mass of the black holes involved in AGN, has turned out to be rather complex. The Fe line intensity does not trivially follow the continuum variations and therefore much work is needed before this technique can be applied.

Soft X-ray broad lines?

A very lively debate has arisen since the launch of *XMM-Newton* on whether or not there are weak, relativistically broadened emission lines corresponding to C, N and O at soft X-ray energies. This stems from the use of the grating spectrographs both in *XMM-Newton* and *Chandra*, which provide spectral resolutions of the order of 200-500. Branduardi-Raymont et al. (2001) were the first to suggest the presence of these features in the RGS spectra of MCG-6-30-15 and Mkn 766, as an alternative to a standard warm absorber picture. Using a *Chandra* observation of MCG-6-30-15, Lee et al. (2001) identified a number of spectral features that were expected from a warm absorber, and even some of them only expected in Fe atoms trapped in dust grains, supporting the dusty warm absorber picture and no evidence for broad emission lines. Mason et al. (2003) have recently reported an analysis of RGS data on Mkn 766, where it is shown that broad relativistic emission lines of C, N and O give a better fit to the data than

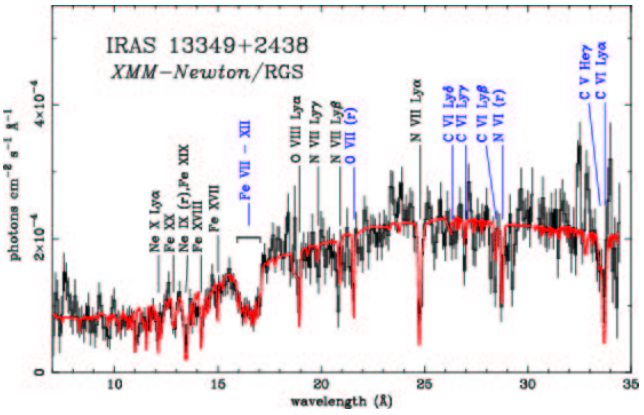

Fig. 6.: *XMM-Newton* RGS spectrum of the QSO IRAS 13349+2438, showing the complexity of the ionized absorber and the presence of a Unresolved Transition Array around 16-17 Å.

a dusty warm absorber. As of today, higher signal to noise *XMM-Newton* data over a larger bandpass appear to favour the presence of relativistic soft X-ray emission lines, and higher spectral resolution *Chandra* data appear to favour the dusty warm absorber interpretation. But the story continues ...

The complexity of the ionized absorbers

The higher spectral resolution provided by RGS has enabled the possibility of studying the ionized absorbers in AGN with much more detail. Sako et al. (2001) conducted the first of such detailed analyses on the QSO IRAS 13349+2438, which was already suspected from the combined *ROSAT*, *ASCA* and optical data to have a complex absorption structure along the line of sight. The RGS spectrum shows a large number of absorption lines of C,N,O,Ne with one and two electrons, as well as a number of Fe lines in various ionisation states. Most remarkably, an Unresolved Transition Array (UTA) of inner-shell lines of Fe M is detected for the first time at X-ray wavelengths, which might be confused, at the lower resolution of non-dispersive CCD imaging spectrographs, with an absorption edge. Absorption lines of Fe are detected in Fe VII - Fe XII and in Fe XVII - Fe XX, but not in the intermediate ionisation states Fe XIII - Fe XVI. This suggests the existence of two distinct absorbers, a low ionisation one, which happens to be outflowing with a velocity $\sim 400\,\mathrm{km\,s^{-1}}$ and a high ionisation absorber basically at rest with the QSO. The low ionization outflowing absorber implies (for normal dust to gas ratio) a reddening coincident with the optical one, but the high ionisation absorber, with a much larger column density, does not appear to have any dust.

Similar deep studies have been conducted on other targets (e.g., Blustin et al. 2002), revealing almost invariably the presence of UTAs, and a complex (at least two-phase) ionisation structure for the absorbers. It must be stressed that we are likely probing the gas in between the broad-line region and the "obscuring torus" in a manner that no other observational strategy could do.

Surveys and the X-ray background

The existence of a cosmic X-ray background (CXRB) was among the very first discoveries of X-ray Astronomy (Giacconi et al. 1962). Its spectrum was well measured by the HEAO-1 mission (Marshall et al. 1980, Gruber 1992) and fits remarkably well a thermal bremsstrahlung model at a temperature of $\sim 30\,\mathrm{keV}$. At galactic latitudes $> 20°$ the CXRB is remarkably isotropic claiming for a true cosmological origin (see Fabian & Barcons 1992 for a review). Most of the energy density in the CXRB resides at $\sim 30\,\mathrm{keV}$, an energy which is not accessible to sensitive enough instrumentation in the current era. Below 1 keV the Galaxy (and probably a local hot bubble) dominates the X-ray intensity, and the extragalactic component is shielded by the interstellar medium, making it difficult to measure. In spite of this, deep *ROSAT* observations resolved $\sim 70\%$ of the CXRB in the 1-2 keV (Hasinger et al. 1998) while *Chandra* has resolved practically 90% of this and $\sim 70\%$ of the 2-7 keV CXRB (Mushotzky et al. 2000).

The lack of spectral distortions of the Cosmic Microwave Background ruled out the presence of substantial amounts of intergalactic gas at the very high temperatures needed to produce the CXRB through thermal bremsstrahlung (Barcons et al. 1991). Finding the sources that produce the CXRB, their astrophysical nature, their cosmic evolution, spatial clustering and so on has been since then the main objective of CXRB studies.

The most popular models for the CXRB make use of the unified model for AGN, and assume a mixture of unabsorbed (presumably type 1) and absorbed (presumably type 2) objects as a function of redshift z (Comastri et al. 1995, Gilli et al. 2001).

Medium sensitivity (Mason et al. 2000) and deep (Lehmann et al. 2002) surveys carried out with *ROSAT* revealed that at soft X-ray energies the X-ray sky is dominated by AGNs, most of which are type 1 Seyferts and QSOs. A small fraction of the AGN were type 2 and other narrow emission line galaxies (e.g., starburst galaxies). However, due to its bandpass limited to soft X-ray photons *ROSAT* missed most of the sources absorbed by H columns in excess to $10^{21}\,\mathrm{cm^{-2}}$.

The large field of view of the EPIC cameras (0.5° in diameter) makes *XMM-Newton* a very powerful tool to conduct X-ray surveys. The Survey Science Centre (SSC) is carrying out a series of serendipitous surveys in order to characterise the content of the X-ray sky

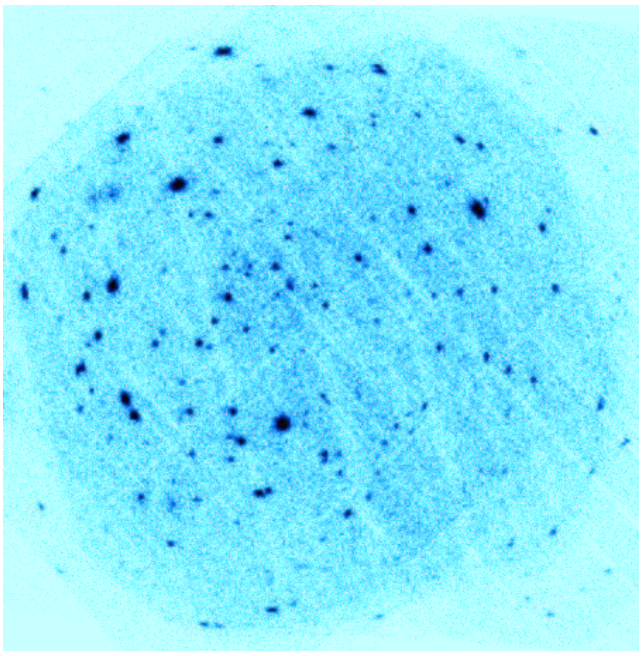

Fig. 7.: *XMM-Newton* EPIC-pn image of the Lockman Hole, totalling an exposure time approaching 1 Ms (about one week).

at different depths. At high Galactic latitudes, 3 samples of $\sim$ 1000 sources each, selected at 0.5-4.5 keV fluxes of $\sim 10^{-13}$, $\sim 10^{-14}$ and $\sim 10^{-15}$ erg cm^{-2} s^{-1} will provide a major handle on this task. A number of surveys are being conducted besides the SSC ones, most of which are discussed in the proceedings of the Workshop *X-ray Surveys, in the light of the new observatories* held in Santander during 4-6 September 2002 (Astronomische Nachrichten, vol 324, issues 1 and 2).

The AXIS programme[4] is providing a substantial leap forward in the *XMM-Newton* SSC medium sensitivity survey. This is a flux limited survey at 2×10^{-14} erg cm^{-2} s^{-1}, in the 0.5-4.5 keV band, with a source density of $\sim$ 100 deg^{-2}, which has the goal of covering $\sim$ 5 deg^{-2} both in the North and in the South. Preliminary results were presented in Barcons et al. (2002) and an update can be found in Barcons et al. (2003a).

The deepest X-ray survey conducted by *XMM-Newton* so far is in the Lockman Hole area, with a total exposure approaching 1000 ks (adding the payload verification, AO-1 and AO-2 data). The scope of this survey is not only to detect the faintest sources, particularly at hard X-ray energies where confusion is still unimportant and *XMM-Newton* is 5-10 times more efficient than *Chandra*, but more importantly to obtain X-ray spectra of the faintest sources. A preliminary account, based on 100 ks data, is presented in Hasinger et al. (2001).

[4]AXIS is an International Time Programme at the Observatorio del Roque de Los Muchachos in La Palma, which was granted 85 observing nights spread on the INT, NOT, TNG and WHT telescopes from April 2000 through April 2002. See http://venus.ifca.unican.es/~ xray/AXIS

Challenging the AGN unified scheme

XMM-Newton is also providing evidence that the one to one association of type 1 AGNs with unabsorbed sources and type 2 AGNs with absorbed sources fails clearly in some cases. For example Barcons et al. (2003b) have shown that the H1320+551 z=0.068 Seyfert 1.9 galaxy (and therefore with a broad line region putatively obscured) does not show any signs of neutral or ionised gas along the line of sight. This is in direct contradiction to the unified AGN model.

On the opposite side, type 1 QSOs are found which display large absorbing columns of neutral gas (e.g., Georgantopoulos et al. 2003), while none or very little was expected. A possible explanation to this is that X-ray absorption occurs very close to the central engine where dust just sublimates and therefore the optical spectrum is unaffected by the surrounding material. This might be a non-isolated situation, as explained by Mateos et al. (2003) in an analysis of the X-ray spectra of XMS sources, where a fraction of type 1 AGNs do require absorbing columns along the line of sight.

Faint and absorbed sources

If anything, the deep observation of Hasinger et al. (2001) demonstrates that the basic picture for the origin of the CXRB, based on absorbed sources, is roughly correct. Indeed, some $\sim$ 40% of the faint sources detected show some hint of absorption in their X-ray colours, in agreement with the general expectations. Quantitatively, however, the situation is still far from clear.

One of the most striking results obtained from the optical identification of *Chandra* deep surveys is that the redshift distribution of type 2 AGN is peaked at significantly lower redshifts ($z \sim 0.8$) than that of type 1 AGN ($z \sim 1.7$) (Hasinger 2002). Similarly, in the XMS all type 2 AGNs are concentrated at low redshifts, while the type 1s reach $z \sim 3$.

This probably means that the models for CXRB need some revision. Following this, Franceschini, Braito & Fadda (2002) have suggested that type 1 AGN arise in the rare highest peaks of the density field in the Universe, but that type 2 AGN result from the evolution and merging of the very massive galaxies, a process that occurs later in the cosmic history.

Optically dull X-ray bright galaxies and obscured accretion

A still intriguing issue raised by the new observatories and studied in detail by *XMM-Newton* is the existence of optically inactive but X-ray luminous galaxies. Such

objects were first highlighted in a *Chandra* deep survey by Mushotzky et al. (2000), as early type galaxies with a large X-ray to optical ratio. Comastri et al. (2002) conducted a multi-wavelength study of one of these objects discovered in their HELLAS2XMM survey, which shows no optical or infrared emission lines, but does show a rather hard X-ray spectrum. They concluded that the counterpart galaxy at $z = 0.159$ hosts a completely obscured active nucleus.

Severgnini et al. (2003) have recently reported on the study of 3 of these objects discovered in the SSC bright source survey. Their X-ray properties are varied, but in all cases reflecting clearly the presence of an X-ray luminous AGN. In that work it is shown that the emission lines related to the more or less obscured AGN are diluted with the galaxy light and therefore very weak and inconspicuous in some cases.

All this appears to support previous suspicions that most, if not all, galaxies host a black hole in their center, many of them active but obscured. Obscured accretion is probably 3 times more frequent in the Universe than unobscured accretion, if the CXRB models are roughly correct. A detailed accounting on the black hole density can then be inferred by assuming a radiative efficiency of the black holes (typically 10%) and compared to other independent estimates of the local black hole density. Fabian (2003) concludes that the estimate based on the CXRB and with what is known from the redshift distribution of obscured sources, converges towards $\sim 4 \times 10^5\,\mathrm{M}_\odot\,\mathrm{Mpc}^{-3}$, a value which is consistent with local estimates. Obscured accretion onto black holes is therefore important, although the "hidden" black hole mass is of the same order than that seen in unobscured AGN.

Gamma-ray burst afterglows

XMM-Newton is making a big effort in observing Gamma Ray Bursts (GRB) following alerts provided by other higher-energy observatories. The absolute minimum reaction time reached is 6-8 hours after the alert. In all observations (conducted as Target Of Opportunity observations, and therefore immediately public) the GRB afterglow has been detected and much has been learnt on this phenomenon from the X-ray data.

GRB011211 (identified to occur in a galaxy of $\sim 25^{\mathrm{mag}}$ at $z = 2.141$) is, perhaps the most interesting case. It was observed by *XMM-Newton* for 27 ks, 11 hours after its detection by *BeppoSAX*. During the first 10 ks of that observation, the EPIC X-ray spectrum showed emission lines which Reeves et al. (2002) identified as Mg XI, Si XIV, SXVI, Ar XVIII and Ca XX but at a significantly blueshifted velocity $\sim 0.1c$ (the detection confidence of these lines has been challenged by Rutledge & Sako 2003 though). If the Reeves et al. (2002) interpretation is correct, then this would provide direct evidence for outflowing material, favouring the model of the collapse of a massive star for GRBs.

Acknowledgments

The work reported herein is based partly on observations obtained with *XMM-Newton*, an ESA science mission with instruments and contributions directly funded by ESA member states and the USA (NASA). We are grateful to Fred Jansen, Christian Motch, Richard Mushotzky and an anonymous referee for comments on an early version that resulted in substantial improvements. XB acknowledges partial financial support by the Ministerio de Ciencia y Tecnología (MCyT), under grant AYA2000-1690. IN is a researcher of the programme *Ramón y Cajal*, funded by the University of Alicante and the MCyT. He acknowledges partial financial support by the MCyT under grants ESP2001-4541-PE and ESP2002-04124-C03-03.

Referencias

[1] Antonucci, R.R.J. 1993, Unified models for active galactic nuclei and quasars, ARAA, 31, 473

[2] Arnaud, M. et al. 2001, Measuring cluster temperature profiles with XMM/EPIC, A&A, 365, L188

[3] Arnaud, M. et al. 2002, *XMM-Newton* observation of the distant (z=0.6) galaxy cluster RX J1120.1+4318, A&A, 390, 27

[4] Audard, M. et al. 2003, A study of coronal abundances in RS CVn binaries, A&A 398, 1137

[5] Barcons, X. et al. 1991, The physical state of the intergalactic medium, Nat, 350, 685

[6] Barcons, X. et al. 2002, The *XMM-Newton* Serendipitous Survey. II. First results from the AXIS high galactic latitude medium sensitivity survey, A&A, 382, 522

[7] Barcons, X. et al. 2003a, The *XMM-Newton* Survey Science Centre medium sensitivity survey, AN, 324, 44

[8] Barcons, X. et al. 2003b, H1320+551: A Seyfert 1.8/1.9 galaxy with an unabsorbed X-ray spectrum, MNRAS, 339, 757

[9] Becker, W., & Aschenbach, B. 2003, X-ray observations of neutron stars and pulsars: First results from *XMM-Newton*, in Becker, W. et al. eds., Proceedings of 270th WE-Heraeus seminar on Neutron stars, pulsars and supernova remnants, MPE Report 278, p. 64 (astro-ph/0208466)

[10] Becker, W., & Trümper, J. 1993, Detection of pulsed X-ray emission from the binary millisecond pulsar J0437−4715

[11] Bhattacharya, D., & van den Heuvel, E.P.J. 1991, Formation and evolution of binary and millisecond radio pulsars, Ph.R. 203, 1

[12] Blustin, A.J. et al. 2002, Multi-wavelength study of the Seyfert 1 galaxy NGC 3783 with *XMM-Newton*, A&A, 392, 453

[13] Bocchino, F.,& Bykov, A.M. 2003, *XMM-Newton* study of hard X-ray sources in IC 443, A&A 400, 203

[14] Bocchino, F. et al. 2001, The X-ray nebula of the filled center supernova remnant 3C 58 and its interaction with the environment, A&A 369, 1078

[15] Branduardi-Raymont, G. et al. 2001, Soft X-ray emission lines from a relativistic accretion disk in MCG-6-30-15 and Mrk 766, A&A, 365, L140

[16] Briel, U.G. et al. 2001, A mosaic of the Coma cluster of galaxies with *XMM-Newton*, A&A, 365, L60

[17] Burwitz, V., et al. 2003, The thermal radiation of the isolated neutron star RX J1856.5−375 observed with *Chandra* and *XMM-Newton*, A&A 399, 1109

[18] Campana, S. 2002, An *XMM-Newton* study of the 401 Hz accreting pulsar SAX J1808.4−3658 in quiescence, ApJ 575, L15

[19] Canizares, C.R. & White, J.L., 1989, The X-ray spectra of high-redshift quasars, ApJ, 339, 27

[20] Cappi, M. et al. 1997, ASCA and *ROSAT* X-Ray Spectra of High-Redshift Radio-loud Quasars, ApJ, 478, 492

[21] Cardiel, N. 1999, Formación estelar en galaxias dominantes de cúmulos, PhD thesis, Universidad Complutense de Madrid

[22] Church, M. J., & Balucinska-Church, M. 2001, Results of a LMXB survey: Variation in the height of the neutron star blackbody emission region, A&A 369, 915

[23] Cohen, D.H., et al. 2003, High-resolution *Chandra* spectroscopy of τ Scorpii: a narrow-line X-ray spectrum from a hot star

[24] Comastri, A. et al. 1995, The contribution of AGNs to the X-ray background, A&A, 296, 1

[25] Comastri, A. et al. 2002, The HELLAS2XMM survey: II. Multiwavelength observations of P3: an X-ray bright, optically inactive galaxy, ApJ, 571, 771

[26] Cottam, J. et al. 2001, High-resolution spectroscopy of the low-mass X-ray binary EXO 0748−67, A&A 365, L277

[27] Cottam, J., et al. 2002, Gravitationally redshifted absorption lines in the X-ray burst spectra of a neutron star, Nat. 420, 51

[28] De Filippis, E. et al. 2003, XMM observation of the dynamically young galaxy cluster CL 0939+4713, A&A, in the press (astro-ph/0304027)

[29] Durret, F. et al. 2003, An *XMM-Newton* view of the extended "filament" near the cluster of galaxies Abell 85, A&A, in the press (astro-ph/0303486)

[30] Esin, A.E. et al. 1998, Spectral transitions in Cygnus X-1 and other black hole X-ray binaries, ApJ 505, 854

[31] Fabian, A.C. & Barcons, X. 1992, The origin of the X-ray background, ARAA, 30, 429

[32] Fabian, A.C., 1994, Cooling Flows in Clusters of Galaxies, ARAA, 32, 277

[33] Fabian, A.C. et al. 2002, A long hard look at MCG-6-30-15 with *XMM-Newton*, MNRAS, 335, L1

[34] Fabian, A.C. 2003, What can be learnt from extragalactic X-ray surveys?, AN, 324, 4

[35] Fabian, A.C. & Allen, S.W. 2003, X-rays from Clusters of Galaxies, in *proceedings of the XXI Texas Symposium on Relativistic Astrophysics*, in the press (astro-ph/0304020)

[36] Favata, F. et al. 2003, An *XMM-Newton*-based X-ray survey of pre-main sequence stellar emission in the L1551 star-forming complex, A&A 403, 187

[37] Feigelson, E.D., & Montmerle, T. 1999, High-energy processes in young stellar objects, ARA&A, 37, 363

[38] Feldmeier, A., et al. 1997, The X-ray emission from cooling zones in O star winds, A&A 320, 899

[39] Fleming, T.A., et al. 1988, The relation between X-ray emission and rotation in late-type stars from the perspective of X-ray selection, ApJ 340, 1011

[40] Franceschini, A. et al. 2002, Origin of the X-ray background and AGN unification: new perspectives, MNRAS, 335, L51

[41] Georgantopoulos, I. et al. 2003, *XMM-Newton* observations of an absorbed z=0.67 QSO: no dusty torus?, MNRAS, in the press (astro-ph/0302375)

[42] George, I.M. et al. 1998, ASCA Observations of Seyfert 1 Galaxies. III. The Evidence for Absorption and Emission Due to Photoionized Gas, ApJS, 114, 73

[43] Giacconi, R. et al. 1962, Evidence for x Rays From Sources Outside the Solar System, Phys Rev Lett, 9, 439

[44] Gilli, R. et al. 2001, Testing current synthesis models of the X-ray background, A&A, 366, 407

[45] Grimm, H.-J., et al. 2003, High-mass X-ray binaries as a star formation rate indicator in distant galaxies, MNRAS 339, 793

[46] Gruber, D.E., 1992, The Hard X-Ray Background, in *The X-ray background*, Barcons, X. & Fabian, A.C. eds, Cambridge University Press.

[47] Guainazzi, M., 2003, The history of the iron K-alpha line profile in the Piccinotti AGN ESO198-G24, A&A, in the press (astro-ph/0302117)

[48] Güdel, M. et al. 2002, Detection of the Neupert effect in the corona of an RS CVn System with *XMM-Newton* and the VLA, ApJ 577, 371

[49] Haberl, F. et al. 2000, A *ROSAT* PSPC catalogue of X-ray sources in the SMC region, A&AS 142, 41

[50] Haberl, F., & Pietsch, W. 2001, The X-ray view of M 33 after *ROSAT*, A&A 373, 438

[51] Haberl, F., et al. 2003, Deep *XMM-Newton* observation of a northern LMC field: I. Selected X-ray sources, A&A, in press (astro-ph/0212319)

[52] Haberl, F. et al. 2003, A broad absorption feature in the X-ray spectrum of the isolated neutron star RBS 1223 (1RXS J130848.6+212708), A&A 403, L19

[53] Hameury, J.-M. et al. 2003, *XMM-Newton* observations of two black hole X-ray transients in quiescence, A&A 399, 631

[54] Harnden, F.R. et al. 1979, Discovery of an X-ray star association in VI Cyg/Cyg OB2, ApJ 234, L51

[55] Hashimoto, Y. et al. 2002, *XMM-Newton* Observation of a Distant X-ray Selected Cluster of Galaxies at z=1.26 with Possible Cluster Interaction, A&A, 381, 841

[56] Hasinger, G. et al. 1998, The *ROSAT* Deep Survey. I. X-ray sources in the Lockman Field, A&A, 329, 482

[57] Hasinger, G. et al., 2001, *XMM-Newton* observation of the Lockman Hole. I. The X-ray data, A&A, 365, L45

[58] Hasinger, G., 2002, The sources of the X-ray background, in *New visions of the Universe in the XMM-Newton and Chandra era*, in the press (astro-ph/0202430)

[59] Helfand, D. J., & Moran, E.C. 2001, The hard X-Ray luminosity of OB star populations: Implications for the contribution of star formation to the cosmic X-ray background, ApJ, 554, 27

[60] Hernanz, M., & Sala, G. 2002, A classical nova, V2487 Oph 1998, seen in X-rays before and after its explosion, Sci 298, 393

[61] van den Heuvel, E.P.J. et al. 1992, Accreting white dwarf models for CAL 83, CAL 87 and other ultrasoft X-ray sources in the LMC, A&A 262, 97

[62] Howk, J.C. et al. 2000, Stagnation and infall of dense clumps in the stellar wind of τ Scorpii, ApJ 534, 348

[63] Iwasawa, K. et al. 1997, The iron K line complex in NGC1068: implications for X-ray reflection in the nucleus, MNRAS, 289, 443

[64] Jansen, F. et al. 2001, *XMM-Newton* observatory. I. The spacecraft and operations. A&A 365, L1

[65] Jimenez-Garate, M.A. et al. 2002, High-resolution X-Ray spectroscopy of Hercules X-1 with the *XMM-Newton* Reflection Grating Spectrometer: CNO element abundance measurements and density diagnostics of a photoionized plasma, ApJ 578, 391

[66] Kaastra, J.S. et al. 2001, *XMM-Newton* observations of the cluster of galaxies Sersic 159-03, A&A, 365, L99

[67] Kahn, S.M. et al. 2001, High resolution X-ray spectroscopy of ζ Puppis with the *XMM-Newton* reflection grating spectrometer, A&A 365, L312

[68] King, A.R. et al. 2001, Ultraluminous X-Ray sources in external galaxies, ApJ 552, L109

[69] King, A.R., et al. 2002, The short-period supersoft source in M31, MNRAS 329, L43

[70] Koptsevich et al. 2003, Deep BVR imaging of the field of the millisecond pulsar PSR J0030+0451 with the VLT, A&A 400, 265

[71] La Palombara, N., & Mereghetti, S. 2002, Timing analysis of the core of the Crab-like SNR G21.5−0.9, A&A 383, 916

[72] Lee, J.C. et al. 2001, Revealing the Dusty Warm Absorber in MCG -6-30-15 with the Chandra High-Energy Transmission Grating, ApJ, 554, L13

[73] Lewin W.H.G., et al. 1993, X-Ray bursts, SSRv 62, 223

[74] Lewin W.H.G., et al. 1995, X-ray binaries, Cambridge Astrophysics Series, Cambridge, MA (Cambridge University Press)

[75] Lorimer, D.R. 2001, Binary and millisecond pulsars at the new millennium, LRR 4,5 (astro-ph/0104388)

[76] Marshall, F.E. et al. 1980, The diffuse X-ray background spectrum from 3 to 50 keV, ApJ, 235, 4

[77] Mason, K.O. et al. 2000, The *ROSAT* International X-ray/Optical Survey (RIXOS): source catalogue, MNRAS, 311, 456

[78] Mason, K.O. et al. 2001, The *XMM-Newton* optical/UV monitor telescope, A&A, 365, L36

[79] Mason, K.O. et al. 2003, The X-ray spectrum of the Seyfert I galaxy Mrk 766: Dusty Warm Absorber or Relativistic Emission Lines?, ApJ, 582, 95

[80] Mateos, S. et al. 2003, X-ray spectra of *XMM-Newton* AXIS serendipitous sources, AN, 324, 48

[81] Matt, G. et al. 2001, The complex iron line of NGC 5506, A&A, 377, L31

[82] Mereghetti, S., et al. 2002a, The X-ray source at the center of the Cassiopeia A supernova remnant, ApJ 569, 275

[83] Mereghetti, S. et al. 2002b, Pulse phase variations of the X-ray spectral features in the radio-quiet neutron star 1E 1207−5209, ApJ 581, 1280

[84] Mewe, R., et al. 2003, High-resolution X-ray spectroscopy of τ Scorpii (B0.2V) with *XMM-Newton*, A&A 398, 203

[85] Miller, J.M. et al. 2002a, *XMM-Newton* spectroscopy of the Galactic microquasar GRS 1758−258 in the peculiar off/soft state, ApJ 566, 358

[86] Miller, J.M. et al. 2003b, Evidence of spin and energy extraction in a Galactic black hole candidate: The *XMM-Newton*/EPIC-pn spectrum of XTE J1650−500, ApJ 570, L69

[87] Miller, J.M. et al. 2003c, *XMM-Newton* spectroscopy of the accretion-driven millisecond X-ray pulsar XTE J1751−305, ApJ 583, L99

[88] Miller, J.M. et al. 2003, X-ray spectroscopic evidence for intermediate-mass black holes: Cool accretion disks in two ultraluminous X-ray sources, ApJ 585, L37

[89] Molendi, S. & Pizzolatto, F. 2001, Is the Gas in Cooling Flows Multiphase?, ApJ, 560, 194

[90] Motch, C., et al. 2002, *XMM-Newton* observations of MR Vel/RX J0925.7−4758, A&A 393, 913

[91] Mushotzky, R.F. et al. 1993, X-ray spectra and time variability of active galactic nuclei, ARAA, 31, 717

[92] Mushotzky, R.F. et al. 2000, Resolving the extragalactic hard X-ray background, Nat, 404, 459

[93] Mushotzky, R.F., 2001, Clusters, in *The Century of Space Science*, Bleeker, J.A.M., Geiss, J. & Huber, M.C.E. eds, p. 473

[94] Nandra, K. & Pounds, K.A. 1994, GINGA Observations of the X-Ray Spectra of Seyfert Galaxies, MNRAS, 268, 405

[95] Narayan, R., McClintock, J.E., & Yi, I. 1996, A new model for black hole soft X-ray transients in quiescence, ApJ 457, 821

[96] Neuhäuser, R. 1997, Low-mass pre-main sequence stars and their X-ray emissions, Sci 276, 1363

[97] Neumann, D. et al. 2001, The NGC4839 group falling into the coma cluster observed by *XMM-Newton*, A&A, 365, L74

[98] Noyes, R.W. et al. 1984, Rotation, convection and magnetic activity in lower main-sequence stars, ApJ 279, 763

[99] Oegerle, W.R. et al. 2001, FUSE Observations of Cooling-Flow Gas in the Galaxy Clusters A1795 and A2597, ApJ, 560, 187

[100] Oosterbroek, T. et al. 2001, *BeppoSAX* observation of the eclipsing dipping X-ray binary X 1658−298, A&A 376, 532

[101] Osborne, J.P. 2001, The central region of M 31 observed with *XMM-Newton*. II. Variability of the individual sources, A&A 378, 800

[102] Oskinova, L.M. et al. 2003, The conspicuous absence of X-ray emission from Carbon-enriched Wolf-Rayet stars, A&A 402, 755

[103] Özel, F., & Psaltis, D. 2003, Spectral lines from rotating neutron stars, AJ 582, L31

[104] Paerels, F. et al. 2001a, First XMM-Newton observations of an isolated neutron star: obtained with XMM-Newton, A&A, 365, L298

[105] Paerels, F. et al. 2001b, A high resolution spectroscopic observation of CAL 83 with *XMM-Newton*/RGS, A&A 365, L308

[106] Parmar, A.N. et al. 2002, Discovery of narrow X-ray absorption features from the dipping low-mass X-ray binary X 1624−490 with *XMM-Newton*, A&A 386, 910

[107] Patterson, J. 1984, The evolution of cataclysmic and low-mass X-ray binaries, ApJS 54, 443

[108] Patterson, J. 1994, The DQ Herculis stars, PASP 106, 209

[109] Peterson, J.R. et al. 2001, X-ray imaging-spectroscopy of Abell 1835, A&A, 365, L104

[110] Peterson, J.R. et al. 2003, High Resolution Spectroscopy of 14 Cooling-Flow Clusters of Galaxies Using the Reflection Grating Spectrometers on *XMM-Newton*, in *New visions of the Universe in the XMM-Newton and Chandra era*, in the press (astro-ph/0202108)

[111] Pietsch, W., et al. 2003, RX J004717.4−251811: The first eclipsing X-ray binary outside the Local Group, A&A 402, 457

[112] Porquet, D., et al. 2003, *XMM-Newton* spectral analysis of the Pulsar Wind Nebula within the composite SNR G0.9+0.1, A&A 401, 197

[113] Pounds, K.A. et al. 1990, X-ray reflection from cold matter in the nuclei of active galaxies, Nat, 344, 132

[114] Pounds, K.A. et al. 2003, A simultaneous *XMM-Newton* and *BeppoSAX* observation of the archetypal Broad Line Seyfert 1 galaxy NGC 5548, MNRAS, in the press (astro-ph/0210288)

[115] Pratt, G.W & Arnaud, M. 2002, The mass profile of A1413 observed with *XMM-Newton*: implications for the M-T relation, A&A, 394, 375

[116] Ramsay, G. & Cropper, M.S. 2002, First X-ray observations of the polar CE Gru, MNRAS 335, 918

[117] Ramsay, G. & Cropper, M.S. 2003, *XMM-Newton* observations of the polars EV UMa, RX J1002−19 and RX J1007−20, MNRAS 338, 219

[118] Rasmussen, A.P. et al. 2001, The X-ray spectrum of the supernova remnant 1E 0102.2−7219, A&A 365, L231

[119] Rauw, G. et al. 2003, Phase-resolved X-ray and optical spectroscopy of the massive binary HD 93403, A&A 388, 552

[120] Reeves, J.N. et al. 2001, *XMM-Newton* observation of an unusual iron line in the quasar Markarian 205, A&A, 365, L134

[121] Reeves, J.N. et al. 2002, The Signature of Supernova Ejecta Measured in the X-ray Afterglow of Gamma-Ray Burst 011211, Nat, 416, 512

[122] Reynolds, C.S. 1997, An X-ray spectral study of 24 type 1 active galactic nuclei, MNRAS, 286, 513

[123] Risaliti, G. et al. 1999, The Distribution of Absorbing Column Densities among Seyfert 2 Galaxies, ApJ, 522, 157

[124] Rutledge, R.E. & Sako, M. 2003, Statistical reexamination of reported emission lines in the X-ray afterglow of GRB 011211, MNRAS, 339, 600

[125] Sakelliou, I. et al. 2002, High Resolution Soft X-ray Spectroscopy of M87 with the Reflection Grating Spectrometers on *XMM-Newton*, A&A, 391, 903

[126] Sako, M. et al. 2001, Complex resonance absorption structure in the X-ray spectrum of IRAS 13349+2438, A&A, 365, L168

[127] Sambruna, R., Eracleous, M., Mushotzky, R.F., 1999, An X-Ray Spectral Survey of Radio-loud Active Galactic Nuclei with ASCA, ApJ, 526, 60

[128] Sarazin, C.L., 1986, X-ray emission from clusters of galaxies, Rev Mod Phys, 58, 1

[129] Sasaki, M., et al. 2000, *ROSAT* HRI catalogue of X-ray sources in the LMC region, A&AS 143, 391

[130] Sasaki, M., et al. 2003, *XMM-Newton* observations of High Mass X-ray Binaries in the SMC, A&A, 403, 901

[131] Schenker, K. et al. 2002, AE Aquarii: how cataclysmic variables descend from supersoft binaries, MNRAS 337, 1105

[132] Severgnini, P. et al. 2003, *XMM-Newton* observations expose AGN in apparently normal galaxies, A&A, in the press (astro-ph/0304308)

[133] Shu, F.H. et al. 1994, Magnetocentrifugally driven flows from young stars and disks. I. A generalized model, ApJ 429, 781

[134] Sidoli, L. et al. 2001, An *XMM-Newton* study of the X-ray binary MXB 1659−298 and the discovery of narrow X-ray absorption lines, A&A 379, 540

[135] Sion, E.M. 1999, White Dwarfs in Cataclysmic Variables, PASP 111, 532

[136] Skinner, S.L., et al. 2002, *XMM-Newton* detection of hard X-ray emission in the Nitrogen-type Wolf-Rayet star WR110, ApJ 579, 76

[137] Smith, D.A. & Done, C. 1996,Unified theories of active galactic nuclei: a hard X-ray sample of Seyfert 2 galaxies, MNRAS, 280, 355

[138] Stelzer, B., & Burwitz, V. 2003, Castor A and Castor B resolved in a simultaneous *Chandra* and *XMM-Newton* observation, A&A 402, 719

[139] Stelzer, B. et al. 2002, Simultaneous X-ray spectroscopy of YY Gem with *Chandra* and *XMM-Newton*, A&A 392, 585

[140] Strohmayer, T.E., & Mushotzky, R.F. 2003, Discovery of X-Ray quasi-periodic oscillations from an ultraluminous X-Ray source in M82: Evidence against beaming, ApJ 552, L109

[141] Strüder, L. et al., 2001, The European Photon Imaging Camera on *XMM-Newton*: The pn-CCD camera, A&A, 365, L5

[142] Supper, R. et al. 2001, The second *ROSAT* PSPC survey of M 31 and the complete *ROSAT* PSPC source list, A&A 373, 63

[143] Sutaria, F.K. et al. 2002, *XMM-Newton* detection of Nova Muscae 1991 in quiescence, A&A 391, 993

[144] Tamura, T. et al. 2001a, *XMM-Newton* observations of the cluster of galaxies Abell 496. Measurements of the elemental abundances in the intracluster medium, A&A, 379, 107

[145] Tamura, T. et al. 2001b, X-ray spectroscopy of the cluster of galaxies Abell 1795 with *XMM-Newton*, A&A, 365, L87

[146] Tanaka, Y. et al. 1995, Gravitationally Redshifted Emission Implying an Accretion Disk and Massive Black-Hole in the Active Galaxy MCG-6-30-15, Nat, 375, 659

[147] Tanaka, Y., & Shibazaki, N. 1996, X-ray novae, ARA&A 34, 607

[148] Tiengo, A. et al. 2002, The anomalous X-ray pulsar 1E 1048.1−5937: Phase resolved spectroscopy with the *XMM-Newton* satellite, A&A 383, 182

Topka, K. et al. 1979, Detection of soft X-rays from Alpha Lyrae and Eta Bootis with an imaging X-ray telescope, ApJ, 229, 661

[149] Trudolyubov, S.P., et al. 2001, Bright X-Ray transients in the Andromeda Galaxy observed with *Chandra* and *XMM-Newton*, ApJ 563, L119

[150] Trudolyubov, S.P. et al. 2002a, On the X-Ray source luminosity distributions in the bulge and disk of M31: First results from the *XMM-Newton* survey, ApJ 571, L17

[151] Trudolyubov, S.P. et al. 2002b, The discovery of a 2.78 hour periodic modulation of the X-Ray flux from Globular Cluster Source Bo 158 in M31, ApJ 581, L27

[152] Turner, M.J.L. et al. 2001, The European Photon Imaging Camera on *XMM-Newton*: The MOS cameras, A&A, 365, L27

[153] Vaiana G.S., et al. 1981, Results from an extensive *Einstein* stellar survey, ApJ 244, 163

[154] Vilhu, O. 1984, The nature of magnetic activity in lower main sequence stars, A&A 133, 117

[155] Warwick, R.S. et al. 2001, The extended X-ray halo of the Crab-like SNR G21.5−0.9, A&A 365, L248

[156] Watson, M.G. et al. 2001,The *XMM-Newton* Serendipitous Survey. I. The role of *XMM-Newton* Survey Science Centre. A&A, 365, L51

[157] White, S.D.M., et al., 1993, X-ray archaeology in the Coma cluster, MNRAS, 261, L8

[158] Wijnands, R., & Van der Klis, M. 1998, A millisecond pulsar in an X-ray binary system, Nat. 394, 344

[159] Wijnands, R. 2003, An *XMM-Newton* observation during the 2000 outburst of SAX J1808.4−3658, ApJ 588, 425

[160] Wilkes, B.J. & Elvis, M.S. 1987, Quasar energy distributions. I - Soft X-ray spectra of quasars, ApJ, 323, 243

[161] Willingale, R. et al. 2002, X-ray spectral imaging and Doppler mapping of Cassiopeia A, A&A 381, 1039

[162] Willingale, R. et al. 2003, The mass and energy budget of Cassiopeia A, A&A 398, 1021

[163] Wilms, J. et al. 2001, XMM-EPIC observation of MCG-6-30-15: Direct evidence for the extraction of energy from a spinning black hole?, MNRAS, 328, L27

[164] Worrall, D.M. & Birkinshaw, M., 2003, The temperature and distribution of gas in CL 0016+16 measured with *XMM-Newton*, MNRAS, in the press (astro-ph/0301123)

Solar Magnetism and Astrophysical Spectropolarimetry

Javier Trujillo Bueno jtb@ll.iac.es
Instituto de Astrofísica de Canarias
38200 La Laguna, Tenerife

Abstract

Polarized light provides the most reliable source of information at our disposal for the remote sensing of astrophysical magnetic fields. In particular, the diagnosis of solar and stellar magnetic fields requires the measurement and theoretical interpretation of polarization signatures in spectral lines, which are induced by various physical effects taking place at the atomic level. The first part of this article presents a 'gentle' introduction to Astrophysical Spectropolarimetry*, emphasizing the importance of developing diagnostic tools that take proper account of the Zeeman effect, scattering polarization and the Hanle effect. Only in this way may we hope to investigate the strength and topology of stellar magnetic fields in a parameter domain which ranges from at least milligauss to many thousands of gauss. The second part of the paper shows some recent applications in solar physics with emphasis on the weakest magnetic fields of the photosphere, chromosphere and corona.*

Resumen

La polarización de la luz nos proporciona la fuente más fiable de información para la detección de campos magnéticos en astrofísica. En particular, el diagnóstico de campos magnéticos en el Sol y en otras estrellas requiere de la medida e interpretación teórica de señales de polarización en líneas espectrales, las cuales son inducidas por varios mecanismos físicos que actúan a nivel atómico. La primera parte de este artículo presenta una introducción a la *Espectropolarimetría en Astrofísica*, enfatizando la importancia de desarrollar técnicas de diagnóstico de plasmas que tengan en cuenta el efecto Zeeman, la polarización por procesos de dispersión ('scattering') y el efecto Hanle. Sólo de esta forma podemos aspirar a obtener información sobre la intensidad y topología de los campos magnéticos estelares en un rango que va desde sólo milésimas de gauss hasta varios miles de gauss. La segunda parte del artículo considera algunas aplicaciones en física solar, con énfasis en los campos magnéticos más débiles de la fotosfera, cromosfera y corona.

Introduction

Most observational work in Astrophysics has so far been carried out mainly on the basis of the intensity of the radiation received from the object observed as a function of wavelength. However, an important but frequently overlooked aspect of electromagnetic radiation is its state of polarization, which is related to the orientation of the electric field of the wave. The state of polarization of a quasi-monochromatic beam of electromagnetic radiation can be conveniently characterized in terms of four quantities that can be measured by furnishing our telescopes with a polarimeter. These observables are the four Stokes parameters (I, Q, U, V) which were formulated by Sir George Stokes in 1852 and introduced into astrophysics by the Nobel laureate Subrahmanyan Chandrasekhar in 1946.

As illustrated in Fig. 1, the Stokes $I(\lambda)$ profile represents the *intensity* as a function of wavelength, Stokes $Q(\lambda)$ the *intensity difference* between vertical and horizontal linear polarization, Stokes $U(\lambda)$ the *intensity difference* between linear polarization at $+45°$ and $-45°$, while Stokes $V(\lambda)$ the *intensity difference* between right- and left-handed circular polarization (cf. Born & Wolf 1994). Note that the definition of the Stokes Q and U parameters requires first choosing a reference direction for $Q > 0$ in the plane perpendicular to the direction of propagation.

There are numerous physical mechanisms that can generate polarized radiation (e.g. Rybicki & Lightman 1979; Landi Degl'Innocenti 2002): the Zeeman effect, which results in the splitting of atomic and molecular energy levels, Thomson, Rayleigh and/or Raman scattering processes, the Hanle effect, polarization due to aligned dust grains, cyclotron radiation produced by electrons spiraling in strong magnetic field lines, synchrotron radiation from relativistic electrons, etc. The polarization signals that are generated at each spatial point of the system under consideration, can often be strongly modified via radiative transfer effects. All the-

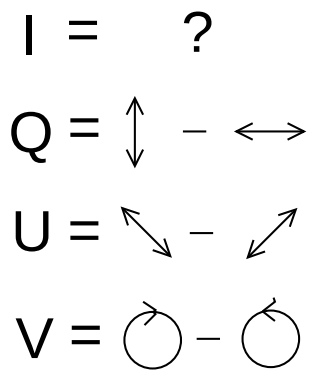

Fig. 1.: Pictorial definition of the Stokes parameters. The observer is facing the radiation source. The Stokes I parameter can be defined in the same way as done for Stokes Q, U or V, but with a '+' sign instead of a '−' sign. Adapted from Born & Wolf (1994) and Landi Degl'Innocenti (2002).

se physical mechanisms leave their 'fingerprints' on the polarization of the electromagnetic radiation that we collect with our increasingly large telescopes. Once the degree of polarization is correctly measured (ideally, for each wavelength), it is necessary to apply plasma diagnostic techniques to extract the information encoded in the Stokes profiles of the observed radiation beam. Such remote sensing techniques are based on the theory and numerical modeling of the generation and transfer of polarized radiation. We thus see that observational and theoretical spectropolarimetry may provide powerful diagnostics of the physical conditions in astrophysical systems, for instance, concerning magnetic fields, which cannot be obtained via conventional spectroscopy. Moreover, since completely unpolarized radiation can be expected only from a perfectly symmetric object, spectropolarimetry may also help us to verify the geometry of the astrophysical object under investigation, even without being possible to resolve it spatially.

Spectropolarimetry is being applied with great success in solar physics. Although its application to other fields of Astrophysics is still in an early stage of development, it is actually becoming increasingly attractive (see *Astrophysical Spectropolarimetry*, edited by Trujillo Bueno, Moreno Insertis & Sánchez 2002*a*). This is mainly due to the observational opportunities opened up by the new generation of ground-based and spaceborne telescopes, as well as to recent advances in the theory and numerical modeling of the generation and transfer of polarized radiation in magnetized plasmas. Particularly relevant examples, besides the Sun and peculiar A- and B-type stars, are young stellar objects and their surrounding disks, symbiotic stars, stellar winds, active galactic nuclei, black hole jets, magnetized neutron stars, X-ray pulsars, the interstellar medium, the cosmic microwave background radiation and its cosmological implications, etc. This introductory paper highlights the increasing interest of astrophysical spectropolarimetry by illustrating how remote sensing techniques based on the Hanle and Zeeman effects are allowing us to investigate the weak magnetism of the extended solar atmosphere.

The generation of polarized radiation

In stellar atmospheres the most important mechanisms that induce (and modify) polarization signatures in spectral lines are the Zeeman effect, scattering processes and the Hanle effect. The interesting point is that the development of diagnostic techniques that combine the Hanle and Zeeman effects in suitably chosen spectral lines may allow us to investigate the strength and topology of stellar magnetic fields in a parameter domain which ranges from at least milligauss to many thousands of gauss.

The Zeeman effect

As illustrated in Figure 2, the Zeeman effect requires the presence of a magnetic field which causes the atomic and molecular energy levels to split into different magnetic sublevels characterized by their magnetic quantum number M. Each level of total angular momentum J splits into $(2J+1)$ sublevels, the splitting being proportional to the level's Landé factor, g_J, and to the magnetic field strength. As a result, a spectral line between a lower level with (J_l, g_l) and an upper level with (J_u, g_u) is composed of several individual components whose frequencies are given by $\nu_{J_l M_l}^{J_u M_u} = \nu_0 + \nu_L(g_u M_u - g_l M_l)$, where ν_0 is the frequency of the line in the absence of magnetic fields and $\nu_L = 1.3996\times10^6 B$ is the Larmor frequency (with B the magnetic field strength expressed in gauss). In particular, a line transition with $J_l = 0$ and $J_u = 1$ has three components (see Fig. 2): one π component centered at ν_0 (or at λ_0), one $\sigma_{\rm red}$ component centered at $\nu_0 - g_u\nu_L$ (or at $\lambda_0 + g_u\Delta\lambda_B$), and one $\sigma_{\rm blue}$ component centered at $\nu_0 + g_u\nu_L$ (or at $\lambda_0 - g_u\Delta\lambda_B$), where $\Delta\lambda_B = 4.6686\times10^{-13}\lambda_0^2 B$ (with λ_0 in Å and B in gauss). The important point to remember is that the Zeeman splitting produces local *sources* and *sinks* of light polarization because of the ensuing wavelength shifts between the π ($\Delta M = M_u - M_l = 0$) and $\sigma_{b,r}$ ($\Delta M = \pm 1$) transitions.

The Zeeman effect is most sensitive in *circular* polarization (quantified by the Stokes V parameter), with a magnitude that, for not very strong fields, scales with the ratio between the Zeeman splitting and the width of the spectral line (which is very much larger than the natural width of the atomic levels!), and in such a way that the emergent Stokes $V(\lambda)$ profile changes its sign for opposite orientations of the magnetic field vector. This so-called *longitudinal* Zeeman effect responds to the line-of-sight component of the magnetic field. Accordingly, if we have a perfect cancellation of mixed magnetic polarities within the spatio-temporal resolution element of the observation, the measured circular polarization would be exactly zero *if* the thermodynamic and dynamic properties of the mixed magnetic components are similar. The antisymmetric shape of the Stokes $V(\lambda)$ profiles illustrated in Fig. 2 can be easily understood by noting the expression of the Stokes-V component of the emission vector:

$$\epsilon_V = \frac{h\nu}{4\pi} N_u A_{ul} \frac{1}{2}[\phi_{\rm red} - , \phi_{\rm blue}] \cos\theta, \qquad (1)$$

where θ is the angle between the magnetic field vector and the line of sight, A_{ul} the Einstein coefficient for the spontaneous emission process, N_u the number of atoms per unit volume in the upper level of the line transition under consideration, while $\phi_{\rm red}$ and $\phi_{\rm blue}$ are profiles that result from the superposition of the Voigt functions corresponding to each individual component.

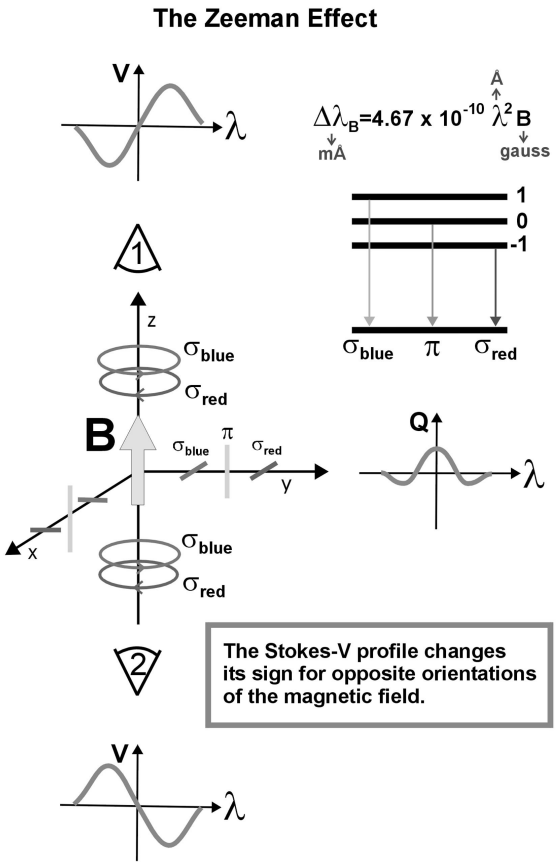

Fig. 2.: The oscillator model for the Zeeman effect indicating the characteristic shapes of the circular and linear polarization profiles as generated locally via the emission process. Note that the Stokes $Q(\lambda)$ profile is invariant to a reversal of the magnetic field direction, while it reverses sign when the transverse field is rotated by $\pm 90°$.

$\phi_{\rm red}$ is displaced to the red side of the central wavelength λ_0, and $\phi_{\rm blue}$ to the blue side. For instance, for the particular case of a line transition with $J_l = 0$ and $J_u = 1$, $\phi_{\rm red}$ is a Voigt profile centered at $\lambda_0 + g_u \Delta\lambda_B$ and $\phi_{\rm blue}$ a Voigt profile centered at $\lambda_0 - g_u \Delta\lambda_B$.

In contrast, the *transverse* Zeeman effect responds to the component of the magnetic field perpendicular to the line of sight, but produces *linear* polarization signals (quantified by the Stokes Q and U parameters) that are normally below the noise level of present observational possibilities for intrinsically weak fields (typically B < 100 gauss for solar spectropolarimetry). The Stokes Q and U profiles induced locally by the Zeeman effect have a three-lobe shape which is also illustrated in Fig. 2. This characteristic shape can be easily understood by noting that the expression of the Stokes-Q component of the emission vector is:

$$\epsilon_Q = \frac{h\nu}{4\pi} N_u A_{ul} \frac{1}{2} [\phi_\pi - (\frac{\phi_{\rm red} + \phi_{\rm blue}}{2})] \sin^2\theta \cos 2\chi, \quad (2)$$

where χ is the angle that the projection line of the magnetic field vector on the plane perpendicular to the direction of propagation forms with the reference direction chosen for $Q > 0$.[5]

Figure 3 shows an interesting example of Stokes profiles produced by the solar atmospheric plasma. The top panel is a section of the Fraunhofer spectrum between 4602 Å and 4610 Å showing the familiar absorption lines corresponding to several chemical elements. The remaining panels give the fractional polarizations $X(\lambda)/I(\lambda)$ (with $X = Q, U, V$). The spectrograph slit has been placed parallel to and 2.5 arcsec inside the limb (at $\mu = 0.07$, where μ is the cosine of the heliocentric angle), such that half of the slit covers a significantly magnetized region, while the other half lies outside it.[6] In the magnetically active region (which corresponds to the lower half of each of the four panels of Fig. 3) we see the characteristic signatures of the Zeeman effect. The V/I panel shows the typical antisymmetric signature of the longitudinal Zeeman effect with a positive and a negative lobe for each spectral line, while in the lower half of the panels for Q/I and U/I we see the typical symmetric signature of the transverse Zeeman effect with two lobes in the wings of opposite sign to the central lobe. Interestingly, as soon as we go outside the facular region (see the upper half of each of the four panels in Fig. 3) we see that the amplitude of the circular polarization is significantly reduced in all atomic lines, while practically the only existing linear polarization signal is the Q/I peak corresponding to the Sr I line at 4607 Å . However, the shape of this Q/I profile is Gaussian-like, suggesting that it is not produced by the transverse Zeeman effect. If it does not result from the Zeeman effect, what, then, could its physical origin be?

Atomic level polarization

The amplitudes of polarization signals induced by the Zeeman effect are very small when the Zeeman splitting becomes a very small fraction of the spectral line width. If there is no Zeeman splitting, there is no wavelength shift between the π and σ transitions, and there is no measurable polarization because the polarizations of such components cancel out.

However, it is easy to see that this is only true if the populations of the individual magnetic sublevels pertaining to the lower and/or upper levels of the spectral line under consideration are assumed to be identical.

[5] If you choose $\chi = 0$ (i.e., $\cos 2\chi = 1$), then $\epsilon_Q \neq 0$ (if the field is inclined with respect to the line of sight), but $\epsilon_U = 0$.

[6] 1 arcsec implies 725 km on the solar surface.

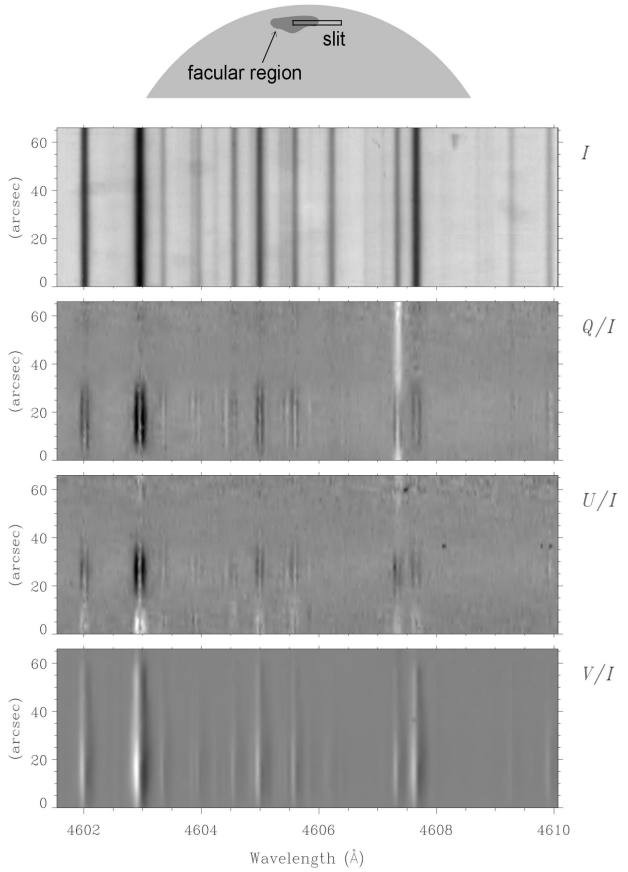

Fig. 3.: Spectropolarimetric observation close to the edge of the solar disk with half of the spectrograph slit crossing a moderately magnetized facular region. Note that while the characteristic signature of the longitudinal Zeeman effect is present at all spatial points along the slit, the signature of the transverse Zeeman effect disappears as soon as one goes outside the facular region. Interestingly, the only spectral line which shows linear polarization outside the facular region is the Sr I line at $\lambda 4607$ Å with a Q/I shape that has nothing to do with the transverse Zeeman effect. From Stenflo (2002).

To this end, consider the case of a line transition with $J_l = 0$ and $J_u = 1$ and choose the quantization axis of total angular momentum along the solar radius vector through the observed point. Assume that the population of the upper-level magnetic sublevel with $M_u = 0$ is *greater* than the populations of the magnetic sublevels with $M_u = \pm 1$. As a result, even in the absence of a magnetic field (zero Zeeman splitting), we can have a non-zero linear polarization signal, simply because the number of π transitions per unit volume and time will be larger than the ensuing number of σ transitions. Thus, a more general expression for the Stokes-Q component of the emission vector would be the following[7]

$$\epsilon_Q = \frac{h\nu}{4\pi} 3A_{ul} \frac{1}{2} [\rho_1(0,0)\phi_\pi - \frac{\rho_1(-1,-1)\phi_{\rm red} + \rho_1(1,1)\phi_{\rm blue}}{2}] \sin^2\theta \quad (3)$$

where θ is the angle between the solar radius vector through the observed point and the line of sight and $\rho_{J_u}(M,M)$ the population of the upper-level sublevel with magnetic quantum number M. This expression shows clearly that in the absence of a magnetic field (i.e., when $\phi_\pi = \phi_{\rm red} = \phi_{\rm blue}$ because their central wavelengths coincide at λ_0 for $B = 0$ gauss) the Stokes-Q profile is equal to the difference between two Voigt profiles: one centered at λ_0 and an extra one centered also at λ_0 but of *smaller* amplitude. This is precisely the explanation of the curious Q/I signal of the Sr I line seen Fig. 3, as observed in weakly magnetized regions close to the edge of the solar disk. Given that this spectral line has $J_l = 0$, its linear polarization is totally due to the population imbalances of the upper level.

On the other hand, it is very important to understand that in the absence of magnetic fields (or in weakly magnetized regions of stellar atmospheres) spectral lines with $J_l = 1$ and $J_u = 0$ can produce linear polarization *only* if there exist population imbalances among the magnetic sublevels of their *lower-level*. If this is the case, then linear polarization can be generated via the *selective absorption* resulting from the population imbalances of the lower level (Trujillo Bueno & Landi Degl'Innocenti 1997; Trujillo Bueno 1999, 2001; Trujillo Bueno et al. 2002*b*). The same applies to $J_l = 3/2 \rightarrow J_u = 1/2$ transitions, like the $\lambda 8662$ Å line of the Ca II IR triplet (Manso Sainz & Trujillo Bueno 2003). Interestingly, lower-level atomic polarization and the ensuing selective absorption mechanism (i.e., 'zero-field' dichroism) is the physical origin of the 'enigmatic' spectral features of the linearly-polarized solar limb spectrum (or *second solar spectrum*) which has been discovered recently using novel polarimeters that allow the detection of very low amplitude polarization signals (with $10^{-6} < Q/I < 10^{-3}$; see Stenflo & Keller 1997; Gandorfer 2000, 2002).

In summary, spectral line polarization can be produced by the mere presence of *atomic level polarization*, i.e., by the existence of population imbalances among the sublevels pertaining to the upper and/or lower atomic levels involved in the line transition under consideration.[8] Upper-level polarization imply *sources* of polarization (through the emission process), while lower-level polarization produce *sinks* of polarization (through the absorption process).

[7] I have chosen here the positive reference direction for $Q > 0$ such that $\cos 2\chi = 1$.

[8] As we shall see below while introducing the Hanle effect, the concept of *atomic polarization* includes also the possibility of quantum interferences (or coherences) among the magnetic sublevels of each J-level, and even among those belonging to different J-levels.

Anisotropic radiation pumping

What is the key physical mechanism that induces atomic level polarization in a stellar atmosphere? The answer is *the anisotropic illumination of the atoms*. This is easy to understand by considering the academic case of a unidirectional unpolarized light beam that illuminates a gas of two-level atoms with $J_l = 0$ and $J_u = 1$ and that is propagating along the direction chosen as the quantization axis of total angular momentum. Since these atoms can only absorb ± 1 units of angular momentum from the light beam, only transitions corresponding to $\Delta M = \pm 1$ are effective, so that no transitions occur to the $M = 0$ sublevel of the upper level. Thus, in the absence of any relaxation mechanisms, the upper-level sublevels with $M = 1$ and $M = -1$ would be more populated than the $M = 0$ sublevel and the *alignment coefficient* $\rho^2_0(J_u = 1) = (N_1 - 2N_0 + N_{-1})/\sqrt{6}$ would have a positive value.

Upper-level selective population pumping occurs when some *upper state* sublevels have more chance of being populated than others. On the contrary, as illustrated in Fig. 4, lower-level selective depopulation pumping occurs when some *lower state* sublevels absorb light more strongly than others. As a result, an excess population tends to build up in the weakly absorbing sublevels (Kastler 1950; Happer 1972; Trujillo Bueno & Landi Degl'Innocenti 1997; Trujillo Bueno 2001). It is also important to note that line transitions between levels having other total angular momentum values (e.g., $J_l = J_u = 1$) permit the transfer of atomic polarization between both levels via a process called *repopulation pumping* (e.g., lower-level atomic polarization can result simply from the spontaneous decay of a *polarized* upper level). The presence of a magnetic field is not necessary for the operation of such optical pumping processes, which can be particularly efficient in creating atomic polarization if the depolarizing rates from elastic collisions are sufficiently low. Figure 5 illustrates the type of anisotropic illumination in the outer layers of a stellar atmosphere.

The Hanle effect

The Hanle effect is the modification of the atomic-level polarization (and of the ensuing observable effects on the emergent Stokes profiles Q and U) caused by the action of a magnetic field that must be *inclined* with respect to the symmetry axis of the pumping radiation field. The basic formula to estimate the magnetic field intensity, $B_{\rm H}$ (measured in gauss), sufficient to produce a sizable change in the atomic level polarization results from equating the Zeeman splitting with the natural width (or inverse lifetime) of the energy level under consideration:

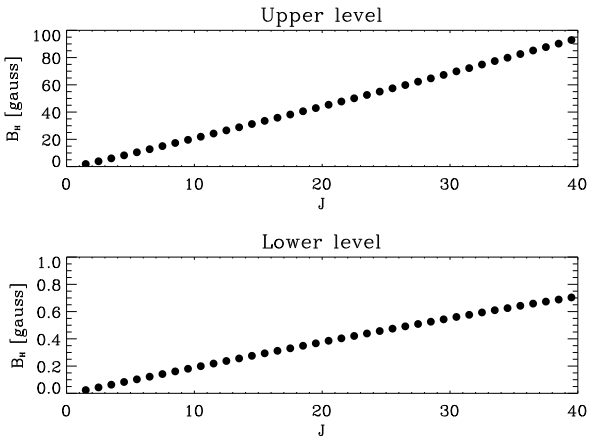

Fig. 6.: Example of the application of Eq. (4) to the lower and upper levels of MgH lines that produce scattering polarization signals on the Sun (see Gandorfer's 2000 Q/I atlas). Each point refers to a spectral line of the Q branch of MgH, whose lines have $J_l = J_u = J$. For each line the upper panel gives the strength of a 'turbulent' field that would be sufficient to produce a sizable change in the atomic polarization of the upper level. The bottom panel gives similar information, but concerning the lower level of each MgH line.

$$2\pi\nu_L\, g_J \;=\; 8.79{\times}10^6\; B_{\rm H}\; g_J \;\approx\; 1/t_{\rm life}\;, \qquad (4)$$

where ν_L is the Larmor frequency, while g_J and $t_{\rm life}$ are, respectively, the Landé factor and the level's lifetime (in seconds), which can be either the upper or the lower level of the chosen spectral line. As illustrated in Fig. 6, this formula shows that the Hanle effect in suitably chosen spectral lines may allow us to diagnose magnetic fields having intensities between 10^{-3} and 100 gauss approximately, i.e., in a parameter domain that is very hard to study via the Zeeman effect alone. Fig. 5 in Trujillo Bueno (2003a) shows an additional example which emphasizes that the observation and physical interpretation of scattering polarization in molecular lines offers a novel diagnostic tool for the empirical investigation of solar magnetoturbulence.

Figure 1 in Trujillo Bueno (2001) illustrates the oscillator model for the Hanle effect including a detailed classical description of the influence of a weak magnetic field on the linear polarization caused by scattering processes (see also Hanle 1924, Mitchell & Zemansky 1934, Landi Degl'Innocenti 1992, Stenflo 1994, Manso Sainz 2002). This classical explanation is relatively easy to understand and the reader is invited to read my 2001 review paper for a suitable introduction to the Hanle effect. In what follows, I provide a very brief description of the Hanle effect within the framework of quantum mechanics, since this is required for a deeper physical understanding of this fascinating mechanism that has

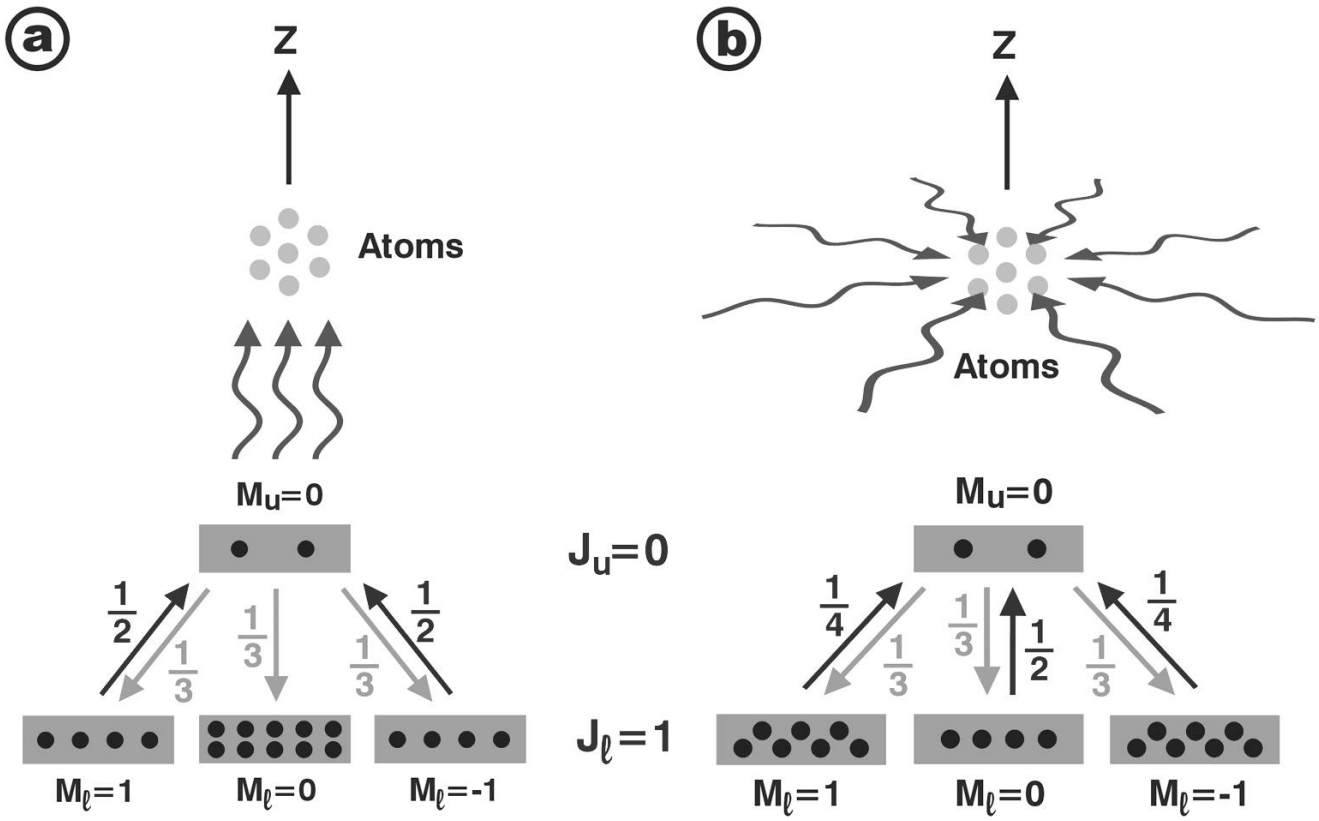

Fig. 4.: Illustration of the *atomic polarization* that is induced in the lower level of a two-level atom (with $J_l = 1$ and $J_u = 0$) by two types of anisotropic illuminations (**a** and **b**). The incident radiation field is assumed to be unpolarized and with axial symmetry around the vertical direction, which is our choice here for the quantization axis of total angular momentum. In both cases, an excess population tends to build up in the weakly absorbing sublevels. Note that the alignment coefficient of the lower level (i.e. $\rho^2_0 = (N_1 - 2N_0 + N_{-1})/\sqrt{6}$, N_i being the populations of the magnetic sublevels) is *negative* in case (**a**) (where the incident beam is *parallel* to the quantization axis), but *positive* in case (**b**) (where the incident beams are *perpendicular* to the quantization axis). The physical understanding of the information provided in this figure is left as an exercise to the reader.

found so many interesting applications in physics (see Moruzzi & Strumia 1991).

To that end, we need to recall first the concept of quantum coherence ($\rho_J(M, M')$) between different magnetic sublevels M and M' pertaining to each J-level. We say that the quantum coherence $\rho_J(M, M')$ is non-zero when the wave function presents a well defined phase relationship between the pure quantum states $|JM\rangle$ and $|JM'\rangle$. It is actually very common to find non-zero coherences while describing the excitation state of an atomic or molecular system under the influence of a pumping radiation field. Let us again consider a two-level atom with $J_l = 0$ and $J_u = 1$ that is being irradiated by an *unpolarized* radiation beam. In the absence of magnetic fields, all coherences of the upper level are zero *if* the quantization axis of total angular momentum is chosen along the symmetry axis of the pumping radiation beam. The same happens if a magnetic field is aligned with the quantization axis and this axis coincides with the symmetry axis of the radiation field that 'illuminates' the atomic system. This is because unpolarized radiation propagating along the quantization axis can only produce *incoherent* excitation of the upper-level sublevels with $M = \pm 1$.[9] If we now rotate the original reference system so that the new quantization axis for total angular momentum forms a non-zero angle with the symmetry axis of the radiation field, then non-zero coherences arise in this new reference system, even in the absence of a magnetic field. As shown below in Eq. (5), a magnetic field will *relax* such quantum coherences.

We thus see that the most general description of the excitation state of a J-level requires $(2J + 1)^2$ quantities: the individual populations ($\rho_J(M, M)$) of the $(2J + 1)$ sublevels and the degree of quantum coherence between each pair of them ($\rho_J(M, M')$). These quantities are nothing but the diagonal and non-diagonal elements of the *atomic density matrix* associated with the J-level, as given by the standard re-

[9]Note that an unpolarized radiation beam may be considered as the incoherent superposition of right-handed and left-handed circular polarization.

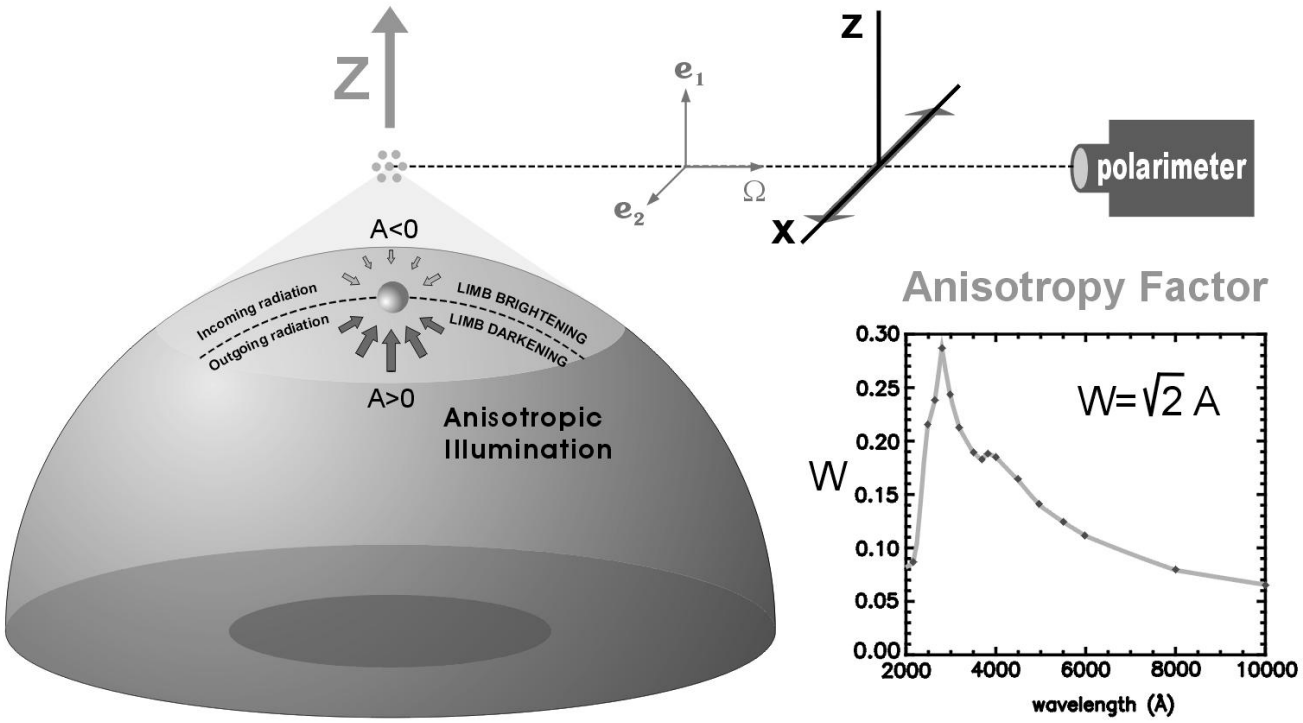

Fig. 5.: Anisotropic illumination of the outer atmospheric layers of a stellar atmosphere, indicating that the *outgoing* continuum radiation shows *limb darkening* while the *incoming* radiation shows *limb brightening*. The figure also illustrates the type of anisotropic illumination experienced by atoms situated at a given height above the visible 'surface' of the star, including the polarization analysis of the scattered beam at 90°. The 'degree of anisotropy' of the incident radiation field is quantified by $A = J^2_0/J^0_0$, where J^0_0 is the familiar *mean intensity* and $J^2_0 \approx \oint \frac{d\vec{\Omega}}{4\pi} \frac{1}{2\sqrt{2}}(3\mu^2 - 1) I_{\nu,\vec{\Omega}}$ (with $I_{\nu,\vec{\Omega}}$ the Stokes-I parameter as a function of frequency ν and direction $\vec{\Omega}$, while $\mu = \cos\theta$, with θ the polar angle with respect to the Z-axis). The possible values of the 'anisotropy factor' W $= \sqrt{2}\,A$ vary between W $= -1/2$, for the limiting case of illumination by a purely horizontal radiation field without any azimuthal dependence (case b of Fig. 4), and W $= 1$ for purely vertical illumination (case a of Fig. 4). It is important to point out that the larger the "anisotropy factor" the larger the fractional atomic polarization that can be induced, and the larger the amplitude of the emergent linear polarization. We choose the positive direction for the Stokes-Q parameter along the X-axis, i.e. along the perpendicular direction to the stellar radius vector through the observed point. The inset shows the wavelength dependence of the anisotropy factor corresponding to the center to limb variation of the *observed* solar continuum radiation. Note that W ≈ 0.14 at 5000 Å. Interestingly, the maximum anisotropy factor occurs around 2800 Å, i.e., very near the central wavelengths of the h and k lines of Mg II, whose polarization may contain valuable information on the magnetic fields and physical conditions of the solar transition region to the 10^6 K coronal plasma. This strongly suggests that we should urgently put a good UV polarimeter on a space telescope.

presentation. Alternatively, we can use the multipole components (ρ^K_Q) of the atomic density matrix, which are given by linear combinations of $\rho_J(M, M')$. The ρ^K_Q elements with $Q = 0$ are *real* numbers given by linear combinations of the populations of the various Zeeman sublevels corresponding to the level of total angular momentum J. The total population of the atomic level is quantified by $\sqrt{2J+1}\rho^0_0$, while the population imbalances among the Zeeman sublevels are quantified by ρ^K_0 (e.g., $\rho^2_0(J=1) = (N_1 - 2N_0 + N_{-1})/\sqrt{6}$ and $\rho^1_0(J=1) = (N_1 - N_{-1})/\sqrt{2}$). However, the ρ^K_Q elements with $Q \neq 0$ are *complex* numbers given by linear combinations of the *coherences* between Zeeman sublevels whose magnetic quantum numbers differ by Q (e.g., $\rho^2_2(J=1) = \rho(1,-1)$). These multipole components of the atomic density matrix provide the most useful way of quantifying, at the atomic level, the information we need for calculating the *sources* and *sinks* of polarization. In this respect, let us mention that the ρ^0_0 elements produce the dominant contribution to the Stokes I parameter, the ρ^1_Q elements (the *orientation* components) affect the circular polarization, while the ρ^2_Q elements (the *alignment* components) contribute to the *linear* polarization signals.

The Hanle effect can be suitably summarized by the following equation (cf. Landi Degl'Innocenti 1985):

$$\rho^K_Q(J_u) \;=\; \frac{1}{1+iQ\Gamma_u}[\rho^K_Q(J_u)]_{B=0}, \qquad (5)$$

where $\Gamma_u = 8.79{\times}10^6\ B\ g_{J_u}/A_{ul}$ and $[\rho^K_Q(J_u)]_{B=0}$ are the ρ^K_Q elements for the non-magnetic case defined in the reference frame in which the quantization axis is aligned with the magnetic field vector. This equation shows clearly that *in the magnetic field reference frame* the population imbalances (i.e., the ρ^K_Q elements with $Q = 0$) are unaffected by the magnetic field, while the ρ^K_Q elements with $Q \neq 0$ are *reduced* and *dephased* with respect to the non-magnetic case. The important point to remember is that the Hanle effect modifies the observed linear polarization because the polarization of the light that is emitted and/or absorbed at each point in the astrophysical system under consideration depends sensitively on the local values of the ρ^K_Q elements along the line of sight. Figure 7 attempts to contrast the diagnostic potential of the Zeeman and Hanle effects.

Finally, it is interesting to mention that the story of the Hanle effect began around 1922, when Wilhelm Hanle was working for his doctoral thesis at Göttingen University. He gave the first correct interpretation of a previously observed phenomenon related to the effect of a weak magnetic field on the *linear* polarization of the spectral-line radiation scattered by mercury vapor illuminated *anisotropically* (see Hanle 1924).[10] With respect to the linear polarization corresponding to the zero magnetic field case (as quantified by the measured Stokes Q amplitude after choosing the reference direction such that $U = 0$), the observed influence of a weak magnetic field (of the order of 1 gauss) was a *rotation* of the plane of linear polarization (i.e., the appearence of a non-zero Stokes-U amplitude) and a *depolarization* (i.e., a reduction in the value of $\sqrt{Q^2+U^2}$). This so-called Hanle effect played a fundamental role in the development of quantum mechanics because it led to the introduction and clarification of the concept of *coherent superposition* of pure states (see Bohr 1924; Hanle 1924, 1925; Heisenberg 1925). As we have hinted above, the Hanle effect is directly related to the generation of coherent superposition of degenerate Zeeman sublevels of an atom (or molecule) by a light beam.[11] As the Zeeman sublevels are split by the magnetic field, the degeneracy is lifted and the coherence (and, in general, also the population imbalances among the sublevels) are modified. This gives rise to a characteristic magnetic-field dependence of the linear polarization of the scattered light that is finding increasing application as a diagnostic tool for magnetic fields in astrophysics (e.g., Trujillo Bueno et al. 2002*a*).

[10] At that time modern quantum mechanics was not yet born and most theoreticians considered his effect as a kind of Faraday effect. Max Planck personally said to Hanle, "your interpretation cannot be correct. It contradicts quantum theory."

[11] A *coherent superposition* of two or more sublevels of a degenerate atomic level is a quantum mechanical state given by a linear combination of pure states of the atomic Hamiltonian.

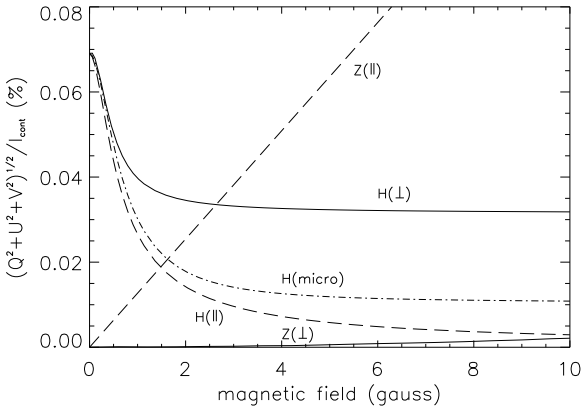

Fig. 7.: The Hanle effect versus the Zeeman effect. The figure shows the maximum polarization degree of a $J_l = 0 \rightarrow J_u = 1$ resonance line (with $A_{ul} = 10^7\ \mathrm{s}^{-1}$ and Doppler width $\Delta\nu_{\mathrm{D}} = 10^{10}\ \mathrm{s}^{-1}$) versus the magnetic field intensity. The simulated observation is close to the limb ($\mu = 0.1$) of a schematic solar atmospheric model. The polarization signals are due either to the Zeeman effect (Z) or to the Hanle effect (H). The dashed–dotted line gives the sensitivity of the Hanle effect to a *microturbulent and isotropic* magnetic field. Note that for this kind of mixed-polarity scenario there is no Zeeman signal. The two other cases are for a magnetic field *parallel* to the stellar surface, and oriented either along the x-axis of Fig. 5 (curves with the symbol $\perp$) or along the y-axis (curves with the symbol $\parallel$). The polarimetric signals corresponding to the transverse Zeeman effect (see the solid line labeled Z($\perp$)) have been multiplied by a factor 10 to make them visible in the figure. Note that for magnetic field intensities greater than 10 gauss (i.e. for the saturated Hanle-effect regime where $\Gamma_u \gg 1$) the "Hanle-effect signal" is *only* sensitive to the *orientation* of the magnetic field vector, but not to its intensity. This can occur for a Zeeman splitting which is still a very small fraction of the width of the spectral line. It is important to point out that a Hanle-effect diagnostics requires comparison of the observed linear polarization with that expected for the zero-field reference case.

The transfer of polarized radiation

In general, the physical interpretation of spectral line polarization requires calculating, for *multilevel* systems, the excitation and ionization state of chemical species of given abundance that is *consistent* with both the *intensity* and *polarization* of the radiation field generated within the (generally magnetized) plasma under consideration. This is a very involved *non-local* and *non-linear* radiative transfer (RT) problem which requires solving the rate equations for the elements of the atomic density matrix (see below) and the Stokes-vector transfer equation for each of the allowed transitions in

the multilevel model. Once such a selfconsistent excitation state is known along the line of sight, it is then straightforward to solve the transfer equation in order to obtain the emergent Stokes profiles to be compared with spectropolarimetric observations.

The Stokes-vector transfer equation

In the polarized case, instead of the standard RT equation for the specific intensity $I(x,\vec{\Omega})$ one has to solve, in general, the following *vectorial* transfer equation for the Stokes vector $\mathbf{I}(x,\vec{\Omega}) = (I,Q,U,V)^\dagger$ ($\dagger$ = transpose):

$$\frac{d}{ds}\begin{pmatrix} I \\ Q \\ U \\ V \end{pmatrix} = \begin{pmatrix} \epsilon_I \\ \epsilon_Q \\ \epsilon_U \\ \epsilon_V \end{pmatrix} - \\ - \begin{pmatrix} \eta_I & \eta_Q & \eta_U & \eta_V \\ \eta_Q & \eta_I & \rho_V & -\rho_U \\ \eta_U & -\rho_V & \eta_I & \rho_Q \\ \eta_V & \rho_U & -\rho_Q & \eta_I \end{pmatrix} \begin{pmatrix} I \\ Q \\ U \\ V \end{pmatrix}. \qquad (6)$$

This equation, whose *general* QED derivation can be found in Landi Degl'Innocenti (1983), can be written in more compact notation as follows:[12]

$$\frac{d}{ds}\mathbf{I} = \mathbf{e} - \mathbf{K}\mathbf{I}, \qquad (7)$$

where s measures the geometrical distance along the ray of direction $\vec{\Omega}$, and $\mathbf{e}$ is the emission vector. Its elements ϵ_I, ϵ_Q, ϵ_U, and ϵ_V account for the contribution of the *spontaneous emission* process to the intensity and polarization that is generated at each spatial point by the physical mechanism under consideration (see Section 2). The propagation matrix $\mathbf{K}$ can also be written as

$$\begin{pmatrix} \eta_I & 0 & 0 & 0 \\ 0 & \eta_I & 0 & 0 \\ 0 & 0 & \eta_I & 0 \\ 0 & 0 & 0 & \eta_I \end{pmatrix} + \begin{pmatrix} 0 & \eta_Q & \eta_U & \eta_V \\ \eta_Q & 0 & 0 & 0 \\ \eta_U & 0 & 0 & 0 \\ \eta_V & 0 & 0 & 0 \end{pmatrix} + \\ + \begin{pmatrix} 0 & 0 & 0 & 0 \\ 0 & 0 & \rho_V & -\rho_U \\ 0 & -\rho_V & 0 & \rho_Q \\ 0 & \rho_U & -\rho_Q & 0 \end{pmatrix}. \qquad (8)$$

This expression helps to clarify that the propagation matrix has three contributions: absorption (the first matrix, $\mathbf{K_1}$, which is responsible for the attenuation of the radiation beam irrespective of its polarization state), dichroism (the second matrix, $\mathbf{K_2}$, which accounts for a selective absorption of the different polarization states), and dispersion (the third matrix, $\mathbf{K_3}$, which describes the dephasing of the different polarization states as the radiation beam propagates through the medium). Actually, the situation is more complicated (and interesting!) because in general the *propagation* matrix $\mathbf{K} = \mathbf{K}^{\rm A} - \mathbf{K}^{\rm S}$, where $\mathbf{K}^{\rm A}$ is the above-mentioned contribution resulting from transitions from the lower-level towards the upper-level, while $\mathbf{K}^{\rm S}$ is the contribution caused by the stimulated emission process. Thus, $\mathbf{K}_1^{\rm S}$ would be the amplification matrix (responsible for the amplification of the radiation beam irrespective of its polarization state), $\mathbf{K}_2^{\rm S}$ would be the dichroism matrix (responsible of a selective stimulated emission of different polarization states), and $\mathbf{K}_3^{\rm S}$ would be the corresponding dispersion matrix. Taking $\mathbf{K}_2^{\rm S}$ and $\mathbf{K}_3^{\rm S}$ into account may be of very great interest for new discoveries in the field of astronomical masers.

The general expressions of the components of the emission vector and of the propagation matrix are very involved and will not be reproduced here (see Landi Degl'Innocenti 1983). They are given in terms of the ρ^K_Q elements of the upper and lower levels of the line transition under consideration and of line-shape profiles, whose dependence on the magnetic quantum numbers cannot be neglected when the Zeeman splittings are a significant fraction of the spectral line width. Such general expressions simplify considerably for several cases of practical interest. For instance, in the case of scattering line polarization in weakly magnetized regions of stellar atmospheres, ϵ_Q (η_Q) is a direction-dependent function of ρ^2_Q(up) (ρ^2_Q(low)), with $Q = 0,1,2$, while ϵ_U (η_U) is a different direction-dependent function of ρ^2_Q(up) (ρ^2_Q(low)), but with $Q = 1,2$. Thus, ϵ_Q and η_Q depend on both the population imbalances (ρ^2_0) and the quantum coherences (Re(ρ^2_1), Im(ρ^2_1), Re(ρ^2_2), Im(ρ^2_2)), while ϵ_U and η_U depend *only* on the coherences. Typically, in stellar atmospheres ϵ_I (η_I) is dominated by the overall population of the upper (lower) levels (i.e. by ρ^0_0(up) or ρ^0_0(low)).

Fortunately, there are situations of practical interest for which the expressions of ϵ_Q and η_Q simplify considerably because the quantum coherences turn out to vanish (i.e. $\rho^2_1 = \rho^2_2 = 0$). To this end, one has to choose the quantization axis of total angular momentum along the symmetry axis of the pumping radiation field (e.g., along the stellar radius vector for a one-dimensional stellar atmosphere model) and to assume that either the medium is unmagnetized or, for example, that the magnetic field is everywhere *microturbulent* and *isotropically distributed* with mixed magnetic polarities within very small scales (i.e., below the photon mean-free path). Under these assumptions a very useful formula can be derived which can be applied to estimate the

[12] The derivation of the Stokes-vector transfer equation is greatly simplified if local thermodynamic equilibrium (LTE) is assumed and the classical model of the radiation-matter interaction is used (e.g., Jefferies, Lites & Skumanich 1989; Landi Degl'Innocenti 1992; Stenflo 1994; del Toro Iniesta 2003; see also the original works of Unno 1956, Stepanov 1958, and Rachkovsky 1962a,b).

emergent fractional polarization at the core of a strong spectral line for an observation along the line of sight specified by $\mu = \cos\theta$ (Trujillo Bueno 1999; 2001):[13]

$$Q/I \approx \frac{3}{2\sqrt{2}}(1-\mu^2)[\mathcal{W}\,\sigma_0^2(\mathrm{up}) - \mathcal{Z}\,\sigma_0^2(\mathrm{low})], \quad (9)$$

where $\sigma_0^2 = \rho_0^2/\rho_0^0$ quantifies the *fractional atomic alignment* or *degree of population imbalance* of the upper or lower level of the line transition under consideration, while $\mathcal{W}$ and $\mathcal{Z}$ are simply numbers which depend on the quantum numbers of the transition (e.g., $\mathcal{W} = \mathcal{Z} = -1/2$ for a transition with $J_l = J_u = 1$). For example, $\sigma_0^2 = 0$ if the magnetic sublevels of the J-level under consideration turn out to be equally populated. Thus, the fractional linear polarization $Q/I = 0$ if $\sigma_0^2 = 0$ in the upper and lower levels of the spectral line under consideration. In Eq. (9) the σ_0^2 values are those corresponding to the optical depth τ where $\tau/\mu \approx 1$ (which means $\tau = 0$ for a solar limb observation at $\mu = 0$). This expression for Q/I shows clearly that the observed fractional polarization produced by scattering processes in a given spectral line in general has two contributions: one from the fractional alignment of the upper-level ($\sigma_0^2(\mathrm{up})$) and an extra one from the fractional alignment of the lower level ($\sigma_0^2(\mathrm{low})$). In general, the first contribution (caused exclusively by the emission events from the polarized upper level) is the only one that is normally taken into account. However, the second contribution (caused by the selective absorption resulting from the population imbalances of the lower level) plays the key role in producing the 'enigmatic' linear polarization signals that have been discovered recently in 'quiet' regions close to the solar limb, as well as in solar coronal filaments (see the reviews by Trujillo Bueno 1999, 2001, 2003*a*; see also Trujillo Bueno & Manso Sainz 2002).

The rate equations for the elements of the atomic density matrix

Since we are interested in the general Non-LTE case in which both collisions and radiative transitions can influence the excitation state, we need also to consider the master equation for the atomic density matrix (see Cohen-Tannoudji et al. 1977, 1992; Landi Degl'Innocenti 1983). Perhaps, the simplest and most famous example of this approach is that formulated by Einstein, who in 1917 introduced rate equations describing the effect of absorption, stimulated emission, and spontaneous emission processes between two levels of an atom immersed in a black-body radiation field (see also Mihalas 1978). The situation is considerably more complex (and interesting!) in the present "polarized case" in which we have *atomic and light polarization* instead of simply overall population of the atomic levels and intensity. For instance, for a multilevel atom devoid of hyperfine structure and taking into account quantum coherences only between the sublevels pertaining to each J-level, the rate of change of the density matrix element $\rho^K_Q(J)$ *in the magnetic field reference system* reads

$$\frac{d}{dt}\rho^K_Q(J) = -2\pi\mathrm{i}\nu_L\, g_J\, Q\, \rho^K_Q(J) \quad (10)$$

$$+\sum_{J_l}\sum_{K_l Q_l} \rho^{K_l}_{Q_l}(J_l)\, T_{\mathrm{A}}(J_l; K_l\, Q_l \rightarrow J; K\, Q)$$

$$+\sum_{J_u}\sum_{K_u Q_u} \rho^{K_u}_{Q_u}(J_u)\, T_{\mathrm{E}}(J_u; K_u\, Q_u \rightarrow J; K\, Q)$$

$$+\sum_{J_u}\sum_{K_u Q_u} \rho^{K_u}_{Q_u}(J_u)\, T_{\mathrm{S}}(J_u; K_u\, Q_u \rightarrow J; K\, Q)$$

$$-\sum_{K' Q'} \rho^{K'}_{Q'}(J)\, R_{\mathrm{A}}(J; K\, Q, K'\, Q' \rightarrow J_u)$$

$$-\sum_{K' Q'} \rho^{K'}_{Q'}(J)\, R_{\mathrm{E}}(J; K\, Q, K'\, Q' \rightarrow J_l)$$

$$-\sum_{K' Q'} \rho^{K'}_{Q'}(J)\, R_{\mathrm{S}}(J; K\, Q, K'\, Q' \rightarrow J_l)$$

$$-D^{(K)}(J)\, \rho^K_Q(J),$$

where $\nu_L = 1.3996 \times 10^6\, B$ is the Larmor frequency (with the magnetic field strength, B, in gauss). Besides including collisional rates like the last term on the rhs, which describes the local depolarization caused by elastic collisions, this equation accounts for radiative rates, both in the *transfer* rates due to absorption (T_{A}), spontaneous emission (T_{E}) and stimulated emission (T_{S}) *from* other levels, and on the *relaxation* rates due to absorption (R_{A}), spontaneous emission (R_{E}) and stimulated emission (R_{S}) *towards* other levels.[14] The explicit expressions for all these transfer and relaxation rates can be deduced from Landi Degl'Innocenti's (1983) polarization transfer theory. In particular, the transfer and relaxation rates due to absorption and to stimulated emission depend explicitly on a number of radiation field tensors which describe the symmetry properties of the radiation field (e.g., the *mean intensity* J^0_0 and the *anisotropy* J^2_0 defined in the caption of Fig. 5).

If the radiation field that illuminates the atomic or molecular system is given, one can then directly solve the statistical equilibrium equations (i.e., $\frac{d}{dt}\rho^K_Q(J) = 0$) in order to obtain the values of the ρ^K_Q elements. This directly solves *the optically thin problem* because,

[13] In this expression, I have chosen the reference direction for $Q > 0$ along the line perpendicular to the stellar radius vector through the observed point, i.e., the parallel to the stellar limb as illustrated in Fig. 5.

[14] For notational simplicity, I have not included the inelastic collisional rates, which are however taken into account in our radiative transfer simulations.

as mentioned above, the I, Q, U and V components of the emission vector are given in terms of the ρ^K_Q elements. However, in *optically thick media* we do not know a priori the radiation field within the medium. Therefore, in this more general case we are obliged to find the selfconsistent ρ^K_Q-values by solving iteratively the *non-local* and *non-linear* system of equations formed by the rate equations for the diagonal and non-diagonal elements of the atomic density matrix and the Stokes-vector transfer equations (see Trujillo Bueno & Manso Sainz 1999; Trujillo Bueno 2003*b*).

Finally, it is important to note that the astrophysical problem of the generation and transfer of polarized radiation is enormously simplified when the approximation of local thermodynamic equilibrium (LTE) is used, i.e., when one assumes that radiative transitions play no role in the populations of the energy levels[15]. As a result, there can be no atomic level polarization (i.e., neither population imbalances nor quantum interferences among the level's substates). In other words, the commonly made assumption of LTE excludes from the outset scattering line polarization and the Hanle effect. Moreover, it restricts the applicability of the Zeeman effect to spectral lines for which the LTE approximation turns out to be justified, and this depends on the particular stellar atmosphere model under consideration. In conclusion, the diagnostic potential of spectropolarimetry is drastically reduced if polarization signatures resulting from 'Non-LTE effects' are disregarded. In order to open a truly empirical window on solar and stellar magnetism we must develop and apply remote sensing techniques based on both the Hanle and Zeeman effects.

Applications in solar physics

This section shows some selected examples which illustrate how remote sensing techniques based on the Hanle and Zeeman effects are allowing us to investigate the weak magnetism of the extended solar atmosphere. I consider only some aspects of the magnetism of the 'quiet' Sun.[16] In fact, this is the only relevant situation during the minimum of the solar magnetic activity cycle, in which no sunspots are seen on the solar surface. However, even during periods of strong magnetic activity, there are many examples of solar plasma structures, such as spicules and prominences, which play a key role with regard to the solar mass flux and energetics, and which owe their very existence to the presence of weak magnetic fields.

The hidden face of solar surface magnetism

When one uses the Zeeman effect as a diagnostic tool of the 'quiet' regions of the solar photosphere (e.g., Lin & Rimmele 1999; Sánchez Almeida & Lites 2000; Collados 2001; Domínguez Cerdeña et al. 2003; Khomenko et al. 2003), one is able to obtain very useful empirical information like that given in Fig. 8, which shows a high-spatial resolution image of the solar 'surface' with bright granules (where the gas is upflowing) surrounded by dark inter-granular lanes (where the gas is downflowing).[17] Overlaid on it we can see solid-line and dotted-line contours indicating the opposite magnetic polarities that were detected by a simultaneously recorded high-resolution longitudinal magnetogram, which is a map of the circular polarization at a given wavelength in the wing of a spectral line. In this case, the visible Fe I line at 6302.5 Å was used, but the Stokes I and V profiles of the nearby Fe I line at 6301.5 Å were also recorded via two-dimensional Fabry-Perot spectropolarimetry. The spatial resolution was $0.5''$ approximately, which implies a spatial resolution element of about 360×360 km^2. This observation of the Zeeman effect in visible lines has been interpreted in terms of magnetic flux concentrations of very small size in diameter having intrinsic field strengths exceeding 1 kG and occupying only about 2% of the solar surface (Domínguez Cerdeña et al. 2003). On the other hand, recent observations of the Zeeman effect using the IR Fe I lines at $\lambda1.56\,\mu$m confirm that the photospheric plasma of the 'quiet' Sun has a *continuous distribution of magnetic field strengths*, from the kilogauss range to *at least* 300 gauss, in such a way that the weaker the field the larger the probability of finding a magnetic field intensity between B and $B + \mathrm{d}B$ when no distinction is made between points located above granules and intergranular lanes (see Khomenko et al. 2003).

In the hydrodynamically controlled photosphere we expect to have highly tangled field lines with resulting mixed magnetic polarities on very small spatial scales, well below the current spatial resolution limit. For this reason, we think that via Zeeman effect diagnostics with the available instrumentation we are seeing only the "tip of the iceberg" of solar surface magnetism ($\sim$1% of the photospheric volume according to Stenflo 1994, Domínguez Cerdeña et al. 2003, and Khomenko et al. 2003). Obviously, it is to be expected that more locations with magnetic fields will be detected via the Zeeman effect when increasing the spatial resolution, and this is only one of the many scientific reasons for pursuing the development of balloon-borne telescopes

[15] The LTE approximation assumes that the level populations are only *locally* controled by collisions with an *isotropic* distribution of colliders.

[16] The interested reader will find several excellent review papers on solar and stellar magnetism in the workshops edited by Sigwarth (2001), Mathys, Solanki, & Wickramasinghe (2001), and Trujillo Bueno & Sánchez Almeida (2003). For the most recent review on sunspot magnetic fields see Solanki (2003). See also the book of Schrijver & Zwaan (2000) on Solar and Stellar Magnetic Activity.

[17] See Bonet (1999) for an overview on high spatial resolution techniques.

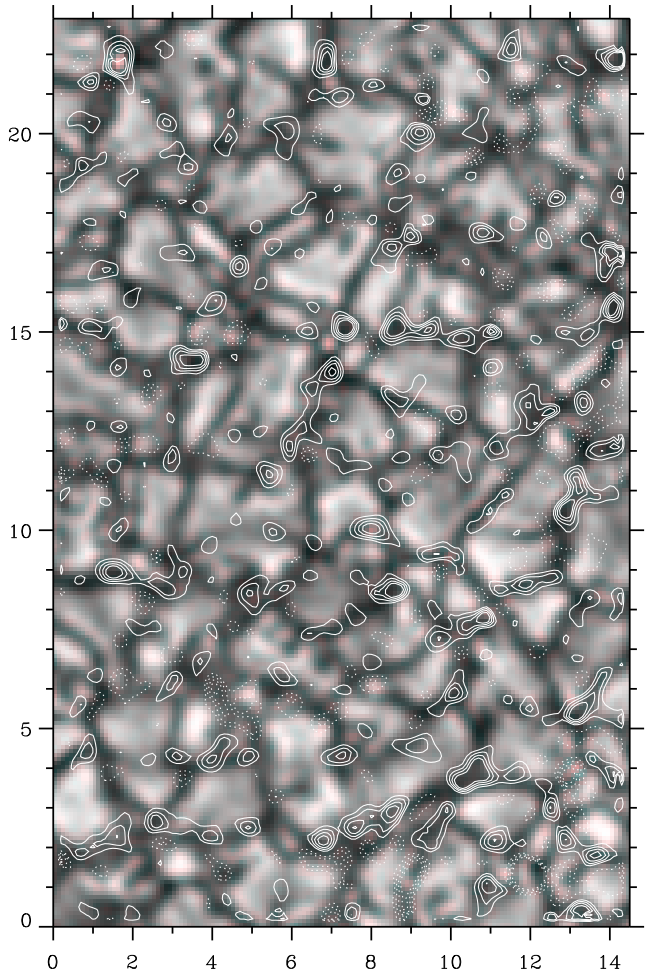

Fig. 8.: Speckle reconstructed broad-band image of the solar 'surface' overlaid with a magnetogram taken in the wing of the Fe I λ6302.5 Å line. The solid and dotted contours indicate opposite magnetic polarities. Note that most of the magnetic flux detected via the longitudinal Zeeman effect in this Fe I line is located in the inter-granular lanes, where the gas is downflowing. The distance between tick marks is 1 arcsec. From Domínguez Cerdeña et al. (2003).

like SUNRISE[18], or space-borne telescopes like Solar-B[19], Solar Orbiter[20] or SDO[21], and large ground-based solar telescopes like GREGOR[22] or the Advanced Technology Solar Telescope[23].

But how to investigate in a reliable way the magnetism of the remaining $\sim 99\%$ of the volume of the 'quiet' solar atmosphere? How to obtain empirical information on the distribution of *intrinsically weak* fields (e.g. with $0 < B < 300$ gauss)? Do such fields carry most of the unsigned magnetic flux of the Sun? Or is this flux dominated by small magnetic flux concentrations in the kG range as some recent investigations seem to suggest (e.g. Socas-Navarro & Sánchez Almeida 2003)? How is energy transported in a mixed magnetic-polarity environment? Can the ensuing magnetic field lines reach the solar chromosphere and corona? As discussed above, Zeeman effect polarization suffers from cancellation effects. Moreover, Zeeman polarization signals of subgauss fields (e.g., with strengths in the milligauss range) have tiny amplitudes, well below the detection limit of the available instrumentation. Therefore, the investigation of magnetoturbulence via spectropolarimetry cannot be done via the Zeeman effect *alone*. We need to complement our Zeeman diagnostic tools developed to interpret the observed *anomalous* Stokes profiles resulting from opposite magnetic polarities that do not cancel completely within the resolution element (e.g., Socas-Navarro & Sánchez Almeida 2002) with new diagnostic techniques based on physical mechanisms whose polarization signals do not suffer from cancellation effects and are sensitive to intrinsically weak fields.

The Hanle effect may well have the required diagnostic potential (e.g., Stenflo 1994; see also Fig. 7), but the problem is how to apply it to obtain reliable information given that a Hanle-effect diagnostics relies on a comparison between the observed linear polarization and that calculated for the zero-field reference case. Shchukina & Trujillo Bueno (2003) have recently demonstrated that reliable diagnostics can be achieved by means of *three-dimensional* (3D) scattering polarization calculations in snapshots taken from realistic simulations of solar surface convection (see Stein & Nordlund 1998; Asplund et al. 2000). These radiation hydrodynamical simulations of the photospheric physical conditions are very convincing because spectral synthesis of a multitude of iron lines shows remarkable agreement with the observed spectral line profiles when the meteoritic iron abundance is chosen (Shchukina & Trujillo Bueno 2001). Therefore, we have used snapshots taken from such time-dependent hydrodynamical simulations in order to calculate the emergent Stokes profiles via 3D scattering polarization calculations using multilevel atomic models. Our first target has been the Sr I line at λ4607 Å, which is a normal triplet transition with $A_{ul} \approx 2 \times 10^8 \mathrm{s}^{-1}$ and Landé factor $g_{J_u} = 1$. We find that the spatially and temporally averaged Stokes profiles give a Q/I that is larger than the observed Q/I, thus indicating the need for invoking magnetic depolarization.

The basic formula of the Hanle effect (see Eq. 4) indicates that a 'turbulent' magnetic field with strength $B_H \approx 23$ gauss is more than sufficient to produce a sizable change in the emergent polarization of the Sr I line at λ4607 Å. In practice, the scattering polarization of this spectral line is sensitive to field strengths between 1 and 300 gauss, approximately. Our numerical simulations of the Hanle effect in the Sr I line taking into

[18] http://star.mpae.gwdg.de/Sunrise/
[19] http://science.msfc.nasa.gov/ssl/pad/solar/solar-b.stm
[20] http://sci.esa.int/home/solarorbiter/index.cfm
[21] http://sdo.gsfc.nasa.gov/
[22] http://gregor.kis.uni-freiburg.de/
[23] http://atst.nso.edu/

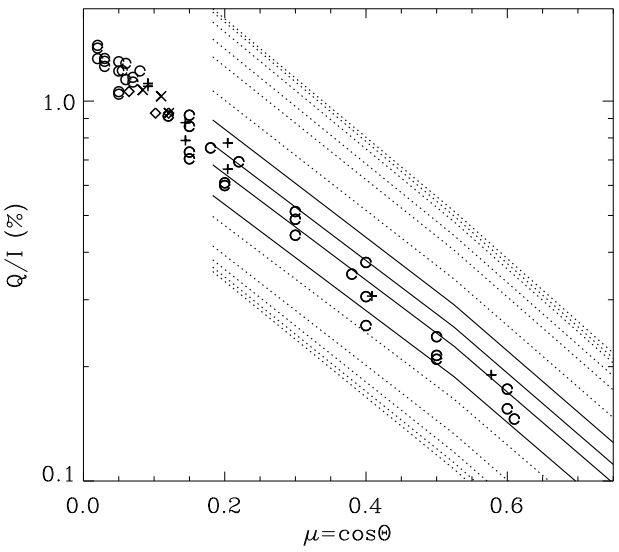

Fig. 9.: Center-to-limb variation of the fractional linear polarization at the core of the Sr I λ4607 line after substraction of the continuum polarization. $\mu = \cos\theta$, with θ the angle formed by the line of sight and the solar radius vector through the observed point. The symbols indicate observations during the minimum of the solar magnetic activity cycle (see the 'circles', from Stenflo et al. 1997, which refer to September–October 1995 observations using the Gregory Coudé Telescope at Locarno) and during the following maximum of the solar cycle (with the 'diamonds' symbols indicating the observations of Trujillo Bueno et al. 2001 taken during May 2000 with the French-Italian telescope THÉMIS at the Observatorio del Teide, with the '×' symbols showing the observations of Bommier & Molodij (2002) taken with THÉMIS during August 2000, and with the '+' symbols showing Bommier's (2002) most recent observations). The dotted and solid lines result from our Hanle-effect simulations for increasing values of a 'turbulent' field. The uppermost dotted line refers to the unmagnetized reference case. The extra lines (from top to bottom) refer to 5, 10, 15, 20, 30, 40, 50, 60, 80, 100, 150, 200, 250, 300 gauss. Note that there is no evidence of a variation of the 'turbulent' field with the solar cycle. From Shchukina & Trujillo Bueno (2003).

account 3D radiative transfer effects in realistic multilevel models show that a microturbulent magnetic field of about 60 gauss leads to a notable agreement with the observed Q/I (see Fig. 9). As seen in this figure, there seems to be an indication that the strength of the 'turbulent' field[24] required to explain the Q/I observations decreases with height in the atmosphere, from the 80 gauss needed to explain the observations at $\mu = 0.6$ to the 40 gauss required to fit the observations at $\mu = 0.1$. This corresponds to an approximate height range of between 200 and 400 km above the solar 'surface' (as seen at continuum optical depth unity).

Alternatively, instead of a single-valued 'turbulent' field that fills the entire photospheric volume, we may assume a continuous distribution of field strengths with a given probability density function (PDF). Unfortunately, with one single spectral line we do not have enough information to constrain the *shape* of the PDF[25]. Nevertheless, if we *assume* that the weak-field part of the PDF has an exponential shape ($e^{-B/B_0}/B_0$), as suggested by recent numerical experiments of turbulent dynamos and magnetoconvection (e.g., Cattaneo 1999; Stein & Nordlund 2003), we then find that $B_0 \approx 130$ gauss yields a fairly good fit to the observed fractional linear polarization. Taking into account that most of the solar surface is occupied by the 'quiet' inter-network regions of mixed polarity fields, and that for an exponential PDF the stronger the field the tinier the fraction of the photospheric volume it occupies, we would then conclude that the *unsigned magnetic flux* and *energy* carried by the intrinsically weak fields (e.g., with $B < 300$ gauss) is much larger than previously thought.

Finally, note that an extra relevant conclusion is the following: *there is no evidence of a variation of the 'turbulent' photospheric field with the solar cycle.* This is particularly important because it help us to choose among several possibilities on the origin of the 'quiet' Sun magnetic fields (e.g., Schrijver & Zwaan 2000). One is that the mechanism responsible for the generation of active regions and the origin of the solar cycle –the familiar solar dynamo that requires *rotation* to produce macroscopic order out of microscopic chaos– is responsible also for the small-scale magnetic activity of the quiet Sun (e.g., through the decay of active regions). The other possibility, strongly supported by our empirical investigation of magnetoturbulence via the Hanle effect, is that the magnetic fields in quiet photospheric regions are generated by *local* dynamo action (Cattaneo 1999) or perhaps by dynamo action within a larger convective domain of ionized gas (Stein & Nordlund 2003).

Chromospheric magnetism and solar spicules

As we have mentioned, most of the photospheric surface is occupied by the 'quiet' inter-network regions of mixed polarity fields and we have lots of good reasons to wish to know how important is the degree of intermittency of the chromospheric field (e.g., Trujillo Bueno & Manso Sainz 2002; Title 2003). Do chromospheric field lines result mainly from the extension of the underlying mixed polarity field of the 'quiet' solar photosphere? Or is the chromospheric field dominated by the field lines from the boundaries of the supergranulation network ?

[24] By 'turbulent' field I simply mean magnetic fields hidden to Zeeman effect diagnostics.

[25] To this end, a good choice would be the linearly polarized spectrum of Ti I whose physical origin has been investigated recently by Manso Sainz & Landi Degl'Innocenti (2002).

The true empirical answer to this type of question is encoded in the polarization of chromospheric spectral lines.

A serious problem is that chromospheric lines like the Ca II IR triplet are relatively broad, which implies that the weak magnetic fields of the 'quiet' chromospheric regions are very difficult to diagnose via sole consideration of the longitudinal Zeeman effect on which magnetograms are based on. Fortunately, in recent years, observational investigations of scattering polarization on the Sun have indicated the existence of 'enigmatic' linear polarization signals in several spectral lines observed in the 'quiet' solar chromosphere close to the solar north pole, which cannot be understood in terms of the classical theory of scattering polarization (Stenflo and Keller, 1997; Stenflo, Keller, & Gandorfer, 2000). These 'enigmatic' features of the linearly polarized solar-limb spectrum have motivated new theoretical investigations of scattering line polarization, which are now making feasible reliable confrontations between spectropolarimetric observations and multilevel radiative transfer simulations of the Hanle and Zeeman effects (see the reviews by Trujillo Bueno 1999, 2001, 2003*a*,*b*; see also Trujillo Bueno & Manso Sainz 2002). Such investigations have been carried out within the framework of the quantum theory of line formation (Landi Degl'Innocenti 1983), which allows us to formulate scattering polarization problems taking into account a key physical ingredient that had been previously neglected: ground-level atomic polarization (i.e., the existence of population imbalances and/or coherences among the Zeeman sublevels of the lower-level of the spectral line under consideration).

Let us consider the modeling issue of the 'enigmatic' linear polarization signatures of the Ca II IR triplet observed by Stenflo et al. (2000) in 'quiet' regions close to the solar limb. This topic has been investigated in detail by Manso Sainz & Trujillo Bueno (2001) and by Trujillo Bueno & Manso Sainz (2002). Fig. 10 shows the fractional linear polarization at the line core of each spectral line calculated at $\mu = 0.1$ (about $5''$ from the limb) assuming magnetic fields of given inclination, but with a random azimuthal component within the spatio-temporal resolution element of the observation. Note, in particular, that the linear polarization of the lines at λ8542 Å and λ8662 Å respond to *milligauss* fields. This is because their linear polarization is caused by the atomic polarization of their *long-lived* lower-levels. Consequently, their observed Q/I signals are sensitive to very weak fields (see Eq. 4). This offers a new diagnostic window onto the magnetism of the solar chromosphere with very interesting applications in other astrophysical contexts too (see Manso Sainz & Trujillo Bueno 2003).

The results of Fig. 10 are really interesting. They indicate that by comparing the observed fractional polarization amplitudes in the three IR lines of ionized calcium, we may hope to investigate empirically whether or not milligauss fields in the 'quiet' solar chromosphere can have a sizable filling factor. Thus, if the Q/I line-core amplitudes of 0.035%, 0.13%, and 0.12% reported by Stenflo et al. (2000) are really accurate, then we could explain them via a distribution of subgauss fields with pretty chaotic field lines. On the other hand, if one opts for chromospheric fields with strengths in the gauss range, then we see in Fig. 10 that there are two possible magnetic-field topologies for which the limb polarization signals of the 8542 and 8662 Å lines can have amplitudes with $Q/I \geq 0.1\%$ (i.e., of the order of the observed ones). As one might have expected, the first topology corresponds to magnetic fields with inclinations $\theta_B \leq 30^\circ$ (because the Hanle effect is not efficient for vertical fields). The second corresponds to magnetic fields which are practically parallel to the solar surface, i.e. 'horizontal' fields with $80^\circ \leq \theta_B \leq 100^\circ$. The physical interpretation of our own spectropolarimetric observations of scattering polarization in chromospheric lines in terms of the Hanle and Zeeman effects indicates that the topology of the solar chromospheric field is considerably more complex than previously thought and with a distribution of field strengths. A physically plausible scenario that might lead to polarization signals in agreement with the observations is that resulting from the superposition of myriads of different loops of magnetic field lines connecting opposite polarities.

Let us now address the following question of how we could investigate the magnetism of the upper solar chromosphere. In my opinion, one attractive possibility is via spectropolarimetric observations of *solar spicules*. These features were described in 1877 by Father Secchi as jet-like, elongated structures in the solar atmosphere. Spicules are best seen when observing a few arcsec off the limb in the chromospheric emission lines of Hα, the H and K lines of ionized calcium at 393 nm and 397 nm, and in lines like the 588 nm and 1083 nm lines of He I. It is commonly believed that most of the chromospheric emission in these lines comes from spicules, and that at heights exceeding 1500 km above the photosphere the solar chromosphere is mainly composed of spicular material. As reviewed by Beckers (1972), these 'geyser-like' plasma structures have a typical height of 9000 km, while their average width is at least an order of magnitude smaller. They show upward velocities reaching 25 km s^{-1} lasting for some 5 min, but with a path that is frequently slanted with respect to the local vertical direction. After reaching a typical maximum height of 9000 km, the ejection stops and is followed by a fading of the spicule brightness or a return of the emitting material to the photosphere. Interestingly, in the upward-moving phase the spicule mass flux exceeds the mass loss of the solar corona through the solar wind by two orders of magnitude!

All theoretical models aimed at explaining the ori-

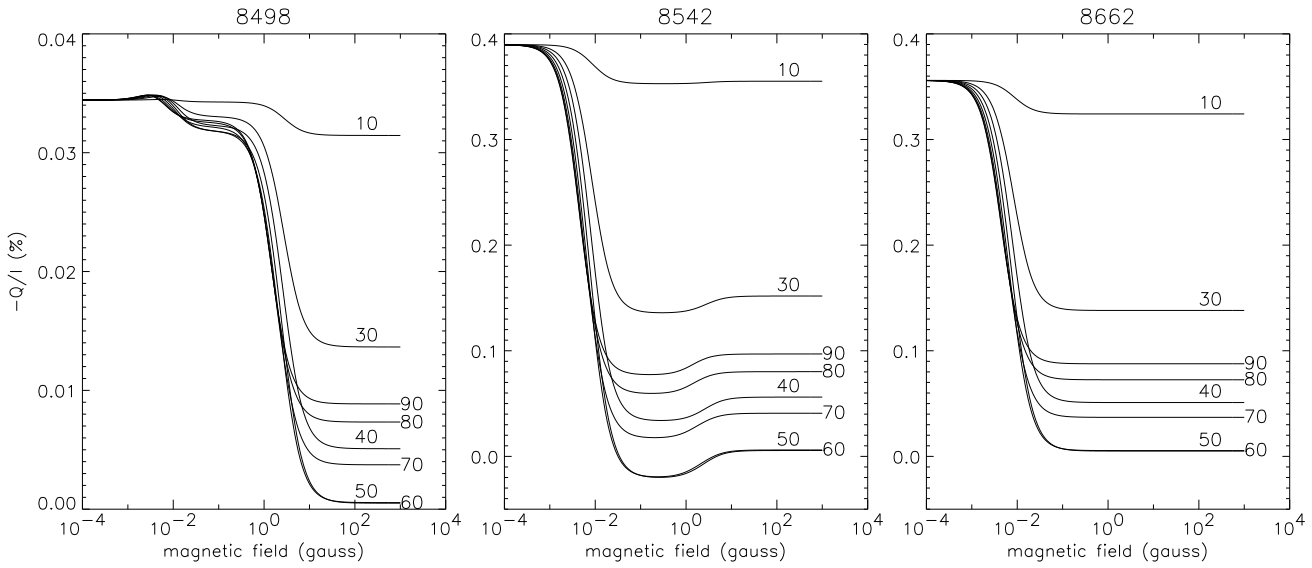

Fig. 10.: The fractional linear polarization of the Ca II IR triplet calculated at $\mu = 0.1$ (about $5''$ from the limb) in a relatively simple model of the solar chromosphere. Each curve corresponds to the indicated inclination (θ_B) of the assumed random-azimuth magnetic field. From Trujillo Bueno & Manso Sainz (2002).

gin of spicules invoke magnetic field effects. What has really been lacking up to now are spectropolarimetric investigations to infer the strength and geometry of the magnetic field that is thought to channel the spicular motion. To fill this gap, our group has recently initiated an investigation which combines observational and theoretical spectropolarimetry.

Figure 11 shows an example of the full Stokes vector of the He I 1083 nm multiplet, which we have observed with the Tenerife Infrared Polarimeter (TIP)[26] attached to the Vacuum Tower Telescope (VTT). The spectrograph slit was located ∼2 arcsec off the limb and parallel to it, thus crossing spicular material as illustrated in the lower part of the figure. This spectropolarimetric observation is very encouraging, especially because of the detection of a non-zero Stokes-U profile. According to the theory of the Hanle effect, this Stokes-U profile is the observational signature of the presence of a weak magnetic field *inclined* with respect to the solar radius vector through the observed point. Note that the Stokes-V signal is at the noise level, indicating that either the field is very weak (the most reasonable possibility) and/or that the field is perpendicular to the line of sight. A best fit to the observations can be achieved, at various levels of sophistication, via theoretical modeling of the Hanle and Zeeman effects. For example, if we assume that the scattering polarization is produced by an optically thin plasma we obtain the solid lines of Fig. 11. Our theoretical modeling of the observed Stokes Q, U and V profiles is notable. The discrepancy found in Stokes-I around the wavelength location of the blue component of the He I 1083 nm multiplet indicates that the optically thin assumption is not suitable for Stokes-I. A more detailed theoretical modeling including radiative transfer effects along a line of sight which goes through many individual spicules yields excellent agreement with the observations and validates the values given in the figure for the strength and orientation of the inferred vector magnetic field.

[26]For a description of the IAC's solar polarimeters see Martínez Pillet, Collados, Sánchez Almeida et al. (1999).

Coronal magnetism and solar prominences

Finally, let us illustrate with a particularly interesting example (i.e., the case of solar prominences) the diagnostic method by means of which we should be able to investigate in the near future the magnetic fields of the solar corona via spectropolarimetric observations of coronal forbidden lines using the Advanced Technology Solar Telescope (ATST).

Solar prominences are relatively cool and dense ribbons of plasma located tens of thousands of kilometers above the visible 'surface' of the Sun and embedded in the 10^6 K solar corona. As pointed out by Priest (1989), prominences represent interesting astrophysical systems where magnetic fields are interacting with plasma in subtle ways, where dense plasma is being supported against gravity and where thermal instability is producing a cool condensation, and so by studying these fascinating objects in detail we can learn how these fundamental processes are likely to operate elsewhere in the Universe. On the other hand, the eruption of a prominence often produces a coronal mass ejection, which may have a dramatic influence on near-Earth space weather.

The Tenerife Infrared Polarimeter allows us to measure the four Stokes parameters with an unprecedented

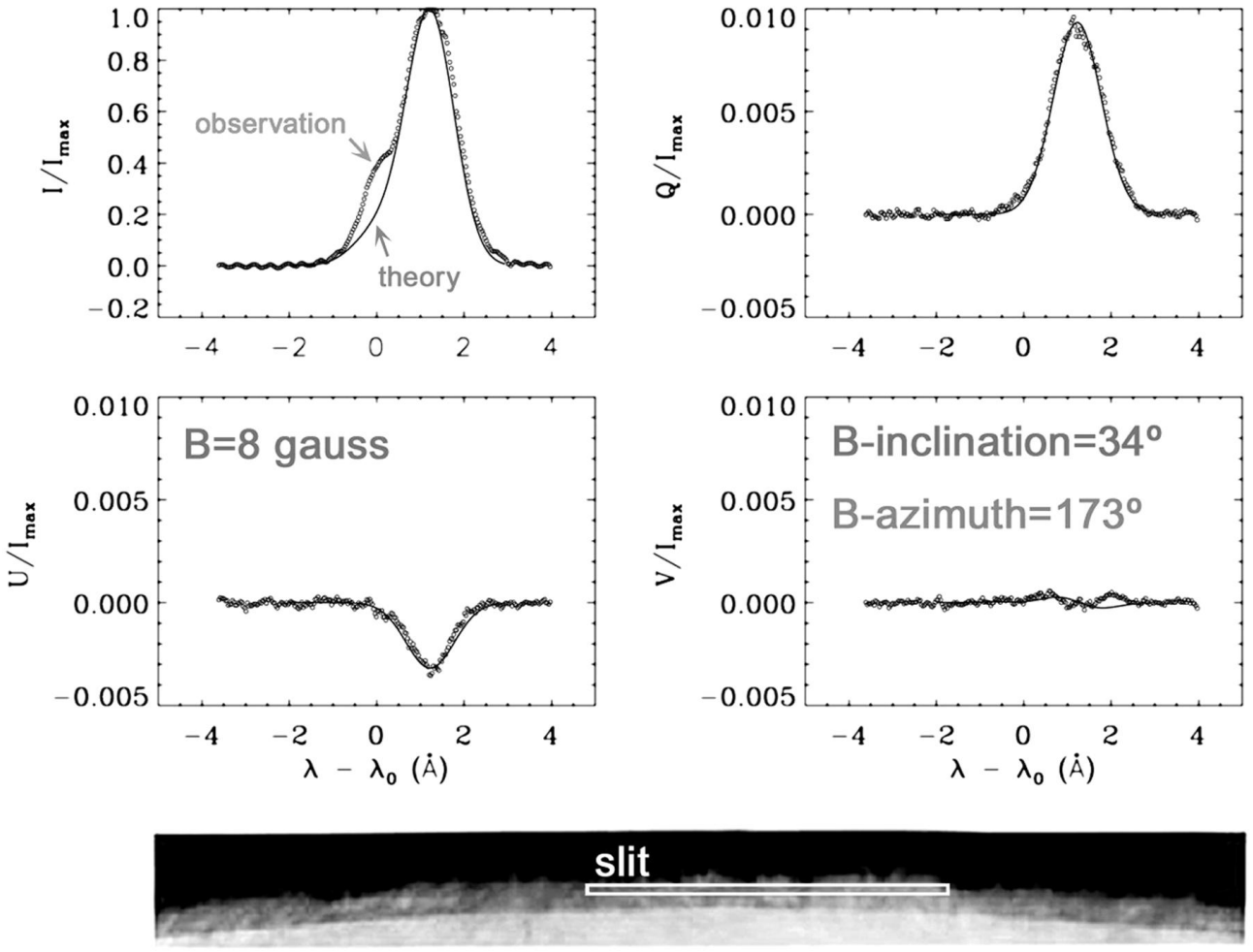

Fig. 11.: Inclination (θ_B), azimuth (χ_B), and strength of the magnetic field vector inferred from the observed He I 10830 polarization in spicules at a given spatial point. The bottom panel illustrates that the light selected by the spectrograph slit stems from chromospheric spicular material.

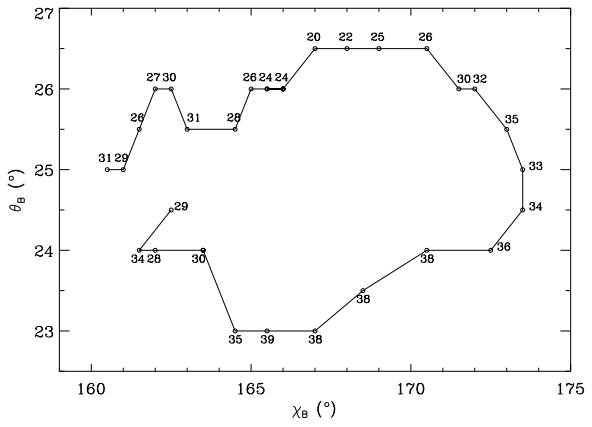

Fig. 12.: Inclination (θ_B), azimuth (χ_B), and strength (in gauss) of the magnetic field vector inferred from the observed polarization in the He I 10830 multiplet at consecutive spatial points along the spectrograph slit.

degree of sensitivity in the near IR. Using this instrument attached to the German Vacuum Tower Telescope and modeling the observed spectral line polarization within the framework of the quantum theory of line formation, we are investigating the three-dimensional structure of the magnetic fields that confine the plasma of solar prominences (see our first results in Trujillo Bueno et al. 2002*b*). To this end, we have developed suitable inversion algorithms for deriving the magnetic field vector from the observed polarization in the He I 10830 multiplet. Figure 3 in the letter by Trujillo Bueno et al. (2002*b*) contrasts our theoretical modeling versus the observed Stokes profiles in one of the many prominences we have observed. Figure 12 shows that the magnetic field vector in a prominence that was located at the solar south pole is *rotating* around a fixed direction in space (given by $\theta_B \approx 25°$ and $\chi_B \approx 168°$) as we move along consecutive spatial points (Merenda, Trujillo Bueno, Landi Degl'Innocenti & Collados 2003; in preparation). This is just an additional example of

how a suitable combination of novel instrumentation, spectropolarimetric observations, theory and numerical simulations is the key to activate new advances in astrophysics.

Concluding remarks

Polarized light provides the most reliable source of information at our disposal for the remote sensing of astrophysical magnetic fields, including those on the Sun. In solar physics we have witnessed interesting observational discoveries thanks to the development of novel polarimeters like the ASP, ZIMPOL or TIP. However, in order to open a true empirical window on the magnetism of the extended solar atmosphere, we urgently need a UV polarimeter in a space telescope and a cleverly-designed large ground-based solar telescope optimized for spectropolarimetric observations, and installed on an excellent site like that chosen by Scharmer et al. (2002) for the Swedish 1m Solar Telescope.

Concerning night-time astronomy, we are still crying out for suitable polarimeters for the present generation of 10m class telescopes.

Acknowledgements

I would like to express my gratitude to the scientists participating in the project AYA2001-1649, which is being funded by the Spanish Ministerio de Ciencia y Tecnología, for stimulating scientific discussions and collaborations on solar magnetism and spectropolarimetry. Thanks are also due to the Editorial Committee of the *Boletín de la SEA* for their kind invitation to write this article.

Referencias

[1] Asplund, M., Ludwig, H.G., Nordlund, Å., & Stein, R.F. 2000, A&A, 359, 669

[2] Beckers, J. 1972, Annual Review of Astronomy and Astrophysics, 10, 73

[3] Bohr, N. 1924, *Naturwissenschaften*, 12, 1115

[4] Bommier, V. 2002, (private communication)

[5] Bommier, V., & Molodij, G. 2002, A&A, 381, 241

[6] Bonet, J. A. 1999, in ASSL Ser. 239, Motions in the Solar Atmosphere, ed. A. Hanslmeier & M. Messerotti (Dordrecht: Kluwer), 1

[7] Born, M., & Wolf, E. 1994, *Principles of Optics*, Pergamon Press, Oxford

[8] Cattaneo, F. 1999, ApJ, 515, L39

[9] Chandrasekhar, S. 1946, ApJ, 105, 424

[10] Cohen-Tannoudji, C. 1977, in *Frontiers in Laser Spectroscopy*, Ecole d'Eté des Houches 1975, North-Holland, Amsterdam

[11] Cohen-Tannoudji, C., Dupont-Roc, J., & Grynberg, G. 1992, Atom-Photon Interactions: Basic Processes and Applications, John Wiley & Sons (p. 257)

[12] Collados, M. 2001, in *Advanced Solar Polarimetry: Theory, Observation and Instrumentation*, M. Sigwarth (ed.), ASP Conf. Series, Vol. 236, 255

[13] del Toro Iniesta, J. C. 2003, *Introduction to Spectropolarimetry*, Cambridge University Press

[14] Domínguez Cerdeña, I., Kneer, F. & Sánchez Almeida, J. 2003, ApJ, 582, L55

[15] Einstein, A. 1917, *Phys. Z.* 18, 121

[16] Fano, U. 1957, Rev. Mod. Phys., 29, 74

[17] Gandorfer A. 2000, *The Second Solar Spectrum*, Vol. 1, ETH, Zürich.

[18] Gandorfer A. 2002, *The Second Solar Spectrum*, Vol. 2, ETH, Zürich.

[19] Hanle, W. 1924, Z. Phys., 30, 93

[20] Hanle, W. 1925, *Ergebnisse der Exakten Naturwissenschaften*, 4, 214

[21] Happer, W. 1972, Rev. Mod. Phys., 44, 169

[22] Heisenberg, W. 1925, Z. Phys., 31, 617

[23] Jefferies, J.T., Lites, B.W., & Skumanich, A. 1989, ApJ, 343, 920

[24] Kastler, A. 1950, J. de Physique, 11, 255

[25] Khomenko, E.V., Collados, M., Solanki, S., Lagg, A., & Trujillo Bueno, J. 2003, A&A, in press

[26] Landi Degl'Innocenti, E. 1983, Sol. Phys., 85, 3

[27] Landi Degl'Innocenti, E. 1985, Sol. Phys., 102, 1

[28] Landi Degl'Innocenti, E. 1992, in *Solar Observations: Techniques and Interpretation*, F. Sánchez, M. Collados and M. Vázquez (eds.), Cambridge University Press, p. 73

[29] Landi Degl'Innocenti, E. 2002, in *Astrophysical Spectropolarimetry*, J. Trujillo Bueno, F. Moreno-Insertis & F. Sánchez (eds.), Cambridge University Press, 1

[30] Lin, H., & Rimmele, T. 1999, ApJ, 514, 448

[31] Manso Sainz, R., 2002, PhD Thesis, University of La Laguna (Tenerife, Spain)

[32] Manso Sainz, R., & Trujillo Bueno, J. 2001, in *Advanced Solar Polarimetry*, M. Sigwarth (ed.), ASP Conf. Series, Vol. 236, 213-220.

[33] Manso Sainz, R., & Landi Degl'Innocenti, E. 2002, A&A, 394, 1093

[34] Manso Sainz, R., & Trujillo Bueno, J. 2003, Physical Review Letters, in press

[35] Martínez Pillet, V., Collados, M., Sánchez Almeida, J. et al. 1999, in *High Resolution Solar Physics: Theory, Observations and Techniques*, T. R. Rimmele, K. S. Balasubramaniam, & R. R. Radick, ASP Conf. Series, Vol. 183, 264

[36] Mathys, G., Solanki, S.K., & Wickramasinghe, D. (eds.) 2001, *Magnetic Fields Across the H-R Diagram*, ASP Conf. Series, Vol. 248

[37] Mihalas, D. 1978, *Stellar Atmospheres*, Freeman and Company, San Francisco

[38] Mitchell, A.C.G., & Zemansky, M.W. 1934, *Resonance Radiation and Excited Atoms*, Cambridge University Press

[39] Moruzzi, G., & Strumia, F. 1991, (eds.), *The Hanle Effect and Level-Crossing Spectroscopy*, Plenum Press, New York

[40] Omont, A. 1977, Prog. Quantum Electron., 5, 69

[41] Priest, E.R. 1989, in 'Dynamics and Structure of Quiescent Solar Prominences', E.R. Priest (ed.), Kluwer, 1

[42] Rachkovsky, D.N. 1962a, *Izv. Krymsk. Astrofiz. Obs.* 27, 148

[43] Rachkovsky, D.N. 1962b, *Izv. Krymsk. Astrofiz. Obs.* 28, 259

[44] Rybicki, G.B., & Lightman, A.P. 1979, *Radiative Processes in Astrophysics*, John Wiley & Sons, New York

[45] Sánchez Almeida, J., & Lites, B. 2000, ApJ, 532, 1215

[46] Scharmer, G.B., Gudiksen, B.V., Kiselman, D., Löfdahl, M.G., & Rouppe van der Voort, L. H. M. 2002, Nature, 420, 151

[47] Schrijver, C. J., & Zwaan, C. 2000, Solar and Stellar Magnetic Activity, Cambridge University Press

[48] Shchukina, N., & Trujillo Bueno, J. 2001, ApJ, 550, 970

[49] Shchukina, N., & Trujillo Bueno, J. 2003, in *Solar Polarization*, J. Trujillo Bueno & J. Sánchez Almeida (eds.), ASP Conf. Series, Vol. in press

[50] Sigwarth, M. (ed.) 2001, *Advanced Solar Polarimetry: Theory, Observation and Instrumentation*, ASP Conf. Series, Vol. 236

[51] Socas-Navarro, H., & Sánchez Almeida, J. 2002, ApJ, 565, 1323

[52] Socas-Navarro, H., & Sánchez Almeida, J. 2003, ApJ, in press

[53] Solanki, S.K. 2003, The Astronomy and Astrophysics Review, 11, 153

[54] Stein, R.F., & Nordlund, Å. 1998, ApJ, 499, 914

[55] Stein, R.F., & Nordlund, Å. 2003, in *IAU Symposium 210: Modeling of Stellar Atmospheres*, N. E. Piskunov, W. W. Weiss, D. F. Gray (eds.), ASP Conf. Series, in press

[56] Stenflo, J.O. 1994, *Solar Magnetic Fields: Polarized Radiation Diagnostics*, Kluwer Academic Publishers

[57] Stenflo, J.O. 2002, in *Astrophysical Spectropolarimetry*, J. Trujillo Bueno, F. Moreno-Insertis & F. Sánchez (eds.), Cambridge University Press, 55

[58] Stenflo, J.O., & Keller, C. 1997, A&A, 321, 927

[59] Stenflo, J.O., Bianda, M., Keller, C. U., & Solanki, S.K. 1997, A&A, 322, 985

[60] Stenflo, J.O., Keller, C., & Gandorfer, A. 2000, A&A, 355, 789

[61] Stepanov, V.E. 1958, *Izv. Krymsk. Astrofiz. Obs.* 18, 136

[62] Stokes, G. G. 1852, *Trans. Cambridge Phil. Soc.*, 9, 399

[63] Title, A. 2003, in *IAU Symposium 210: Modeling of Stellar Atmospheres*, N. E. Piskunov, W. W. Weiss, D. F. Gray (eds.), ASP Conf. Series, in press

[64] Trujillo Bueno, J. 1999, "Towards the Modeling of the Second Solar Spectrum", in *Solar Polarization*, K. N. Nagendra & J. O. Stenflo (eds.), Kluwer Academic Publishers, 73

[65] Trujillo Bueno, J. 2001, "Atomic Polarization and the Hanle Effect", in *Advanced Solar Polarimetry: Theory, Observation and Instrumentation*, M. Sigwarth (ed.), ASP Conf. Series, Vol. 236, 161

[66] Trujillo Bueno, J. 2003*a*, "Astrophysical Spectropolarimetry and Magnetic Field Diagnostics", in *IAU Symposium 210: Modeling of Stellar Atmospheres*, N. E. Piskunov, W. W. Weiss, D. F. Gray (eds.), ASP Conf. Series, in press

[67] Trujillo Bueno, J. 2003*b*, "The Generation and Transfer of Polarized Radiation in Stellar Atmospheres", in *Stellar Atmosphere Modeling*, I. Hubeny, D. Mihalas & K. Werner (eds.), ASP Conf. Series, Vol. 288, 551

[68] Trujillo Bueno, J., & Manso Sainz, R. 1999, ApJ, 516, 436

[69] Trujillo Bueno, J., & Landi Degl'Innocenti, E. 1997, ApJ Letters, 482, L183

[70] Trujillo Bueno, J., Collados, M., Paletou, F., & Molodij, G. 2001, in *Advanced Solar Polarimetry*, M. Sigwarth (ed.), ASP Conf. Series, Vol. 236, 141

[71] Trujillo Bueno, J., & Manso Sainz, R. 2002, Il Nuovo Cimento, Vol. 25 C, No. 5-6, 783

[72] Trujillo Bueno, J., Moreno Insertis, F., & Sánchez, F. (eds.) 2002*a*, *Astrophysical Spectropolarimetry*, Cambridge University Press

[73] Trujillo Bueno, J., Landi Degl'Innocenti, E., Collados, M., Merenda, L., & Manso Sainz, R. 2002*b*, Nature, 415, 403

[74] Trujillo Bueno, J., & Sánchez Almeida, J. (eds.) 2003, *Solar Polarization*, ASP Conf. Series, Vol. in press

[75] Unno, W. 1956, *Publ. Astron. Soc. Japan* 8, 108

Tesis doctorales

Scattering Line Polarization and the Hanle Effect in Weakly Magnetized Stellar Atmospheres

Rafael Manso Sainz rsainz@ll.iac.es

Director/es: Javier Trujillo Bueno
Centro: Instituto de Astrofísica de Canarias
Lectura: 1 de julio de 2002

La iluminación anisótropa de los átomos en las regiones externas de una atmósfera estelar induce diferencias entre las poblaciones, así como coherencias cuánticas, entre los subniveles magnéticos de los niveles atómicos (esto es, polarización atómica). Como consecuencia, la luz emergente está, en general, linealmente polarizada (*scattering line polarization*). El efecto Hanle es la modificación de la polarización atómica, y por consiguiente de la polarización de la luz observada, por la acción de un campo magnético débil que rompe parcialmente la degeneración de los subniveles. El análisis de la polarización de la luz dispersada en líneas espectrales abre por tanto la posibilidad de estudiar tales campos magnéticos. En esta tesis se plantea una jerarquía de problemas de transporte radiativo con polarización y se presenta el desarrollo y aplicación de métodos para su resolución numérica. El objetivo es comprender la formación de señales espectropolarimétricas de este tipo y así desarrollar nuevas técnicas de diagnóstico para plasmas astrofísicos.

En primer lugar establecemos los fundamentos de los métodos numéricos para el transporte de radiación polarizada en un gas de átomos de dos niveles, teniendo en cuenta el efecto Hanle debido a un campo magnético microturbulento e isótropo. Hemos generalizado a este caso una serie de métodos previamente desarrollados para el caso estándar no polarizado: el método de la *iteración-*Λ *acelerada*, basada en el método iterativo de Jacobi, y los esquemas iterativos basados en la iteración Gauss-Seidel y el método SOR introducidos por Trujillo Bueno y Fabiani Bendicho (1995, ApJ, 455, 646). Demostramos la excelente tasa de convergencia de estos métodos, que no requieren la construcción o inversión explícita de grandes matrices, y que conservan la simplicidad y tiempo de cómputo por iteración similares a la elemental *iteración-*Λ.

Consideramos además el problema de la polarización por *scattering* resonante en átomos de dos niveles y el efecto Hanle para el caso general de una atmósfera estelar multidimensional. Resolvemos el problema del transporte radiativo aplicando los métodos iterativos mencionados anteriormente, para lo cual hemos desarrollado dos códigos numéricos para geometría Cartesiana arbitraria. De esta manera hemos investigado cómo efectos de transporte radiativo horizontal, debidos a inhomogeneidades del plasma estelar, compiten con los campos magnéticos débiles para modificar las señales de polarización por *scattering* en líneas espectrales, y cómo esto puede afectar al diagnóstico de campos magnéticos débiles en la atmósfera solar.

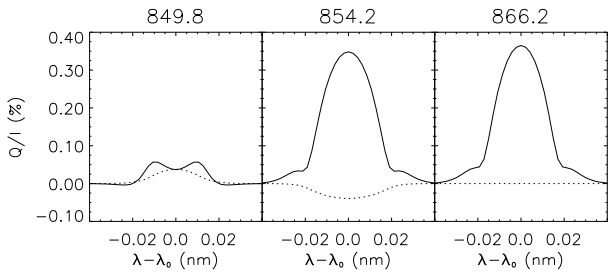

Fig. 1.: Simulación numérica de la polarización lineal debida a *scattering* observada en el triplete IR del Ca II. Líneas continuas: teniendo en cuenta el efecto de la polarización atómica de los niveles inferiores de tales transiciones. La forma de los perfiles y las amplitudes relativas Q/I están en buen acuerdo con las observaciones. Líneas discontinuas: despreciando la polarización atómica.

Tambien hemos resuelto, por primera vez, el problema de la generación y transporte de polarización por *scattering* en el espectro de átomos de muchos niveles. Para ello tenemos en cuenta la generación y distribución de polarización atómica entre todos los niveles del sistema atómico debida a absorciones, emisiones y colisiones. Se ha llevado a cabo un estudio sistemático de la polarización por *scattering* resonante en atmósferas estelares, considerando que ambos niveles atómicos son, en general, polarizables. En el caso general de un átomo de varios niveles, hemos demostrado, en particular, que las señales de polarización "enigmáticas" observadas en el triplete infrarrojo del Ca II son debidas a que los niveles metaestables $^2D_{3/2}$ y $^2D_{5/2}$ están significativamente polarizados. Como consecuencia, la polarización en la línea 866.2 nm, y prácticamente toda la de la línea 854.2 nm, es debida a absorción selectiva (Trujillo Bueno y Landi Degl'Innocenti 1997, ApJL, 482, 183), lo que demuestra que el "dicroísmo a campo nulo" opera en la cromosfera solar (véase la Fig. 1).

Finalmente, investigamos la influencia de campos magnéticos débiles sobre las señales de polarización por *scattering* en los espectros de átomos de muchos niveles en atmósferas estelares. Se presenta, por primera vez, un estudio del transporte radiativo considerando el efecto Hanle en sistemas atómicos arbitrarios en los que cualquier nivel puede estar polarizado. En particular, se extiende el estudio sistemático para átomos de dos niveles al caso magnetizado y se generaliza el estudio del Ca II, enfatizando las nuevas posibilidades de diagnóstico de campos magnéticos débiles que esto supone. El código numérico desarrollado para este estudio permite realizar simulaciones numéricas de los efectos Hanle y Zeeman actuando conjuntamente en atmósferas estelares débilmente magnetizadas. La aplicación de esta nueva herramienta de transporte radiativo a observaciones espectropolarimétricas está actualmente ayudándonos a descifrar la intensidad y topología de los campos magnéticos de la cromosfera solar.

Estudio de vórtices anticiclónicos y ciclónicos en la atmósfera de Júpiter

Raúl Morales Juberías rm.juberias@louisville.edu

Director/es: Agustín Sanchez Lavega
Centro: E.S.I. - Universidad del País Vasco
Lectura: 25 de octubre de 2002

En este trabajo de Tesis Doctoral presentamos los resultados de dos líneas de investigación independientes pero complementarias que nos permiten avanzar en el conocimiento que actualmente tenemos de las propiedades físicas de la atmósfera de Júpiter.

Desde un punto de vista observacional, presentamos los resultados del estudio estadístico sistemático y exhaustivo de algunas de las propiedades físicas de los sistemas meteorológicos más representativos y ubicuos de la atmósfera Joviana: Los vórtices anticiclónicos y ciclónicos de escala superior a 1000 km. Es el primer estudio de este tipo que se realiza en base a observaciones continuas tomadas durante un periodo de tiempo tan largo (seis años, 1994 - 2000) y abarcando medidas en un rango de latitudes del planeta tan amplio ($\pm 75°$)(Morales-Juberías et al. 2002, Icarus, 157, 76; Morales-Juberías et al. 2002, Icarus, 160, 325). Además, presentamos por primera vez en la historia de observaciones del planeta, la caracterización observacional detallada de la fusión de dos de los vórtices anticiclónicos más grandes (tamaño $\gtrsim$ 10,000 km) y longevos (tiempo de vida $\gtrsim$ 60 años) de su atmósfera (Sánchez-Lavega *et al.* 2001, *Icarus* 149, 491).

Como principal fuente de datos para este estudio utilizamos imágenes de Júpiter del archivo del *Telescopio Espacial Hubble (HST)* tomadas con la *Wide Field Planetary Camera 2* en los filtros de 410, 890 (banda de absorción del metano) y 953 nm, los cuales permiten sondear, según los modelos fotométricos estándares West *et al.* 1995, Science, 267, 1296), distintas alturas en la atmósfera del planeta entre $\approx$ 0.1 y 1 bar de presión. Para completar el estudio en las fechas en las que no disponiamos de imágenes del *HST*, recurrimos al análisis de un grán número de imágenes CCD provenientes de las campañas de vigilancia continua de Júpiter que se realizan con el Telescopio Planetario de 1 metro (*T1M*) del Observatorio del *Pic du Midi* (Francia), así como con el Telescopio Infrarojo de 3-m (*ITRF-NASA*) del Observatorio de *Mauna Kea* (Hawai, *US*). El estudio de la evolución temporal a largo plazo de las propiedades de estos sistemas meteorológicos lo completamos analizando un gran número de imágenes tomadas por las naves *Voyager* en 1979, en filtros similares a los usados por el *HST*. Para la caracterización detallada de la morfología y dinámica del nuevo vórtice gigante surgido en la fusión observada, utilizamos imágenes propias de alta resolución tomadas en tiempo de observación reservado del *HST* el 2 de septiembre de 2000. Desde un punto de vista teórico, presentamos los resultados de distintas simulaciones numéricas de algunos de los fenómenos observados.

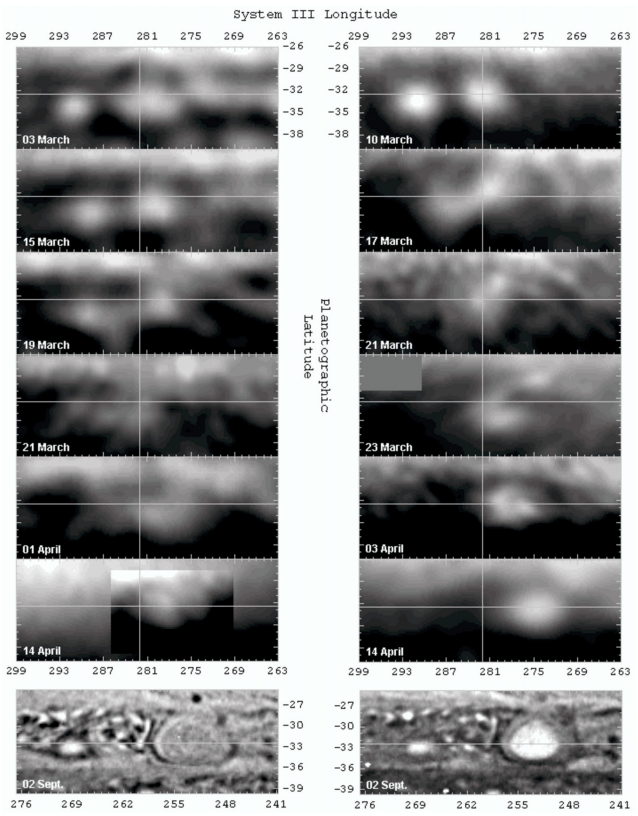

Fig. 1.: Secuencia de proyecciones cilíndricas de las imágenes de la interacción entre dos vórtices gigantes en la atmósfera de Júpiter, tomadas con filtros sensibles a diferentes alturas en la atmósfera. Serie de la izquierda: arriba, filtros 840 nm y 1.58 μm, abajo, imagen de alta resolución del *HST* en 953 nm (P $\approx$ 0.4-1 bar). Serie de la derecha: arriba, filtros 890 nm y 3.78 μm, abajo, imagen de alta resolucion del *HST* en 890 nm (P $\approx$ 0.2 bar).

Como herramienta de trabajo utilizamos el modelo meteorológico de circulación general EPIC (*Explicit Planetary Isentropic Coordinate Model*; Dowling *et al.* 1998, *Icarus* 132, 221), el cual integra explícitamente las ecuaciones primitivas de circulación atmosférica en coordenadas isentrópicas y geometría esférica. Principalmente estudiamos bajo qué condiciones podemos reproducir el fenómeno observado (Fig. 1) de que durante el proceso de fusión los vórtices gigantes orbitaran entre ellos respecto a un centro común en los niveles altos de la atmósfera y que sin embargo no lo hicieran en los niveles bajos. Presentamos cuál es el espacio de parámetros a los que esta dicotomía vertical es principalmente sensible y caracterizamos la región del mismo en la que se dan las condiciones suficientes para que esta dicotomía se produzca (Morales-Juberías et al. 2003, Icarus, enviado).

Diagnóstico de galaxias H II *en el rojo lejano*

Enrique Pérez Montero enrique.perez@uam.es

Director/es: Ángeles I. Díaz Beltrán
Centro: Universidad Autónoma de Madrid
Lectura: 5 de febrero de 2003

La principal motivación que ha tenido este trabajo de tesis ha sido el estudio de la importancia que tiene el rango espectral en el rojo lejano e infrarrojo cercano en la correcta descripción de las nebulosas de gas ionizado (*i.e.* regiones H II). Para ello se ha observado en este rango (entre 7000 Å y una micra) con el *Isaac Newton Telescope* una muestra de 12 galaxias H II cercanas pertenecientes al Segundo Catálogo de Byurakan y que ya habían sido observadas en el rango óptico. Estos objetos resultan de interés debido a su baja metalicidad y alto brillo superficial. La aportación más significativa de las nuevas observaciones la constituye la observación de las líneas aurorales de [O II] y [S III], así como las líneas nebulares intensas de [S II] y [Si III].

Los valores obtenidos en la espectrofotometría de estas observaciones junto a las imágenes en B y R recabadas en la bibliografía muestran variaciones en las propiedades físicas que no son propias de una familia de objetos homogénea y que corresponden a valores de luminosidad, tasa de formación estelar presente y pasada o proporción en la masa de hidrógeno ionizado muy diferentes. Es esperable, por tanto, que dichas diferencias se reproduzcan para una edad del Universo más joven, en contraste con las suposiciones vertidas sobre Galaxias Compactas Azules a corrimiento al rojo mayor.

La determinación de la densidad y de al menos tres temperaturas electrónicas (t([O II]), t([O III]) y t([S III])) ha sido posible en todos los objetos, así como la de [S II] en siete de ellos. El análisis de estas cantidades ha permitido determinaciones más fiables de las abundancias iónicas así como un estudio de la estructura interna de ionización de estos objetos, la cual refleja una cierta tendencia hacia el esquema t([S III]) > t([O III]) > t([O II]) y alerta ante la utilización de relaciones entre temperaturas obtenidas a través de modelos simples para hallar las correspondientes abundancias iónicas. Además existen factores adicionales de incertidumbre tales como la variación en los coeficientes atómicos y la dependencia con la densidad de t([O II]) y de t([S II]). Las abundancias iónicas deducidas resultan ser, en toda la muestra, valores menores que 0.2 veces las abundancias solares. Asimismo es reseñable la sobreabundancia de N/O en Mrk709, anormalmente alta para su metalicidad, y que pensamos puede estar relacionada con la sobreestimación de las líneas de [N II] por efectos ajenos a la fotoionización.

La modelización individual de los objetos ha permitido estimar los parámetros funcionales de los mismos (*i.e.* parámetro de ionización, temperatura efectiva del cúmulo ionizante y metalicidad) no conocidos así como estimar los factores de corrección de ionización (ICF) del azufre y el nitrógeno. Estos modelos han permitido

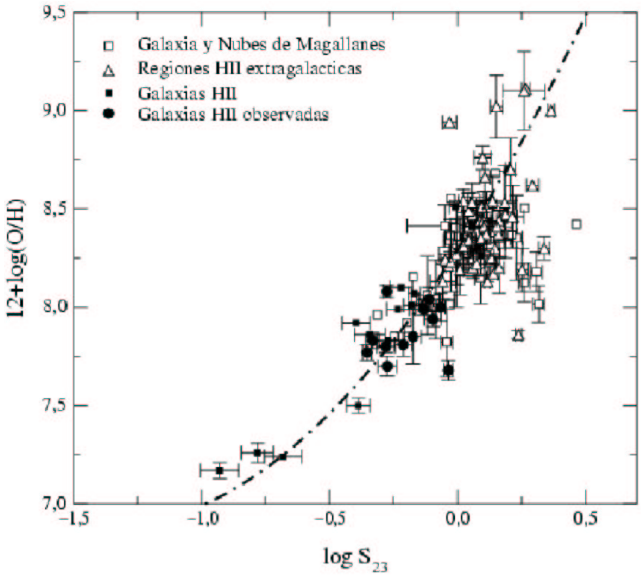

Fig. 1.: Relación entre el parámetro S_{23} y la metalicidad para una muestra de diversas familias de regiones de gas ionizado

confirmar las hipótesis de $O^0/H^0 \approx O/H$ y de $N^+/O^+ \approx N/O$. Asimismo, los modelos no parecen reproducir fielmente la estructura de ionización del azufre y de los ICF(S) obtenidos se deducen valores de S^{3+} de acuerdo a las predicciones que le otorgan un valor menor a pesar de lo que indican las observaciones en el IR medio de la línea de [S IV] a 10.52 μm para un objeto de la muestra (Mrk 209). Todos estos factores de incertidumbre concurren para no poder dar una estimación precisa del comportamiento de la curva universal de S/O frente a O/H en el régimen de bajas metalicidades. En cuanto a las propiedades de la población estelar ionizante inferidas de los resultados de estos modelos parecen estar de acuerdo con la existencia de brotes de formación estelar anteriores al del actual cúmulo ionizante.

La parte final del trabajo se ha dedicado a estudiar los principales parámetros empíricos de determinación de metalicidad. Para ello se ha reunido una muestra a partir de la bibliografía de 347 objetos con una abundancia de oxígeno determinada de manera directa y una medición de las líneas más intensas. De la muestra compilada, 160 tenían medidas las líneas de [S III] en el IR cercano, incluyendo las observadas en este mismo trabajo. Asímismo, con la intención de identificar las fuentes de incertidumbre en las calibraciones hechas a partir de estos parámetros empíricos se han usado modelos de fotoionización que cubrían las condiciones físicas de los objetos de la muestra. Los resultados obtenidos confirman al parámetro S_{23} como aquel a partir del cual se obtienen estimaciones más precisas de la metalicidad en relación al parámetro R_{23} o al parámetro N2.

Análisis espectroscópico de fragmentos cometarios y asteroidales a su entrada en la atmósfera terrestre

Josep Maria Trigo i Rodríguez

Director/es: Juan Fabregat Llueca (UV) y Jordi Llorca Piqué (UB)
Centro: Departament d'Astronomia i Astrofísica, Universitat de València
Lectura: 28 Junio 2002

Se analiza el origen y composición de la materia interplanetaria a partir de una perspectiva nueva basada en el estudio de los fenómenos luminosos que producen estas partículas a su entrada a la atmósfera terrestre, llamados meteoros. Tales partículas, procedentes mayoritariamente de la degradación de las superficies de cometas y asteroides, cuando se hallan en órbita solar se denominan genéricamente meteoroides. Dependiendo de la geometría orbital del encuentro con la Tierra alcanzan la atmósfera a velocidades comprendidas en el rango de 11 a 73 km/s. A alturas entre 120 y 70 km la densidad atmosférica causa que las colisiones atómicas sean frecuentes sobre el meteoroide, calentándolo por encima de 1500 K en la denominada ablación. Como consecuencia de ese proceso se produce la fase luminosa denominada meteoro que, visible a grandes distancias, puede ser estudiada con técnicas fotográficas, CCD o vídeo desde la superficie terrestre.

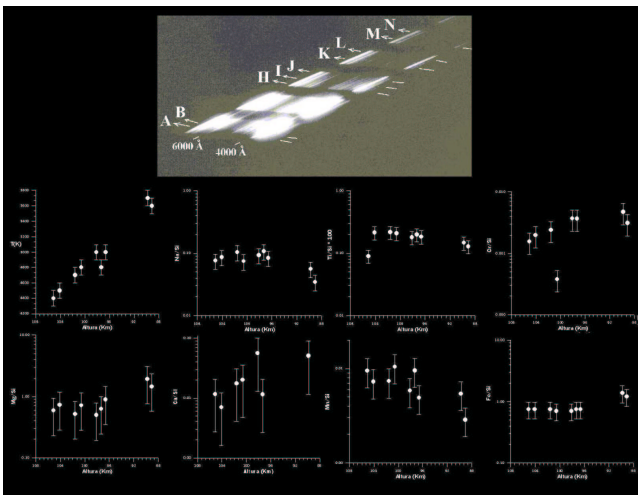

Fig. 1.: Espectro del bólido LEO de magnitud absoluta –12 producido por un fragmento del 55P/Tempel-Tuttle con una masa de 250±80 gramos. Se muestra dependiendo de la altura sobre la superficie terrestre la temperatura y abundancias químicas relativas al silicio de diferentes elementos.

En la primera parte de la tesis se analizan las imágenes en doble estación de 24 meteoros, la mayoría obtenidos durante la tormenta de Leónidas acaecida en 1999. De las imágenes estereoscópicas desde varias estaciones fotográficas ubicadas en la superficie terrestre se realiza la reconstrucción de las trayectorias reales en la atmósfera y la órbita heliocéntrica, calculada la velocidad geocéntrica de los meteoroides. Las órbitas calculadas permiten asociar los meteoros fotografiados a fragmentos procedentes de los cometas 55P/Tempel-Tuttle, 109P/Swift-Tuttle y 3P/Encke, así como también uno de ellos procedente del asteroide Faetón. En la segunda parte de la tesis se estudia el campo de la espectroscopía de meteoros a partir del análisis de quince espectros pertenecientes a trece brillantes meteoros (bólidos) registrados desde el Observatorio de Ondrejov (República Checa). Primero se determina la sensibilidad del espectrógrafo a partir de la cual se calibra la intensidad de las diversas líneas espectrales. Una vez calibrada se ajustan los espectros observados a un espectro sintético construido a partir de fijar unos valores típicos de la densidad de tonos en la columna meteórica, la temperatura y el área radiante. Cambiando esos parámetros por el método de los mínimos cuadrados, el espectro sintético alcanza valores de intensidad similares al registrado. En ese momento se varían a su vez las abundancias relativas de los diferentes elementos químicos para mejorar la calidad del ajuste de la intensidad de las líneas. De esa manera se obtuvo a lo largo de la trayectoria de cada bólido un espectro sintético en el intervalo comprendido entre 3800 y 6500Å, de donde se dedujeron finalmente las abundancias químicas relativas al Si de diferentes elementos químicos: Na, Mg, Ca, Ti, Cr, Mn, Fe, Co y Ni. El rango de masa de los meteoroides progenitores de los espectros analizados está a medio camino entre las partículas de polvo interplanetario (IDPs) y los meteoritos condríticos más pequeños. Comparando las abundancias químicas con las características de IDPs, del polvo del cometa 1P/Halley y de meteoritos condríticos se llega a interesantes conclusiones. Una de ellas es una mayor abundancia en Na de la deducida para el 1P/Halley. Asimismo se ha confirmado el efecto de evaporación incompleta del calcio que abandona el meteoroide sin fundirse, probablemente en forma de polvo refractario. Los resultados sugieren también que las medidas realizadas por la sonda Giotto del polvo del cometa 1P/Halley no pueden considerarse representativas del polvo cometario dado que varias abundancias químicas son diferentes en meteoroides de otros cometas. Probablemente tales diferencias sean debidas a que los espectrómetros de masas detectasen sólo partículas pequeñas de masa equivalente a la de los componentes principales de la matriz de las IDPs. Estos componentes principales, que suelen ser granos minerales, no suelen tener composición condrítica pese a que el conjunto del IDP sí puede poseerla. La espectroscopía de meteoros constituye un campo innovador que permite profundizar en esos procesos y determinar las abundancias y anomalías químicas de estos objetos si bien con una precisión mucho menor que la obtenida del análisis *in situ* en laboratorio. A pesar de ello posee la ventaja de permitir determinar las abundancias químicas dentro de un rango de error aceptable aun cuando las partículas se desintegren por completo en la atmósfera y no puedan ser por tanto recuperadas para su posterior análisis. En definitiva, el análisis de espectros meteóricos puede convertirse en una herramienta de gran valor en el estudio de la composición química de la materia interplanetaria que alcanza la Tierra. Este tipo de estudios puede complementar muy bien misiones mucho más costosas de recogida de materia cometaria in situ, como las misiones *Stardust* o *Rosetta* de la NASA y la ESA.